SYNTHESIS AND CHARACTERIZATION OF A PHYSICALLY ENTANGLED DNA HYDROGEL AND ITS APPLICATIONS

A Dissertation

Presented to the Faculty of the Graduate School

of Cornell University

In Partial Fulfillment of the Requirements for the Degree of

Doctor of Philosophy

by

Songming Peng

August 2014

SYNTHESIS AND CHARACTERIZATION OF A PHYSICALLY ENTANGLED DNA HYDROGEL AND ITS APPLICATIONS

Songming Peng, Ph. D.

Cornell University 2014

DNA is commonly viewed as a genetic material in all life forms, which is responsible for storing and encoding genetic information. However, from a materials perspective, DNA is an inherently generic polymeric material. Since this generic material is derived from biology, it has many unique properties that are not possessed by any other materials, including molecular recognition capability, defined base composition, and precise manipulation by enzymes. These properties have enabled extensive usage of DNA in nanotechnology for creating delicate DNA nanostructures as well as assembling nanomaterials. For real-world applications, however, it is necessary and important to create DNA materials in bulk-scale. Therefore, special attention needs to be paid to the efficiency and the yield for the synthesis of DNA materials. Unfortunately, these two objectives have not been fully explored in the field. In this thesis, I present a novel method to create a bulk-scale physically entangled DNA hydrogel. By designing two enzymatic processes, rolling circle amplification and multi-primed chain amplification, DNA chains are greatly amplified, both in length and in quantity, to entangle with each other to form a DNA hydrogel. Due to the power of enzymatic amplification, a bulk-scale hydrogel is easily produced with low cost and readily to be scaled up. Interestingly, our DNA hydrogel possesses properties

that are not found in nature of any kind: it has both solid-like and liquid-like properties. When the gel is immersed in water, it memorizes its original shape and behaves like a solid. However, the hydrogel become free-flowing “liquid” after taken out of water, and metamorphoses back to its original shape upon addition of water. More interestingly, the hydrogel is composed of uniformly sized DNA microspheres. To our surprise, the DNA density in each microsphere reaches as high as the human chromosome density. Thus, the DNA microsphere effectively concentrates unprecedentedly high dose DNA drugs that have never been achieved. This super-condensed ultra-high dose DNA effectively protects the condensed DNA, efficiently enters the cell and releases the DNA, enabling a superior therapeutic effect. This condensed DNA format is potential to serve as a versatile platform to compact and deliver all DNA-based therapeutics.

BIOGRAPHICAL SKETCH

Songming was born and raised in Jingmen, Hubei, China. He had a lovely childhood with his parents and grandparents in a beautiful village. At the age of twelve, his parents sent him to a boarding middle school in the city, which helped him to be independent at very early age. He later attended Longquan High School, where he luckily met a lovely girl, Cong Ye, and happily married her in 2012. After high school, he went to Shanghai Jiaotong University and studied Chemical Engineering. In addition to enjoying the colorful college life and travelling to Wuhan to see his girlfriend Cong, he spent two years conducting research in biodegradable polymer synthesis at Professor Changming Dong's lab, where he developed a great interest in biomaterials. He was admitted to the Master of Engineering program in Biomedical Engineering at Cornell University to follow his interest. At Cornell, he luckily attended a seminar given by Professor Dan Luo, and got fascinated by the idea of treating DNA as generic materials. He then applied for the Ph.D. program in Biological and Environmental Engineering at Cornell University and pursued his Ph.D. degree with Professor Dan Luo, focusing on developing bulk-scale DNA materials and their biomedical applications. Besides devoting himself to the exciting research, he served as the executive vice president for the Cornell Chinese Students and Scholars Association for one year to help the community and spread Chinese culture in Cornell. After enjoying the gorgeous natural scenery and extremely cold winter at Cornell for five years, he is now ready to move on to Caltech to start his new journey as a postdoc with Professor James Heath at Chemical Engineering.

To my family and friends

ACKNOWLEDGMENTS

I would like to express my special appreciation to my Ph.D. advisor and my committee chair Professor Dan Luo, for his great guidance and valuable advice throughout my dissertation, as well as my professional development. Even though Dan is super-busy, he is always there to help whenever needed. Without his continuous help and support, it will not be possible for me to finish this dissertation. I could not have imagined having a better advisor and mentor for my Ph.D. study. I am also very much indebted to my other two committee members Professor John March and Professor Chung Yuen Hui for their great and constructive advice on my research projects. I would like to thank all my committee members for their great recommendation letters, which has enabled me to continue my postdoc work at Caltech.

In addition, I would like to acknowledge my lab mates and my collaborators, especially Chuanying Xu, Jong Bum Lee, Chunyan Li, Yuerui Lu, Dayong Yang, Jason Kahn, Shawn Tan, Mike Campolongo, Thua Tran, Mark Hartman, Pichamon Kiatwithinon, Young Hoon Roh, Roanna Ruiz, Thomas Derrien, Ed Rice, Duo An, Jiajie Yu, Xuejuan Xu, Jinhui Cui, Huaimin Wang and Ru Cheng for their help, suggestions and discussions in both my profession and my life.

Last but not the least, I would like to thank my wife and my true friend, Cong Ye, for the love and happiness she has brought to me during the past ten years. Furthermore, I would like to thank my parents, Weiguo Xu and Chunfang Peng, for their endless love and financial support, which helped me devote myself to the

research. I would also like to thank my parents-in-law for taking care of my wife and me. Moreover, I want to thank my three roommates (Yuerui Lu, Han Wang and Han Zhang), as well as my other good friends at Cornell for the numerous happy times (eating, texas hold'em, skiing and traveling) we have been through together for the past five years.

TABLE OF CONTENTS

LIST OF FIGURES

LIST OF TABLES

CHAPTER 1: INTRODUCTION

1.1 DNA as a generic material

DNA is commonly viewed as a genetic material in all life forms, which is responsible for storing and encoding genetic information. However, from materials science and engineering perspective, DNA can be treated as a generic polymer composed of four different deoxy-nucleoside monomers: Adenine (A), Thymine (T), Guanine (G), and Cytosine (C). These four monomers are connected by the phosphodiester bonds to form a polymer chain, which is termed single-stranded DNA (ssDNA, Figure 1.1). Unlike conventional polymers in which the monomer sequences are randomly distributed, the base arrangement in the DNA chains can be specifically designed and precisely controlled. Typically, one end of the DNA strand contains a phosphate group on the 5' carbon of the sugar ring (defined as the 5' end), while the other end has a hydroxyl group on the 3' carbon of the sugar ring (defined as the 3' end). Since DNA is derived from biology, it possesses many unique properties that are not owned by any other materials.

Biologically, DNA has the molecular recognition capability at the nanoscale. If two ssDNAs are complementary, they will be able to recognize each other and hybridize into a double-stranded DNA (dsDNA) in anti-parallel directions (one strand from 5' to 3' and the other from 3' to 5') through the base paring rules (i.e., A pairs with T and G pairs with C, Figure 1.1). This property can be used to control molecular recognition of different DNA chains. For instance, by designing the sequence of ssDNAs to be either complementary or non-complementary, different ssDNAs can

either hybridize into dsDNA or remain in the ssDNA form. In addition, DNA hybridization is entirely reversible: dsDNA can be separated into two ssDNAs at elevated temperature (a process called denaturing) and the separated ssDNAs can be re-hybridized to the dsDNA at lower temperature (a process called renaturing). This reversible feature allowed the possibility of using temperature to regulate DNA states (ssDNA or dsDNA).

In addition, a myriad of enzymes can be employed to precisely manipulate DNA at the molecule level[1-3]. For example, a ligase can covalently link two pieces of DNA together (Figure 1.2). On the other hand, an endonuclease can cleave one piece of DNA into two pieces at specific sequences (Figure 1.2). A polymerase can elongate one DNA using the other DNA as a template (Figure 1.2). Till now, more than one thousand enzymes have been discovered that can be utilized to precisely manipulate DNA at the angstrom level[2, 4, 5]. These enzymes provide a versatile toolbox to engineer DNA materials for specific applications.

Chemically, DNA can be easily synthesized and modified. Virtually, any DNA sequence can be synthesized with high monodispersity, using technologies such as solid-state synthesis techniques[6, 7] and recombinant DNA technology[7]. The error rate of the synthesized DNA can be as low as 1 per 10 000 nucleotides[7, 8]. In addition, many chemical moieties such as primary amines, alkynes, thiols and biotins can be easily attached to the 5' or 3' end groups of DNA strands[2]. The modified DNA can be easily conjugated with other materials such as proteins[9-16], polymers[17-22], and gold nanoparticles[23-30] to build hybrid materials.

Physically, each helical turn of dsDNA consist of ten base pair (bp) with the

length of 3.4 nm, and the width of 2 nm. Surprisingly, the Young's modulus of DNA strands is as high as the Plexiglass[31, 32], allowing long DNA chains in the range of micrometers (thousands of bps) to be used despite its diameter of 2 nm. Moreover, the rigidity of DNA chains can be easily tuned by changing the length of DNA or states of DNA (dsDNA or ssDNA). In general, dsDNA shorter than 150 bp (which is the persistence length of DNA, approximately 50 nm)[33] is very rigid, while dsDNA is flexible when it is longer than the persistence length. On the other hand, ssDNA has a persistence length of about 1 nm[34] (corresponds to 1-3 base), thus, most ssDNAs are flexible. These properties provide a simple strategy to tailor the flexibility and rigidity of a desired DNA structure by adjusting the length of DNA or the composition of ssDNA and dsDNA.

Due to these unique properties, DNA has been extensively employed to build a variety of well-controlled and sophisticated nano-scale structures and devices[35-54], such as DNA cube[38], DNA smiley face[41], and DNA buckyball[44]. In addition, DNA has been utilized as a nano-organizer to assemble inorganic nanoparticle to form one-dimensional (1-D) polymers[55-57], two-dimensional (2-D) lattices[23, 24, 58, 59] and three-dimensional (3-D) crystals[25, 28, 30, 60, 61]. In light of these achievements, however, most of these structures were hard to scale up due to the high error rate and low yield of self-assembly[36, 51, 54]. Among many challenges, bulk-scale preparation is essential for the applications of DNA materials. In this thesis, I will focus on the methods of creating bulk-scale DNA materials and their biomedical applications.

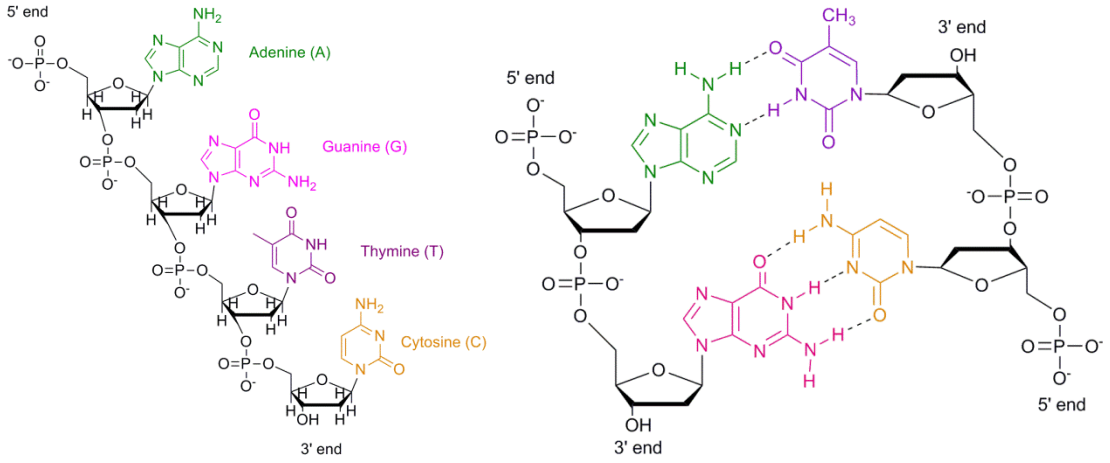

Figure 1.1. DNA as a polymer and the base pairing rules. A DNA polymer is composed of phosphodiester bonds, with four different bases (i.e. A, T, G, and C) dangling on the backbone. Two DNA polymers can antiparallelly hybridize with each other to form a dsDNA following the base paring rules (A with T and G with C).

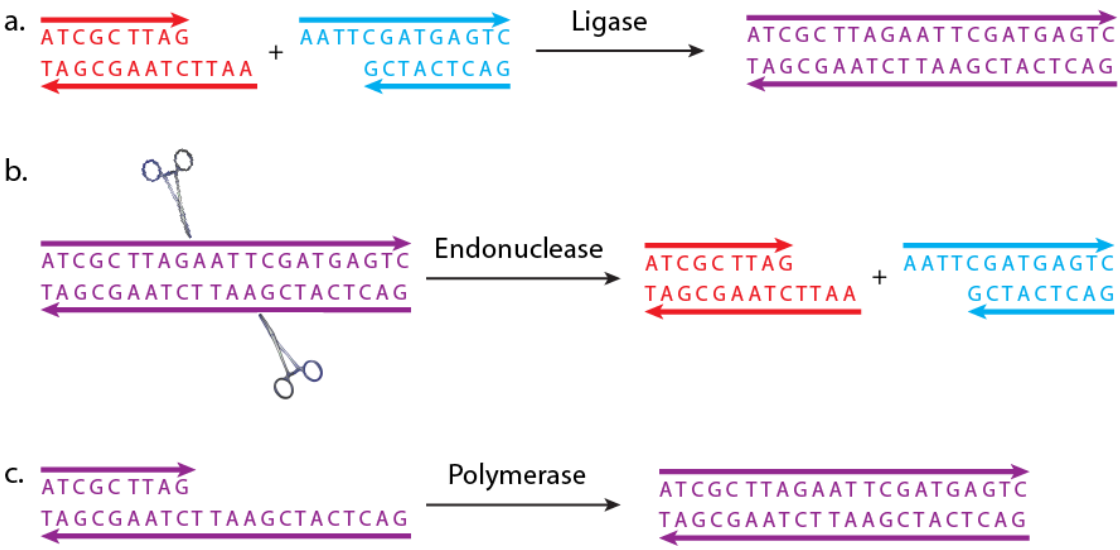

Figure 1.2. Enzymatic manipulation on DNA. Ligase links two pieces of DNA together (**a**), while endonuclease cuts one DNA into two pieces at specific sequence (**b**). Polymerase elongates one DNA strand using the other one as a template (**c**).

1.2 Linear DNA-based bulk materials and their applications

Linear DNA, which includes both ssDNA and dsDNA, is the natural DNA topology. It has been widely used as molecular probes for DNA detection. In addition, DNA can be easily conjugated to different functional moieties, including nanoparticles, proteins and polymers, to create hybrid materials. These DNA-hybrids possess the attributes of both DNA and the other material, enabling the creation of novel materials with new functions. Moreover, the DNA-hybrids can be precisely arranged in the nanoscale by other DNA templates to achieve higher ordered structures and new applications.

As one of the early attempts of using DNA as a generic material, Mirkin and co-workers pioneered in functionalizing gold nanoparticles (AuNP) with thiol modified DNA and organizing the AuNPs into macroscopic materials[26, 62]. They further applied the DNA functionalized AuNP for highly sensitive, colorimetric DNA detection[26, 63]. They first functionalized the AuNPs with two different thiolated ssDNAs, each with a partial complementary sequence to the target DNA. Without target DNA, the AuNPs were homogenously dispersed in the solution, showing a reddish color. However, when the target DNA was present, the AuNPs were brought together to form aggregates by the DNA hybridization. The close proximity of the AuNPs changed the solution from red color to purple color due to a red shift in the surface plasmon resonance of the AuNPs (Figure 1.3). The colorimetric change enabled a detection limit as low as 10 femtomoles of target DNA with naked eyes. More interestingly, the aggregates exhibited a sharp melting transition (from aggregates to solution at high temperature), allowing one to distinguish target DNA

sequence that contained one base mismatch, deletion or insertion from the fully complementary targets. In addition to AuNPs, DNA has been utilized to organize other nanomaterials including quantum dots[64-67], carbon nanotubes[68-71] for creation of multiplexed detection platform and development of semiconductor devices.

To further explore the molecular recognition capability of linear DNA, it was used to precisely control the placement and assembly of proteins at the nanoscale. Niemeyer and coworkers demonstrated this concept by using the DNA as a template to arrange DNA-protein (i.e. streptavidin) conjugates to form the protein arrays[72]. This approach was further applied to fabricate multi-enzyme complexes (MEC) by attaching multiple enzymes to a linear DNA template[73]. The MEC greatly enhanced the multi-step catalytic efficiencies due to the close proximity of these enzymes. Specifically, two enzymes (oxidoreductase and luciferase), which catalyzed two consecutive reaction steps, were first conjugated to linear DNA. The formed DNA-protein hybrids were then brought together by a complementary DNA template to form the MEC, allowing the consecutive reaction to occur more efficiently (Figure 1.4). Indeed, the resulted MEC showed a three-fold increase in catalytic efficiency compared to a random distribution of enzymes in solution. Similar concepts have been used to enhance the catalytic activity of other enzymes including glucose oxidase and horseradish peroxidase[11, 74]. This technique of DNA-directed assembly of proteins is extremely useful for developing enhanced catalytic systems for biomedical and biological applications[14, 15, 75].

The aforementioned examples have fully taken advantage of molecular recognition capability of DNA in the DNA-protein hybrids. On the other hand,

proteins, especially antibodies, carry many biological functions, including antigen recognition and binding. By utilizing the antibody function in the DNA-antibody conjugate, Cantor and colleagues developed immuno-polymerase chain reaction (Immuno-PCR), which has enabled ultrasensitive antigen detection[9, 10, 76]. In detail, DNA was first conjugated to monoclonal antibody to form the DNA-antibody hybrid. The hybrid bound specifically to an antigen, forming the antigen-antibody-DNA complex. Then, the DNA was amplified by PCR to greatly increase the signal that indicated the presence of the target antigen (Figure 1.4). Due to the specificity and amplification power of PCR, the detection limit for Immuno-PCR was 100 - 10 000-fold more sensitive than that of enzyme-linked immunosorbent assays (ELISA)[77]. This technique can be potentially applied detect a signal antigen molecule, enabling a broad range of applications in immunological research and clinical diagnostics[9, 77, 78].

In addition to assemble nanoparticles and proteins, DNA has also been used to synthesize novel copolymers[20]. The linear DNA can be designed either into the backbone to form block copolymers[21, 79] or into the side chain to from DNA-polymer brushes. For example, Herrmann and coworkers attached one or two ssDNAs to polyethylene glycol (PEG) polymer to form DNA-polymer hybrids (i.e. ssDNA-PEG, and ssDNA-PEG-ssDNA). These hybrids were then assembled to different block copolymers, including PEG-dsDNA-PEG, PEG-dsDNA-PEG-dsDNA-PEG and PEG-dsDNA-PEG-dsDNA-PEG-dsDNA-PEG[79]. Theoretically, the PEG-DNA block can be repeated as many times as wanted to generate super molecular weight block copolymers. Interestingly, the DNA length in the block copolymer can be easily elongated with enzymatic reactions such as PCR[21]. In addition, the PEG can be easily

changed to other polymers including polystyrene and polypropylene oxide to produce amphiphilic DNA block polymers[80, 81]. These amphiphilic polymers self-assembled into the nanoscale micelle in solution, which can effectively load the hydrophobic chemotherapeutic drugs such as doxorubicin and efficiency enter and kill the cancer cells[82].

One the other hand, when the DNA is attached to the backbone of the polymer, a brush DNA-polymer is created. Since the DNA adopts ssDNA state in the brush polymer, it can recognize other complementary ssDNA to form higher ordered structures such as DNA-based hydrogel. Langrana and coworker have produced two brush DNA-acrylamide polymers by separately copolymering two different acrydite-functionalized DNAs with acrylamide monomers[83]. In the presence of a linker DNA, which was partially complementary to the two ssDNAs, those two different brush DNA-polymers were brought together to form a DNA-based hydrogel. In this system, the three hybridized DNA strands replace the traditional chemical crosslinkers. Due to the reversibility property of DNA hybridization, the hydrogel crosslinking is reversible, either by high temperature to denature the hybridized DNA, or by specific removal DNA strands which have a higher affinity to the linker DNA (Figure 1.5). This switchable hydrogel has been used as a stimuli responsive material in controlled release of nanoparticles[84, 85] and proteins[86, 87] for therapeutic applications. Recently, Liu and coworker further adopted this DNA-based hydrogel for ultrasensitive colorimetric mercury detection and removal in water[88-90]. In this application, ssDNA was specially designed to contain many thymine bases, two of which could bind to Hg^{2+}. In the absence of Hg^{2+}, the hydrogel showed yellow fluorescence, upon addition

of SYBR Green I dye. However, in the presence of Hg^{2+}, the selective biding of Hg^{2+} between two thymine bases induced the formation of a hairpin structure, which allowed the intercalation of SYBR Green I dye into the DNA. Thus, the hydrogel changed from yellow fluorescence to green fluorescence. This sensor was successfully used to detect and remove Hg^{2+} from samples of Lake Ontario water spiked with mercury.

For the purpose of discussion, we distinguish DNA-based hydrogel and DNA hydrogel. In DNA-based hydrogel, DNA adopts a liner topology and serves only as a crosslinking role in the hydrogel formation. Since the function of these DNA is presented by the hybridization of linear DNA, we categorized DNA-based hydrogel in the linear DNA-based bulk materials. In contrast, in the DNA hydrogel, the DNA consists of the scaffold of the material in which DNA is linked with each other to form a three dimensional network structure. Thus, we categorized DNA hydrogel under network topology.

Besides assembling proteins, polymers and nanoscale materials, more recently, Khademhosseini, Yin and coworkers has demonstrated the power of DNA to assemble macroscopic objects[91], furthering proving the capability of DNA as a generic material. Specifically, short DNA strands (48 nt) were first modified with PEG-acylate to introduce crosslinkable group into the DNA. The modified DNA was then copolymerized with PEG diacrylate in square holes, forming 250×250×250 μm hydrogel cubes. The DNA on the surface of the hydrogel was then amplified with rolling circle amplification to produce giant long ssDNAs. When hydrogel cubes carrying complementary giant DNA strands (48 nt) were mixed together, they

assembled into aggregates (Figure 1.6). This giant-DNA-dependent nature of the assembly was further verified by the DNA degradation experiment in which the aggregates became dispersed after DNase treatment, proving the assembly was indeed due to the giant DNA on the hydrogel surface. The DNA assisted assembly of macroscopic hydrogels enable the possibility of creating complex self-assembled macro-structures for diverse biomedical application such as patterned cell culture, controlled cell interactions and tissue engineering. For instance, by encapsulating specific different cells inside each hydrogel, the self-assembled structures could be utilized to build the basic architectures of native tissues[91].

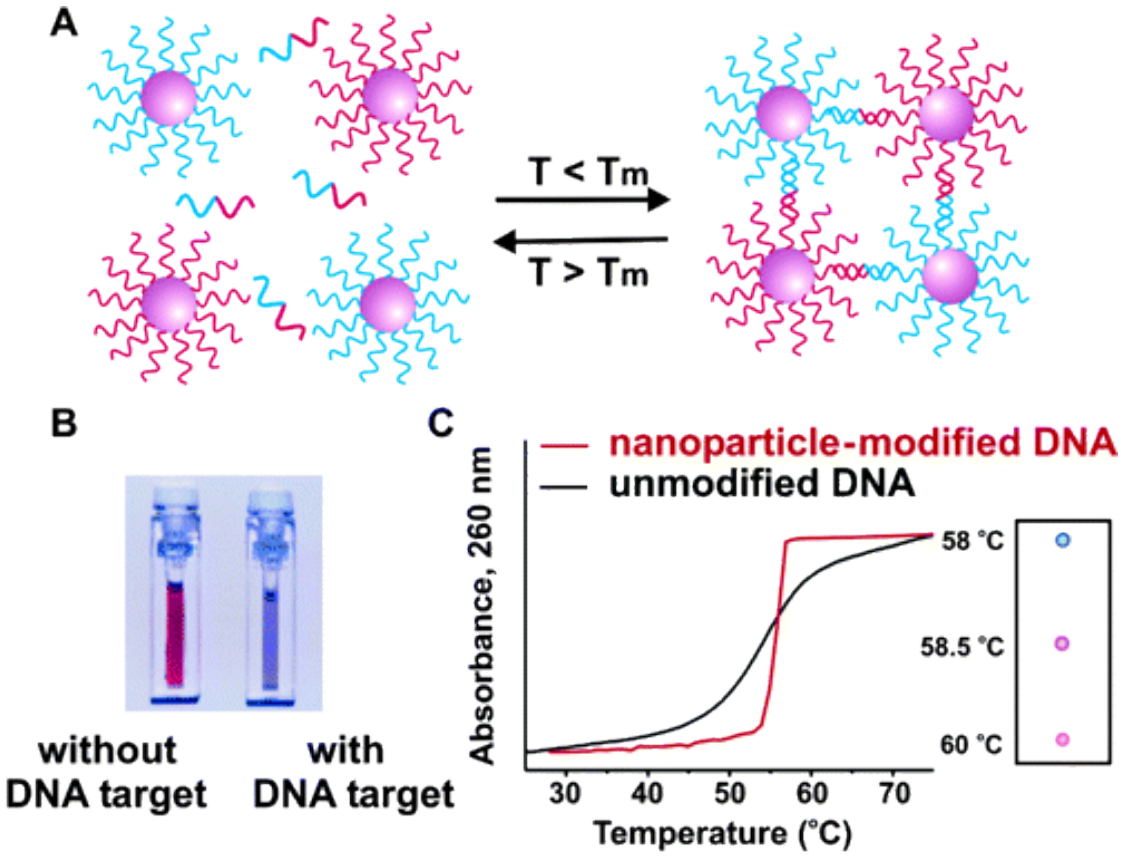

Figure 1.3. DNA functionalized AuNP for highly sensitive and colorimetric DNA detection. AuNPs are first modified with different thiolated ssDNAs. In the presence of complementary target DNA, DNA functionalized AuNPs will form aggregates (A), resulting in a solution color change from red to purple (B). The solution-to-aggregation transition is reversible by controlling the temperature. The aggregates show a sharp melting transition monitored by UV-vis spectroscopy (C). [26, 62]

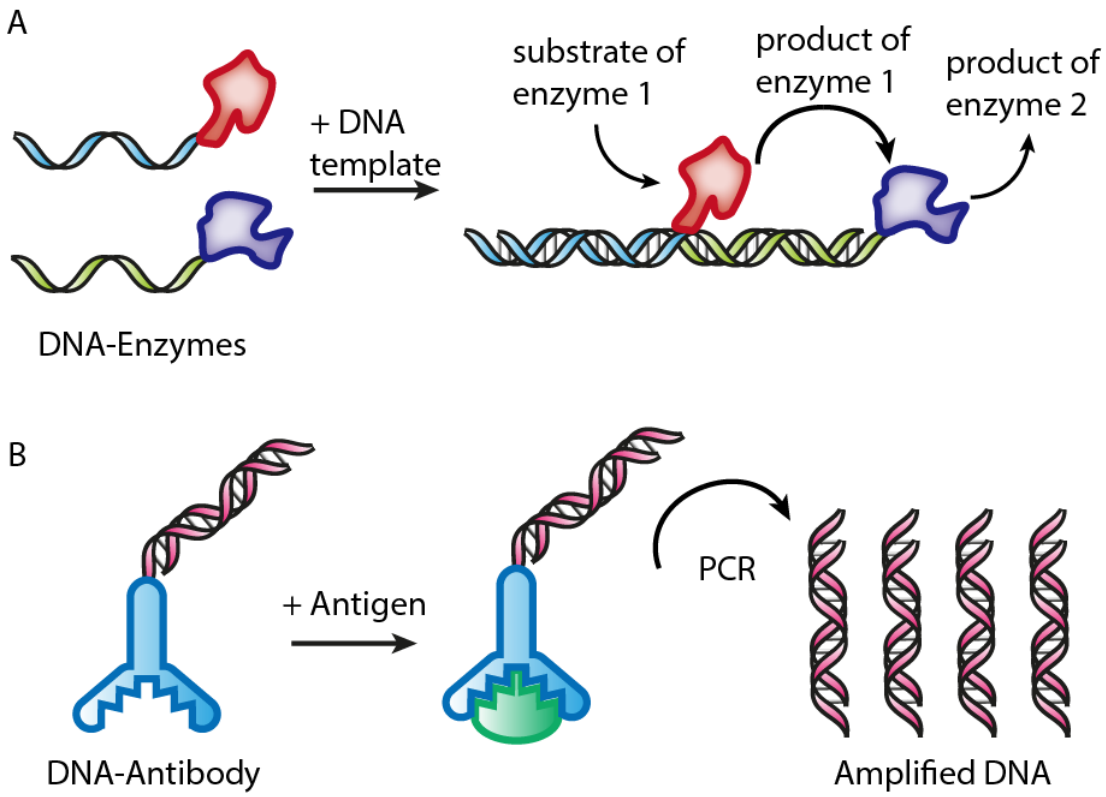

Figure 1.4. Schematic illustration of applications of protein–DNA conjugates. (A) Construction of the artificial multi-enzyme complexes. Two DNA-enzyme hybrids are obtained by conjugating different enzymes to two linear DNA strands. Upon the addition of the DNA template, they are assembled to form the multi-enzyme complexes. Since the product of enzyme 1 serves as the substrate for enzyme 2, the proximity of these two enzymes exhibits a much higher catalytic efficiency compared to a random distribution of enzymes in solution. (B) Immuno-PCR for detection of antigen. The DNA-antibody conjugate specifically recognizes and binds to the target antigen. Then the DNA is greatly amplified by PCR, indicating the presence of antigen and achieving ultra-low detection limit. [2, 9, 73]

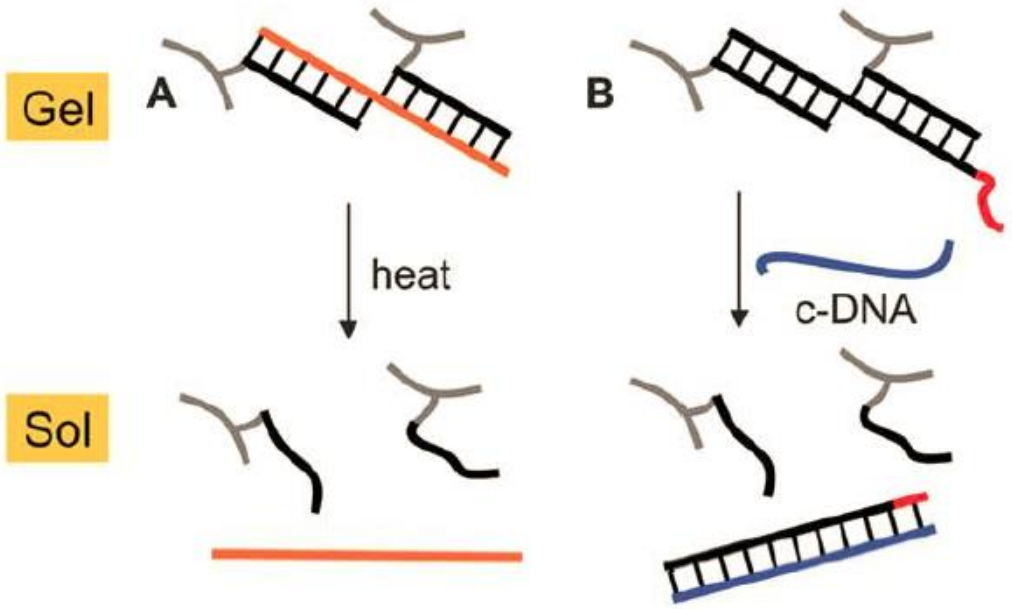

Figure 1.5. Stimuli responsive gel to solution transition of DNA-functionalized hydrogels. ssDNAs are attached to the backbone to polymers to form a DNA-brush polymer. In the presence of a linker DNA, the brush-polymers are brought together to form a DNA-based hydrogel. The hydrogel formation is reversible due to the reversibility of the DNA hybridization. Different stimuli can be used to induce the gel to solution transition. (A) Transition is induced by change of temperature in which the hybridized dsDNA are denatured to adopt ssDNA state. (B) Transition can also be induced by the complementary DNA, which has a higher affinity to the linker DNA strand.[83, 89]

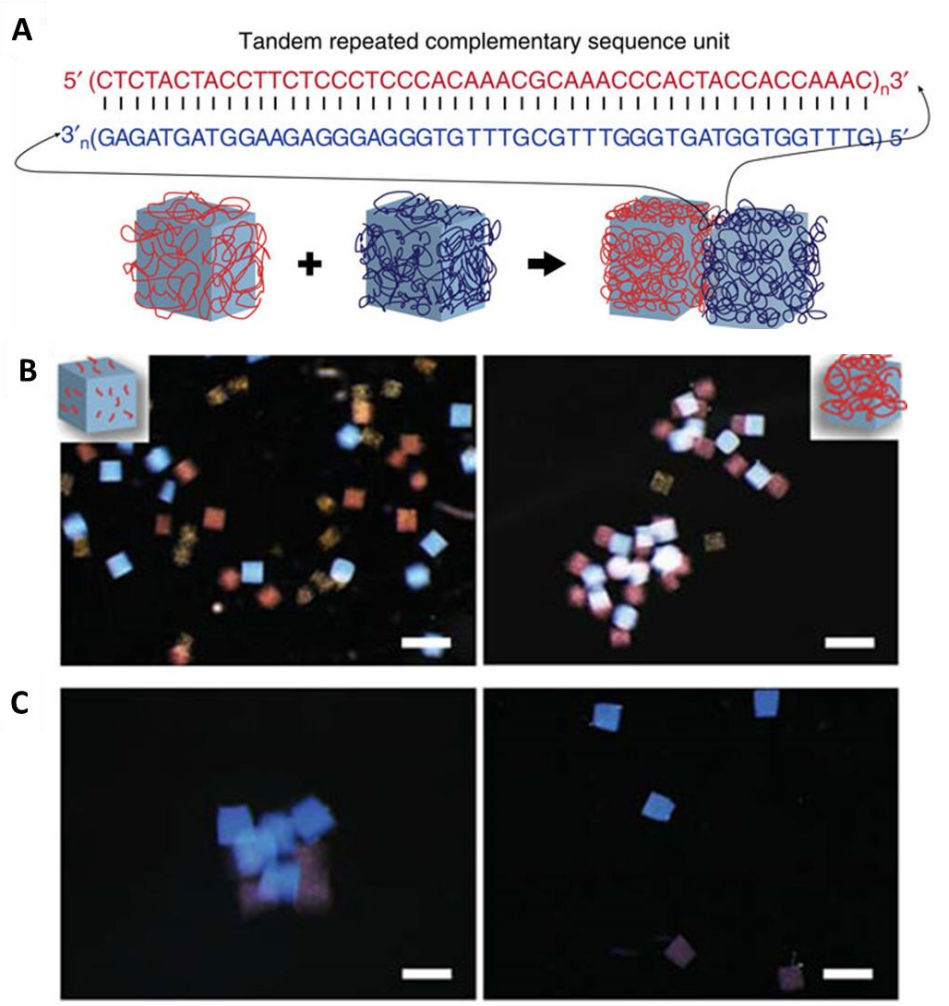

Figure 1.6. DNA guided macroscopic hydrogel assembly. (A). Giant DNA containing tandem repeats of complementary 48-nt sequences was amplified on the surface of red and blue hydrogel cubes. Hybridization between the complementary DNA sequences resulted in the hydrogel assembly. (B). Red and blue hydrogel cubes carrying complementary short DNA strands failed to assemble into aggregates (left), while hydrogels with giant DNA succeeded to do so (right), in the presence of yellow hydrogels that were not modified with DNA. (C) Aggregates assembled from red and blue hydrogels carrying giant DNA fell apart after 1 h DNase treatment (left: before DNase treatment; right: after DNase treatment). Scale bar, 500 μm.[91]

1.3 Branched DNA-based bulk materials and their applications

While promising and widely used, linear DNA is limited by its linear structure and topology as a material building block. To overcome these constraints, branched DNA has been developed. The branched DNA extended the DNA topology from one dimension to two dimensions, bringing many unique advantages that cannot be achieved by linear DNA. For example, branched DNA is inherently multivalent, allowing the design of various functional moieties on different branches. In addition, branched DNA can be engineered to be either isotropic or anisotropic by simply selecting different sticky-ends for each branch. Moreover, hybridization and ligation of branched DNA structure can result more complex 2-D and 3-D DNA structures.

Towards that end, our group developed branched Y-shaped, T-shaped and X-shaped DNA structures[92]. More specifically, Y-shaped DNA was achieved by designing three ssDNAs (Ya, Yb and Yc) to be partially complementary to each other. When those ssDNAs were mixed with equal moles, they recognized each other and assembled into a Y-shaped DNA (Y-DNA) with close to 100 % yield (Figure 1.7). T-shaped and X-shaped DNA were also synthesized in a similar manner. In order to achieve a higher-generation branched DNA structure, sticky ends, which are the single-stranded overhangs at the ends of dsDNA, are designed to each arm of the Y-DNA. An important concept for sticky ends design is palindromic *versus* non-palindromic sequences. Palindromic sticky ends contain the same 5' to 3' sequence as their complementary DNA sequences. For instance, 5'-GAATTC-3' has the exact same sequence as its complementary strand, which is 5'-GAATTC-3', thus allowing for self-hybridization. On the other hand, non-palindromic sticky ends are not self-

complementary, inhibiting the formation of the self-hybridized structure. To better control the branched DNA structure, non-palindromic sticky ends were chose for the core Y-DNA (G0). Another three peripheral Y-DNAs, which had a complementary sticky end to the core Y-DNA, were ligated to the core to form the first generation of dendrimer-like DNA (DL-DNA, G1). Similarly, higher generation structures were produced by repeatedly ligating peripheral Y-DNAs to the previous generation (Figrure 1.7).

The DL-DNA possesses the advantages of traditional chemical dendrimers, such as tunable size, diverse architecture, and availability of multiple surface groups (multivalency), which can be achieved by altering the composition and length of the individual Y-DNA building blocks comprising the DL-DNA. In fact, the fine tunability on the size of DL-DNA in the nanoscale has been utilized to reveal structural requirements for IgE receptor signaling in mast cells[93]. More importantly, the synthesis of DL-DNA was catalyzed by the T4 ligase enzyme, giving close to 100 % yield, which enabled to create the DL-DNA in bulk scale. In addition, DL-DNA spans a greater range of diameters than traditional dendrimers. For example, DL-DNA can reach a size of 50 nm in the second generation, while PAMAM dendrimers can only reach 11 nm in the ninth generation[94]. This dendrimer structure and broad size range can greatly enhance the DL-DNA diffusion speed and facilitate endocytosis by cells[95]. Moreover, the degraded products of the DNA are nucleotides, which are naturally occurring metabolites in the body-rendering the DL-DNA non-toxic and biocompatible. These properties render the DL-DNA a superior candidate for biomedical applications.

Indeed, the DL-DNA structure has been successfully utilized for biomedical applications such as multiplexed diagnosis[96-98], vaccine and drug delivery[93, 99-101]. In particular, our lab reported a DL-DNA based fluorescence nanobarcode for multiplexed detection of pathogen DNA[96, 102]. The nanobarcode consisted of first generation DL-DNA with varying modified branches, each labeled with unique fluorescence dyes (green or red) or molecular probes (Figure 1.8). By controlling the number of the green/red fluorescent dyes, multi-colored nanobarcodes were created, allowing multiplexed detection of different bacterial pathogen DNAs simultaneously. We demonstrated that the DNA nanobarcodes were able to simultaneously detect four different pathogen DNA (i.e. *Bacillus anthracis*, *Francisella tularensis*, Ebola virus and the severe acute respiratory syndrome (SARS) coronavirus) with attomole sensitivity in less than a minute. The results demonstrated that the DL-DNA can be used as both structure scaffolds and functional diagnostic probes.

More recently, the DNA barcode has been extended from a DNA detection system to a universal protein detection system[103]. Specifically, a universal adapter was first created by conjugating a linear DNA strand with an Ezz protein domain. The universal adapter can interface between IgG antibodies and DNA dendrimer-based reporters. The IgG antibody detects specific antigen, while the DNA dendrimer reporter reveals the detection signal. As a demonstration of the capability, multiple proteins were detected with labeled dendrimer DNA reporters, including fluorescent dyes, quantum dots and horseradish peroxidase enzyme. This universal protein detection system permits multiplexed protein detection with multiple reporters, further revealing the modularity and high capacity of the DL-DNA.

Multifunctional dendrimers are powerful materials for real-world applications, because they can build different functional moieties into a single entity[104]. However, it is extremely complicated and difficult to synthesize anisotropic dendrider structure to achieve multi-functions[104]. Branched DNA can easily overcome this limitation by virtue of simply designing different sticky ends to each DNA branch. In light of this, we created an anisotropic branched crosslinkable (ABC) monomer by using the anisotropicity of branched DNA[97]. The ABC monomer was prepared by linking Y-DNA with different functional moieties (modules) to the core X-DNA (Figure 1.9). The modules can be tracers (fluorescent dyes, quantum dots or gold nanoparticles), sensors (ssDNA molecular probes), effectors (therapeutic small interfering RNA, siRNA, or small molecular drugs) or chemical linkers (photocrosslinkable groups). As formed ABC monomer possess multi-functions including pathogen detection, multiplexed drug delivery and therapy. For instance, when the sensor module was designed into the ABC monomer, it served as a detection platform. In the presence of target pathogen DNA, two ABC monomers with the complementary sensing sequences were brought together, initiating the photopolymerization under UV light. This pathogen-driven polymerization was used to detect SARS, Ebola and Anthrax simultaneously[97]. On the hand, when the effector module was designed into the ABC monomer, it served as a multiplexed drug delivery platform[105]. Other applications such as imaging can be achieved if imaging reagents such as quantum dots, fluorescent dyes or carbon nanotubes is introduced into the anisotropic structure. These results indicated that the capability and versatility of branched DNA structure for real-world applications.

In addition to diagnostics, the branched DNA structure has been successfully employed to enhance the therapeutic effect of DNA drugs[99, 100]. Similar to the gene sequence that encodes protein information, some special DNA sequences can encode immunological information. For example, CpG motif with the sequence of 5'-GACGTT-3' has immunostimulatory effects[106-109], while other sequence motif such as 5'-TTAGGG-3' has immunosuppressive therapeutic potentials[110-112]. Thus, the DNA molecule itself can be used as an immune-modulator for DNA vaccine and DNA drugs. However, the potency of linear DNA is very limited. Takakura, Nishikawa and co-workers[99] has designed to CpG motif into the DL-DNA structure to enhance its potency. Their results showed that much higher immune response was triggered compared to the linear DNA with the same dose of CpG motif, suggesting that the DL-DNA structure contributed to the immunostimulatory enhancement. Other motifs such as 5'-TTAGGG-3' which has immunosuppressive function can also be imaged to be designed into the DL-DNA to create novel DNA drugs with higher potency against autoimmune disease such as multiple sclerosis and inflammatory arthritis.

Since DNA can be easily degraded by nuclease, it can also be used as a sacrificial template to assist the synthesis of other functional materials. In light of this property, Lu and coworker created novel enzyme nanocomplexes with superior catalytic efficiency[113]. Exemplified by the synthesis of a triple-enzyme nanocomplex, the inhibitors of these three enzymes were first conjugated to different branches of X-DNA. Those three different enzymes were then mixed with the X-DNA to form the triple-enzyme complex. Subsequent *in situ* polymerization led to the formation of a polymer shell around the enzyme complex. Finally, remover of the X-DNA-inhibitor

scaffold by nucleases resulted in a highly robust enzyme complexes colocalized in a polymer shell (Figure 1.10). Such a close proximity of those enzymes enabled active transport of the reaction intermediates among the enzymes, leading to significantly enhanced catalytic efficiency. In addition, encapsulating those enzymes within the polymer shell effectively stabilized them in a non-physiological environment and protected them against protease degradation. Furthermore, the polymer shell can be easily modified to introduce other functions such as desired surface properties and targeting capability[113]. Interestingly, the enzyme complex containing alcohol oxidase and catalase effectively reduced blood alcohol levels in intoxicated mice, creating a novel antidote and prophylactic for alcohol intoxication.

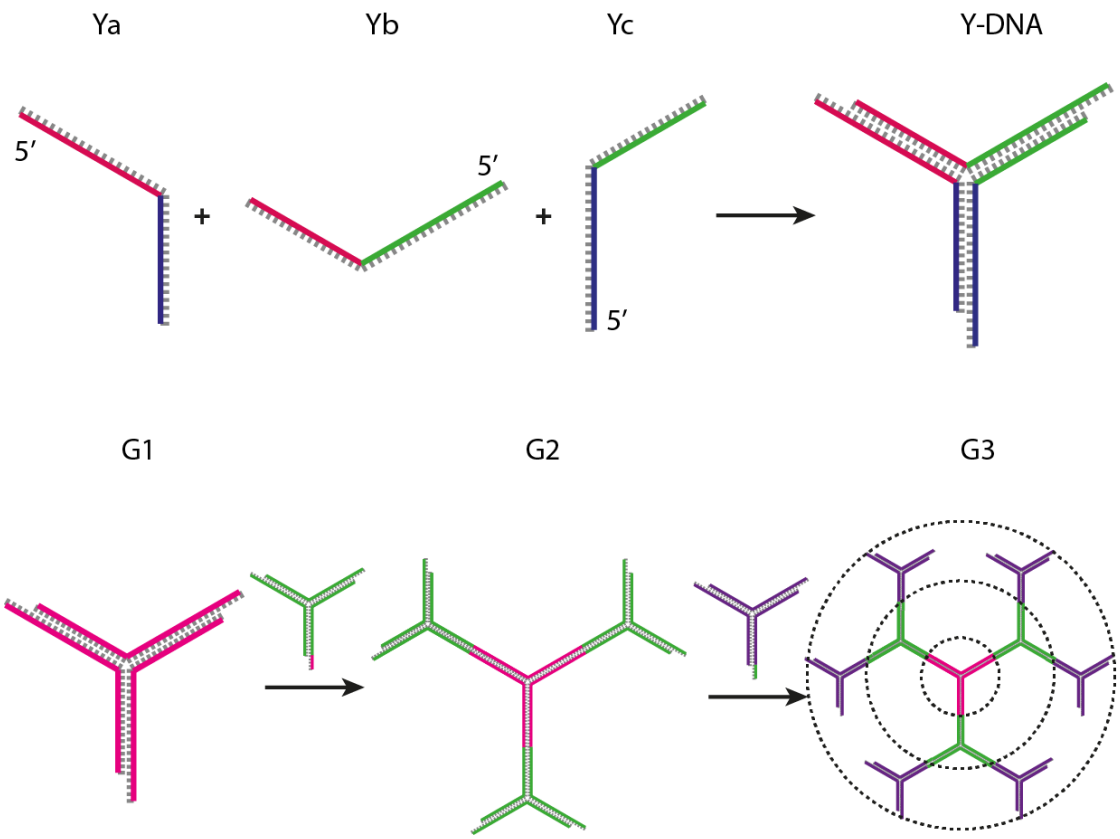

Figure 1.7. Schematic illustration of dendrimer-like DNA formation. Three partially complementary ssDNA (Ya, Yb & Yc) recognized and hybridized with each other to form the Y-shaped DNA (G0). By designing the sticky ends at the core G0 to be non-palindromic, peripheral Y-DNA was added to the core in a controlled fashion to form the dendrimer-DNA (G1), through DNA hybridization and ligation. In a similar manner, higher generations of dendrimer-DNA were obtained.[92]

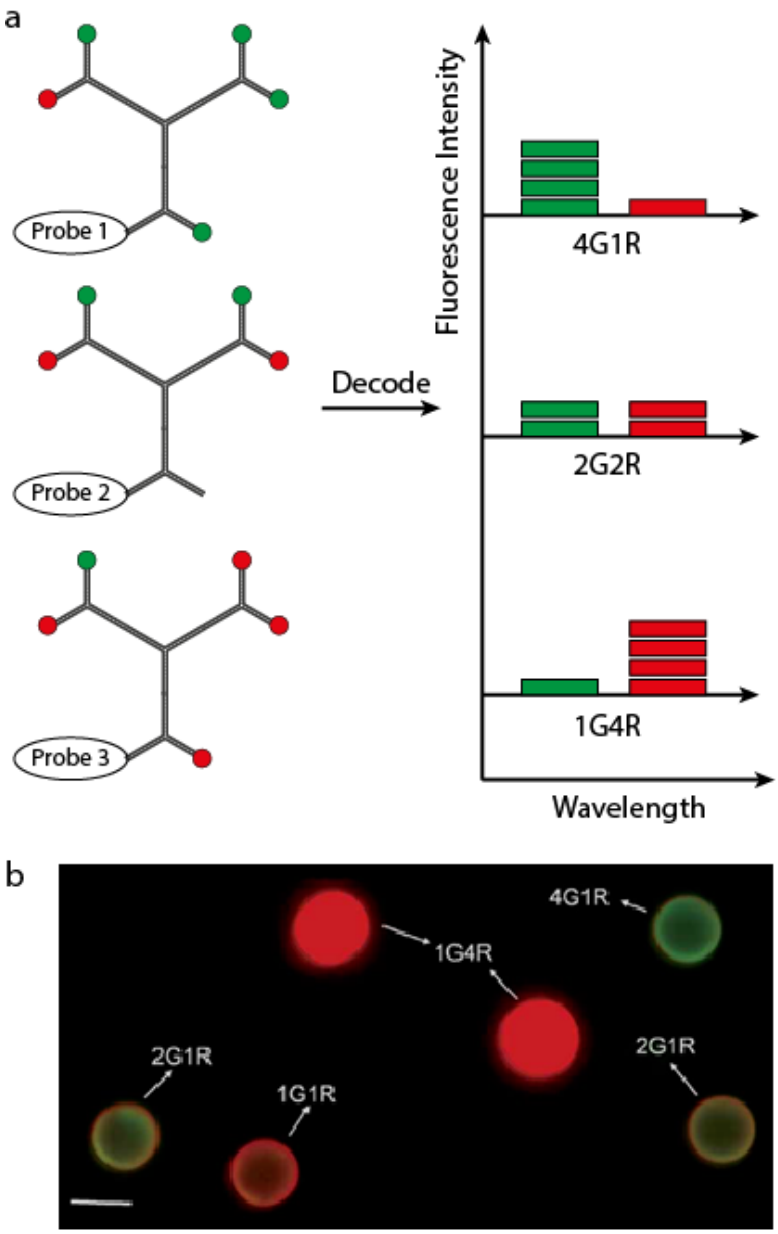

Figure 1.8. DNA barcode for multiplexed pathogen detection. The nanobarcodes with different detection probes were decoded based on the ratio of fluorescence intensity (**a**, G = green and R = red). Multiple target detection (a total of four targets) was achieved using nanobarcodes and microbeads (**b**, scale bar, 5 μm).[96]

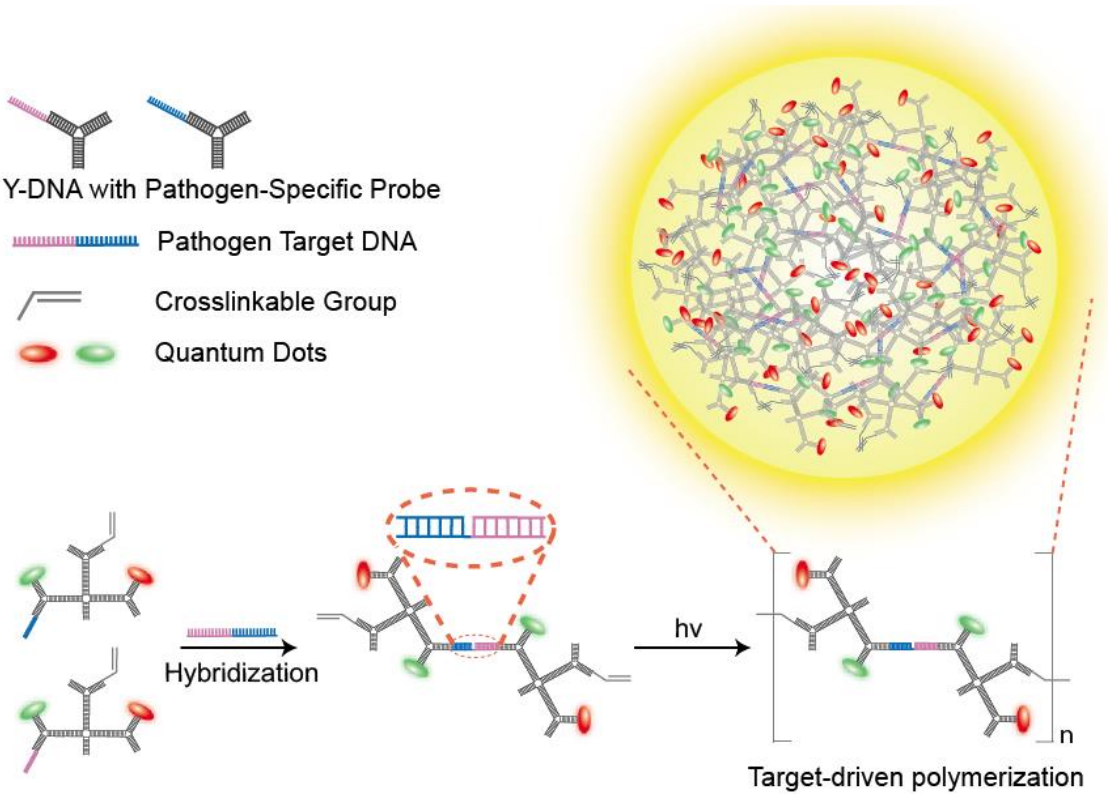

Figure 1.9. Schematic illustration of target-driven polymerization for pathogen detection. Different functional moieties were introduced to the Y-DNA, which included pathogen target DNA, corsslinkable group and quantum dots. These Y-DNAs were linked to the specific arms of X-DNA through pre-designed sticky ends, to form the anisotropic branched crosslinkable (ABC) monomer. In the presence of pathogen DNA, two ABC monomers were brought together by the DNA hybridization. The hybridized DNA was then photopolymerized in UV light to form aggregates, which enabled multiplexed pathogen detection.[97]

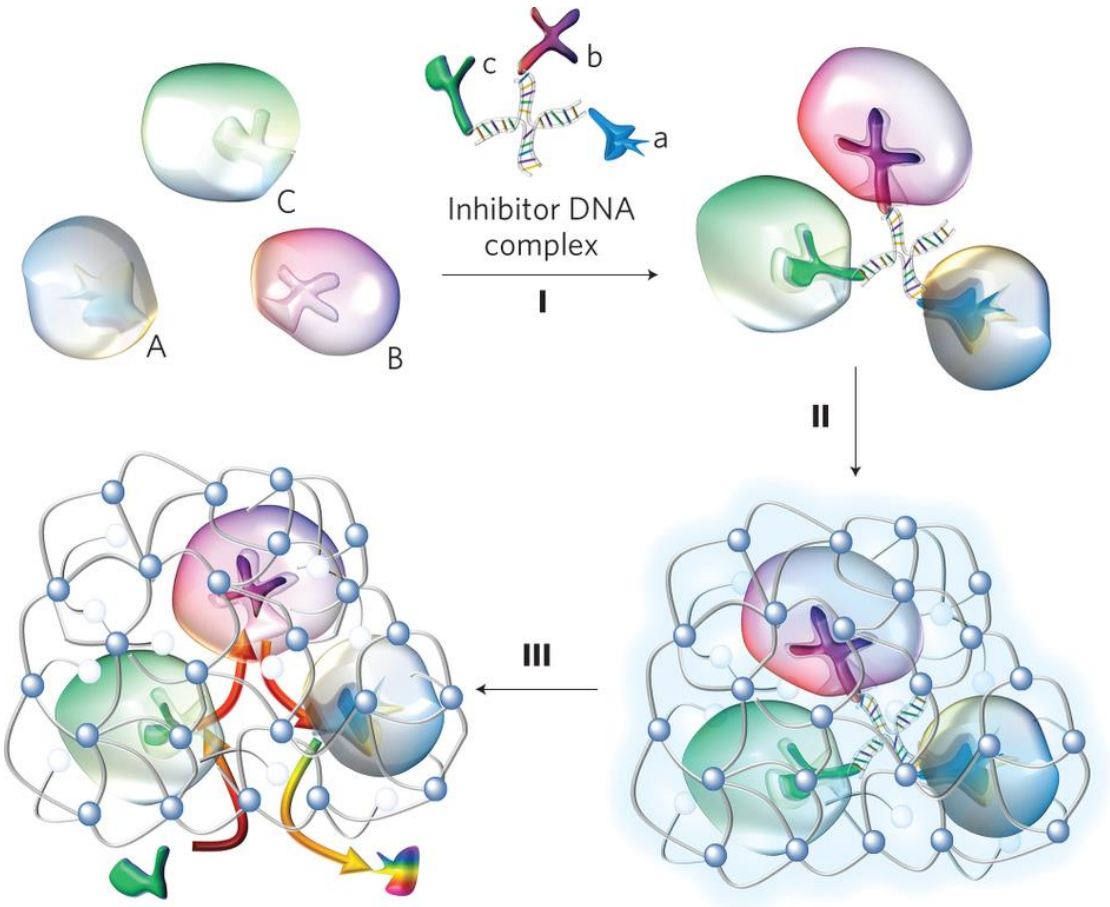

Figure 1.10. Schematic illustration of the synthesis of a triple-enzyme complex. Spontaneous assembly of invertase (A), glucose oxidase (B) and horseradish peroxidase (C) with an inhibitor-DNA scaffold containing their respective competitive inhibitors, lactobionic acid (a), glucosamine (b) and 4-dimethylaminoantipyrine (c), leading to the formation of a X-DNA triple-enzyme structure (I). *in situ* polymerization resulted a thin polymer shell around the enzyme complex (II). Removal of the DNA scaffold by nucleases leading to the formation of triple-enzyme complexes with significantly enhanced stability and catalytic activity.[113]

1.4 Networked DNA-based bulk materials and their applications

Hydrogel is inherently a bulk-scale material, which has tremendous biomedical applications including drug delivery[114-120], cell encapsulation[120-124], 3-D cell culture[123-126] and tissue engineering[114, 124, 125, 127-137]. DNA, a superb naturally born biocompatible and biodegradable biomaterial, however, had limited demonstrations in these promising applications. The main hurdle is the challenge of synthesizing DNA materials in bulk-scale.

Toward that end, our group pioneered in extending the 2-D branched DNA topology to create a 3-D networked DNA hydrogel[138]. By using branched DNA (X-shaped, T-shaped, and Y-shaped DNA), we demonstrated a bulk-scale hydrogel entirely from DNA for the first time. The branched DNA were designed to have the palindromic sticky ends, thus allowing them to self-hybridize and ligate with each other to form a networked structure (Figure 1.11). Unlike conventional hydrogels, the DNA hydrogel gelation process was catalyzed by an enzyme, T4 ligase, which functions in neutral pH, room temperature, physiological relevant salt condition and aqueous environment. This offers the advantage of *in situ* encapsulating of drugs including small molecule drugs and therapeutic proteins, as well as live mammalian cells, eliminating the drug-loading step and also avoiding denaturing conditions. Indeed, without any loading step, we have demonstrated that the DNA hydrogel can successfully encapsulate and culture both Chinese hamster ovarian cells (adherent cells) and Hela S3 cells (floating cells). In addition, since the DNA hydrogel can be degraded by nucleases, it allowed the release of the encapsulated cells/drugs. Moreover, by simply changing the types and concentrations of the branched DNA, the

physical properties such as the modulus and pore size can be easily tuned.

In addition to biomedical applications, the DNA hydrogel has also used in fabricating supercapacitors for energy storage[139], as well as synthesizing ultrasmall AuNP for catalytic applications[140]. DNA is a naturally occurred polyelectrolyte, which has a negative charge due to the deionization of the phosphate group in the DNA backbone. By taking advantage of this property, Kim and coworkers prepared a capacitor by depositing other polyelectrolyte on top of the DNA hydrogel substrate[139]. Since the DNA hydrogel was formed in the physiological relevant conditions, it enabled the device to utilize physiological fluids as a source of electrolyte, allowing the device to be potentially implanted inside fluid rich organs such as blood vessel and bladder. On the other hand, Murata and coworkers concentrated Au precursors inside the DNA hydrogel, due to the high affinity of DNA base to transition metals[141, 142]. Further reduction of Au^{3+} yielded well dispersed, uniformly distributed and non-aggregated AuNP of 2-3 nm size[140]. Such small AuNP is usually unstable due to the large surface area; however, the DNA hydrogel provides an excellent matrix to prevent the AuNP aggregation. As formed AuNP-DNA hydrogel hybrid showed superior catalytic activity in hydrogenation reaction of nitrophenol to aminophenol.

Instead of using enzyme to chemically crosslink DNA together, Liu and co-workers created another DNA hydrogel based on DNA molecular recognition[143]. Rather than designing palindromic sticky ends to the Y-DNA structure, they introduced i-motif, a cytosine-rich sequence, to the end of Y-DNA. At high pH values (pH > 8), the i-motifs are unprotonated, resulting the Y-DNA to electrostatically repel each other. When the pH value is adjusted to slightly acidic, the i-motifs become

partially protonated, which lead to the formation of hydrogen bond between protonated and unprotonated cytosines[144]. As formed hydrogen bond will cause the interlocking of the i-motifs among Y-DNAs and result the formation of a DNA hydrogel within minutes (Figure 1.12). The fast transformation of the i-motifs enables the DNA hydrogel to quickly release cargos such as gold nanoparticles upon the change of the environmental pH. More recently, they have developed another type of DNA hydrogel with thermal and enzymatic responsiveness from pure DNA self-assembly[145]. In this design, they produced Y-DNA with 8 bp non-palindromic sticky ends, and a dsDNA linker with 8 bp complementary sticky ends. When the Y-DNA was mixed with the dsDNA, they spontaneously assembled into a networked structure to form a hydrogel. Since the hydrogel is not covalently crosslinked, it can transit from a gel state to a sol state when the temperature is above the melting temperature of the 8 bp sticky ends. Indeed, they demonstrated that the gel switched between gel and sol state when changing the temperature from 25 to 50 °C, and this process was cycled many times. More interestingly, by designing enzymatic cutting site into the dsDNA linker, the hydrogel was also responsive to enzymatic manipulation, exhibiting a gel-sol transition.

The responsive feature of the DNA hydrogel to exploited as a smart material to envelop and release single cells[146]. Trapping and sealing single cells in microwells are very useful to generate cell array for single cell analysis. Traditional sealing materials such as glass[147] and polydimethylsiloxane (PDMS)[148] fail to provide a permeable environment for media and oxygen, thus causing negative influence on cell behavior such as cell death. Liu and coworkers utilized the enzymatic responsive DNA

hydrogel to successfully seal and release the cells[146]. The cells were trapped in the microwells. Upon addition of the Y-DNA and the dsDNA linker, a hydrogel was formed spontaneously to seal the microwells. Due to the porous structure of the DNA hydrogel, the cover was permeable leading to a high survival rate of cells enveloped. Interestingly, the hydrogel cover can be opened by a restriction enzyme to cleave the DNA hydrogel, releasing cells on demand.

In a similar fashion to the aforementioned branched-DNA, the DNA hydrogel can also be engineered to contain the immunostimulatory sequence and encapsulate doxorubicin, which functioned as a sustained delivery system for both immunostimulatory CpG motifs and intercalated doxorubicin for cancer treatment[100]. More recently, the molecular recognition properties of the DNA has been used to prepare an injectable, self-gelling, biodegradable and immunomodulatory DNA hydrogel for antigen delivery[149]. The branched-DNA monomers were injected to the mice, and gelation occurred instantaneously following injection at the physiological condition. The *in situ* formed DNA hydrogel can efficiently deliver tumor antigens with higher potency and less toxicity than clinically available vaccine adjuvants.

Besides using DNA as a generic material for diagnostics and therapeutics, we also took advantage of DNA's genetic function, which cannot be achieved by any other material, to create the first ever cell-free protein producing gel (P-gel, Figure 1.13)[150]. The P-gel was composed of X-DNA and linearized plasmids, which were covalently ligated together by T4 ligase. The X-DNA served as the scaffold, while the plasmid functioned for protein production. After incubating with the transcription/translation-related enzymes, amino acids, and ATPs, P-gel produced

proteins in a cell-free environment with an up to 300 fold increase than the current solution-based systems. Such enhanced efficiency was due to fact that the bulk-scale DNA hydrogel format can improve the gene stability, increase local gene concentration and enzyme turnover rate as a result of the closer proximity of genes. Since the P-gel can produce protein in a cell-free fashion, it can generate a greater number of proteins including toxic and membrane proteins than the conventional cell-based protein expression system. The gel-based protein production platform revealed that the complicated transcription and translation processes can be replicated outside the cells in a gel network, indicating that the P-gel can serve as a general protein production technology.

Even though temperature can be used to change the gel state from gel to sol, however, sometimes intact branched DNA structure is desirable at high temperatures, such as PCR. Toward that end, we designed a thermostable branched DNA structure[151], by using psoralen, a naturally occurring reagent that intercalates and cross-links DNA[152]. The psoralen-crosslinked branched DNA structure can withstand denaturing conditions without disruption of their integrity. Thus, the thermostable branched DNA was successfully utilized as primers for PCR, enabling high temperature multiplexed detection. Moreover, by using GFP gene as the PCR template, the gene sequence was amplified and incorporated into the thermostable branched DNA structure to form a protein producing gel. Due to the generality of psoralen crosslinking, this thermostable concept can also be extended to all other DNA based structure.

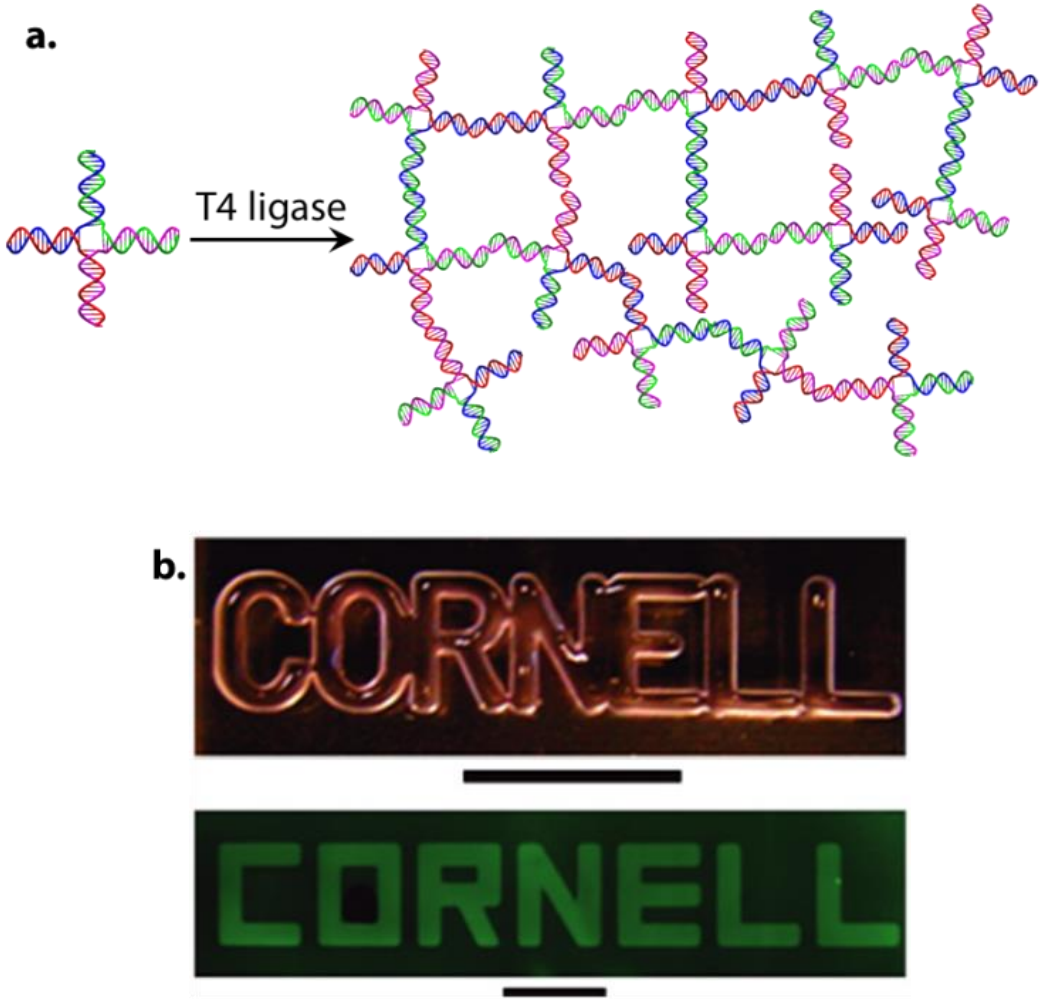

Figure 1.11. Formation of bulk-scale DNA hydrogel. X-DNA with palindromic sticky ends were linked together by the T4 ligase to form the DNA hydrogel (**a**). Photographs of DNA hydrogel patterned into CORNELL shapes (scale bar is 1 cm and 500 um for the top and bottom images, respectively (**b**). The bottom gel was stained with a DNA-specific fluorescent dye: SYBR I).[138]

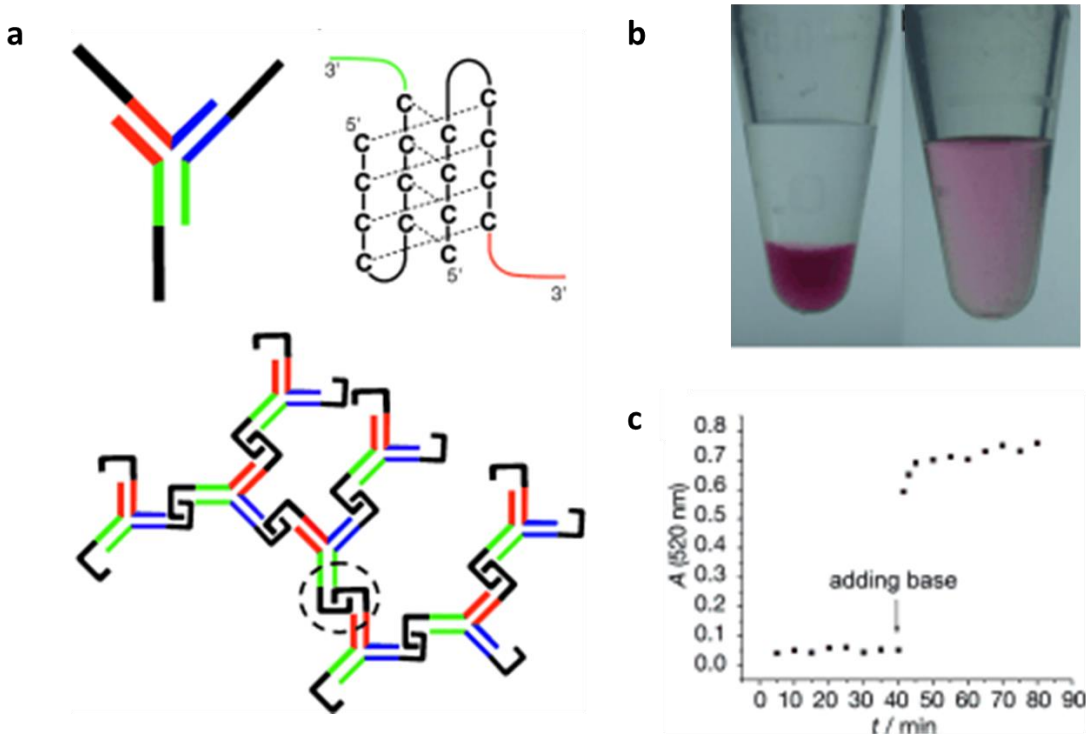

Figure 1.12. Principle structure of the pH-responsive DNA gel. a) A Y-shaped DNA nanostructure with three free interlocking domains (Y unit); b) enlargement of the circled region in (c) to show the formation of inter-Y-unit i motif: two black domains from neighboring DNA Y units form an i motif to cross-link adjacent Y units; c) DNA hydrogel made from the three-dimensional assembly of DNA Y units. The sequences (with different domains in different colors) of the three DNA strands used in the assembly. Gel transition switched by pH change (visualized with GNPs. a) 7 nM GNPs were trapped in DNA hydrogel (40 μL) with a covering layer of 50 mM MES buffer (pH 5.0, 50 mM NaCl). b) After the pH value of the buffer had been changed to pH 8.0, the GNPs were released from the DNA hydrogel to form a uniform solution. c) Time trace of the absorption at 520 nm for the upper part of the solution before and after addition of NaOH.[143]

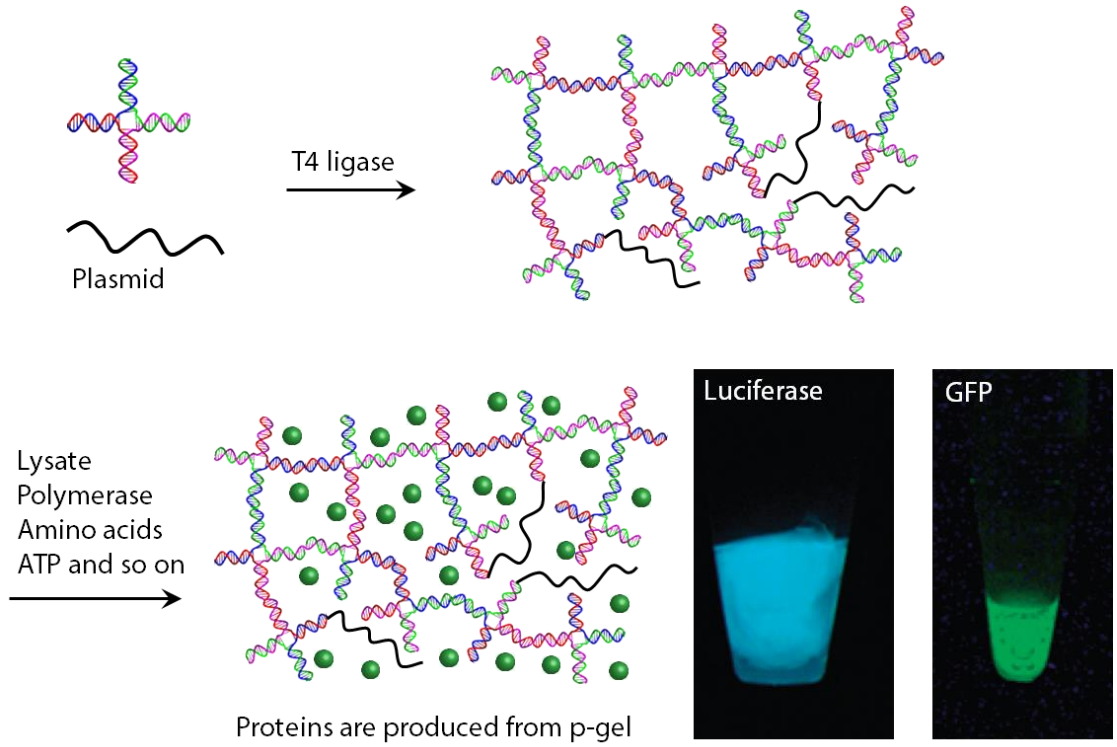

Figure 1.13. Formation of DNA-based, cell-free protein producing gel (P-gel). X-DNA were ligated with the plasmids to form the P-gel. After incubating the P-gel with the transcription and translation related reagents, such as lysate, polymerase, amino acid, ATP and so on, proteins were expressed with high efficiency from the P-gel. The blue color and green color indicated that functional proteins of luciferase and green fluorescent protein were produced from P-gel.[150]

1.5 Significance of this dissertation

Even though extensive efforts has been made in bulk-scale DNA materials and their application, methods for creating bulk-scale DNA materials, especially DNA hydrogels, are still limited. All current methods for producing DNA hydrogels are based on the following processes: forming branched DNA structures and crosslinking them together either by ligation or hybridization. In this dissertation, I will introduce an entirely novel method to create a DNA hydrogel by physical entanglement for the first time. Instead of resorting to branched DNA, I utilize enzymatic amplifications to produce long ssDNAs, both in length and in quantity, and entangle them to form a DNA hydrogel. Due to the power of enzymatic amplification, a bulk-scale hydrogel is produced with low cost and readily to be scaled up. Interestingly, the hydrogel consists of uniformly sized DNA microspheres. Those microspheres can be easily isolated from the hydrogel, and to our surprise, the DNA density in each microsphere reaches as high as the human chromosome density in the metaphase. Such high DNA density enables the DNA microsphere to concentrate unprecedentedly high dose DNA drugs that have never been achieved. This super-condensed ultra-high dose DNA (scudDNA) effectively protects the condensed DNA, efficiently enters the cell and releases the DNA, resulting a superior therapeutic effect.

CHAPTER 2: SYNTHESIS AND CHARACTERIZATION OF A PHYSICALLY ENTANGLED DNA HYDROGEL

2.1 Introduction

DNA hydrogel has shown tremendous potential in biomedical applications. However, the method of synthesizing DNA hydrogel is very limited. From the hydrogel structure perspective, it can be classified into two categories, chemical gel in which the crosslinking points are linked with each other, and physical gel in which the crosslinking points are entangled with each other. All the current methods for producing DNA hydrogels are based on linking the branched DNA structures, either by ligating them[138] or hybridizing them[143, 145] to form a chemical DNA gel. Therefore, developing a novel method to create physically entangled DNA hydrogel can greatly expand the DNA hydrogel reservoir.

To do so, we designed a totally different approach: instead of using branched DNA structures, we elongated linear DNA chains and "wove" them non-covalently into a physical hydrogel via a polymerase. To fabricate the physical DNA hydrogel, we chose a special polymerase: Φ29, a bacteria phage polymerase that was capable of DNA chain elongation and chain displacement, thus amplifying and weaving DNA. Φ29 used a single-stranded DNA (ssDNA) as a template to elongate the primer while at the same time displacing the newly synthesized strands into ssDNA products. Based on Φ29, we designed a unique combination of two sequential processes: (i) a Rolling Circle Amplification (RCA, or R) followed by (ii) a Multi-primed Chain Amplification (MCA, or M).

In more detail, Primer-1 was first hybridized to a circular DNA template. In the presence of Φ29, Primer-1 was elongated using the circular DNA as a template (Figure 2.1). After running the RCA for x hours (hrs), a long ssDNA-1 was generated with the tandem repeats of the circular DNA template sequence. Then excess amount (1000 fold of Primer-1) of Primer-2 and Primer-3 were introduced to the solution to initiate the MCA. Primer-2 had the complementary sequence to the ssDNA-1, while Primer-3 had the same sequence of ssDNA-1. First, a number of Primer-2 was periodically hybridized to the ssDNA-1 and elongated using ssDNA-1 as a template. During this process, old strands, which were previously produced on same ssDNA-1, were displaced by the advancing new strand. This newly displaced ssDNA became a new template, ssDNA-2. Then a number of Primer-3 was hybridized to ssDNA-2. In a similar fashion, Primer-3 was elongated and displaced by the polymerase to generate ssDNA-3. Since ssDNA-3 possessed the same sequence repeats as ssDNA-1, it can be utilized as a template for Primer-1 again. Thus, a chain reaction was established and large amounts of ssDNA-1 and ssDNA-2 were generated. Since the RCA and MCA products were very long (greater than 46 milliion Da[153]), and since the produced ssDNA-1 was complementary to ssDNA-2, these long and linear DNA chains would entangle together as well as hybridize to each other at multiple points, resulting in entangling the whole system into a gel-state[154] (Figure 2.1). To the best of our knowledge, this is the first time that a DNA hydrogel is synthesized by physical entanglement, and from a pure enzymatic amplification process.

Interestingly, our DNA hydrogel had properties that were not found in nature of any kind: it had both solid-like and liquid-like properties. When the gel was

immersed in water, it memorized its original shape and behaved like a solid. However, the hydrogel became free-flowing “liquid” when taken out of water, and went back to its original shape upon re-introducing water. The whole process of gel-to-liquid transition can be repeated many times and were triggered by simply adding or removing water. The unusual properties were further examined by the unique internal structure of the hydrogel, as well as the mechanical stresses applied to the hydrogel. As a potential application for the liquid-like and solid-like behavior, we utilized the hydrogel to create an electric circuit that used water as a switch.

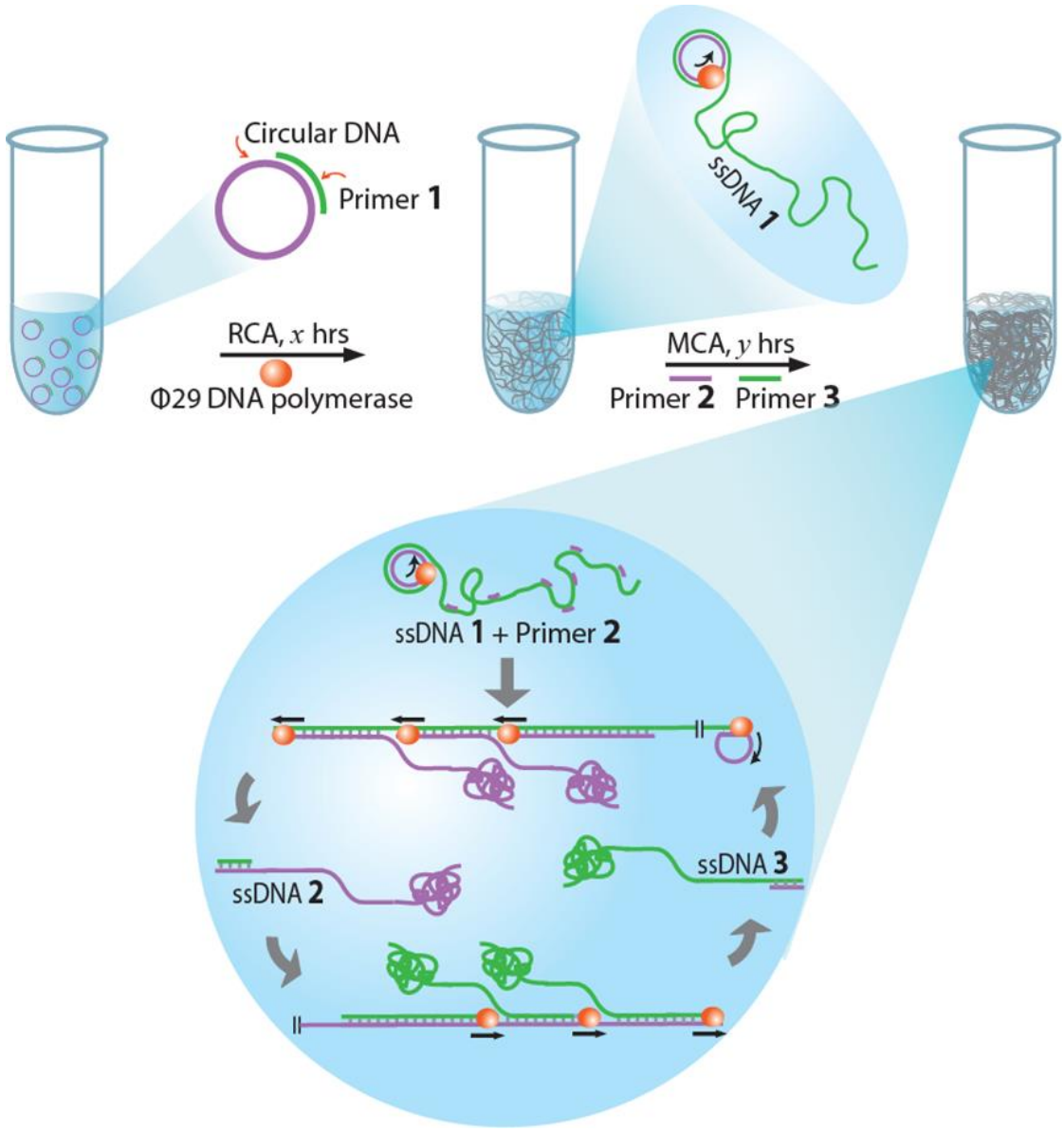

Figure 2.1. Schematic diagram of step-wise approach for the physically entangled DNA hydrogel synthesis. The RCA and MCA processes were carried out as follows. (i) For the R-process: a circular ssDNA template was first produced and then a complementary primer for RCA (Primer-1) was added, which produced elongated ssDNA products (termed as ssDNA-1: tandem repeats of the sequences that was complementary to the original circular ssDNA template). (ii) For the **M**-process: after

RCA we added two additional primers (Primers-2 and Primer-3) for subsequent chain amplification: Primer-2 was elongated to generate ssDNA-2 (which was complimentary to ssDNA-1); Primer-3 was used to create ssDNA-3 (which was complementary to ssDNA-2, thus ssDNA-3 and ssDNA-1 had the exact same sequences). As a result, Primer-2 was also able to produce more ssDNA-2 using newly synthesized ssDNA-3 as templates, leading to the chain amplification.[154]

2.2 Materials and Methods

2.2.1 Chemicals and DNA sequences

Φ29 DNA polymerase, Exonuclease I and Exonuclease III were purchased from New England Biolabs (Beverly, MA). CircLigase^{TM} ssDNA Ligase was purchased from Epicentre Biotechnologies (Madison, WI). Oligonucleotides were commercially synthesized and PAGE purified (Integrated DNA Technologies, Coralville, Iowa). Sequences of the oligonucleotides are listed in Table 2.1.

2.2.2 Preparation of circular DNA templates

Phosphorylated linear ssDNA template (0.5 μM) was treated with of CircLigase^{TM} ssDNA Ligase (5 unit/μl) overnight at 65 ºC in 200 μL of reaction buffer (50 μM of ATP, 2.5 mM of $MnCl_2$) to circularize the linear DNA. The ligase was then inactivated by incubating the reaction solution at 80 ºC for 10 min. To remove the non-circularized linear ssDNA template, excess amount of exonucleases (i.e. 300 U of Exonuclease I and 3,000 U of Exonuclease III) were added to the solution. This solution was then incubated at 37 ºC for 3 hrs and denatured at 80 ºC for 40 min to inactivate the exonucleases. YM-10 (10 000 Da molecular weight cutoff) columns were used to purify and concentration the circularized DNA. The formation and purity of the circularized DNA template was examined by 10 % denatured polyacrylamide gel electrophoresis (PAGE) at 600 V at 25 °C for 1 hour with Tris-borate-EDTA buffer (TBE, pH 8.3). The PAGE was stained by SYBR II (Molecular Probes, USA) following the manufacturer's protocol.

2.2.3 Synthesis of DNA hydrogel by DNA polymerization

The circular DNA template was first hybridized with Primer-1 at room temperature for 2 hrs by incubating an equal molar amount of them in TE buffer (pH 8.0, 10mM Tris, 1mM EDTA). Hybridized circular DNA templates (50 nM) were incubated with Φ29 DNA polymerase (1 unit/μl) at 30 °C for x hrs in 100 μl of the reaction buffer (50mM Tris-HCl, 10mM $(NH_4)_2SO_4$, 10 mM $MgCl_2$, 4 mM dithiothreitol, 200 μg/ml bovin serum albumin and 10 - 50 mM dNTP). Primer-2 and Primer-3 (50 μM of each) were then added into the reaction solution to initiate the multi-primed chain reaction y hrs at 30 °C without adding additional reagents.

2.2.4 Characterization of the DNA hydrogel

a. Gel formation process monitoring

The solution for DNA polymerization was first prepared in a 96-well plate without Φ29 DNA polymerase. After Φ29 DNA polymerase was added, optical density (OD) at 600 nm was evaluated by a microplate reader (BioTek Synergy4 Plate Reader, BioTek Instruments, Inc., Winooski, Vermont) every hour at 30 °C for a total duration of 20 hrs.

b. Staining of the DNA hydrogel

The formed DNA hydrogel was stained with GelGreen, a green fluorescent nucleic acid dye designed to stain both dsDNA and ssDNA, at 4 ^{o}C overnight. The stained gel was imaged under UV light at 254 nm.

c. Rheology Test of the DNA hydrogel

A Rheometric Scientific Inc. (RSI) rheometer with parallel cone and plate

fixtures was used to measure the mechanical properties of the DNA hydrogel. 200 μl DNA hydrogel was sandwiched between the cone and plate. A dynamic frequency sweeping mode (from 0.1 to 100 rad/s) was used, with the strain fixed at 50%. The storage modulus and loss modulus of the DNA hydrogel were recorded in real time.

d. Scanning Electron Microscope (SEM) imaging

Zeiss Ultra SEM (Carl Zeiss Inc., Germany) was used to obtain high resolution images of the DNA hydrogel. The DNA hydrogel was placed onto the top of the SEM holder and air dried. The sample was metal-coated with Au/Pd.

e. Focused-Ion Beam

FEI Strata 400 STEM FIB (FEI Company, USA) was used to cut individual DNA microsphere. The DNA microsphere was isolated from the DNA hydrogel and placed onto the top of SEM holder. The sample was metal-coated with Au/Pd. After cutting, the internal structure of the DNA microsphere was observed using SEM.

f. Electrical Property Measurement

To test the capability of DNA hydrogel as an electric circuit switch, gel was first formed in a mold. Gold nanoparticles of 10 nm were doped into the gel during the gelation. The current vs voltage curves were measured using a Keithley 6430 (Keithley Instruments, Inc., USA), both before or after adding water to the DNA hydrogel.

2.3 Results and Discussions

2.3.1 Fabrication of the circularized DNA template

Linear ssDNA before and after circularization was run in 10% denature PAGE gel. A clear band shift was observed for the circularized DNA compared to the linear DNA (Figure 2.2), indicating the successful formation of the circular DNA template. The lower mobility of the circular DNA in the PAGE gel was due to the loss of its free ends after the circularization[155]. In addition, no leftover of linear DNA was presented in the circularized DNA sample, suggesting that the exonucleases had totally removed the unreacted linear DNA template. We emphasized that the purity of the circular DNA template was critical to the DNA hydrogel formation.

2.3.2 Formation of the DNA hydrogel

The enzymatic processes were monitored by the optical density (OD) at 600 nm. For example, when **R**-process was fixed at 4 hrs, the OD increased with the duration of **M**-process (Figure 2.3). After **M**-process reached 16 hrs (i.e., $\mathbf{R}_4\mathbf{M}_{16}$), a totally opaque hydrogel was formed (Figure 2.3). On the other hand, **R**-process itself for as long as 20 hrs ($\mathbf{R}_{20}\mathbf{M}_0$) only produced a viscous solution (Figure 2.3). Moreover, there was no detectable signal for $\mathbf{R}_{20}\mathbf{M}_0$ solution in the rheometer, proving that $\mathbf{R}_{20}\mathbf{M}_0$ was just a liquid. We further examined the gel formation by varying the time combinations of x and y and found that a minimum of x = 2 hrs and y = 16 hrs was required in order to create a DNA hydrogel (Table 2.2). These results indicated that both RCA process, which produced long DNA chains, and MCA process, which initiated chain reaction and generated many long DNA chains, were needed in order to

form a physically entangled DNA hydrogel.

The opaque solution formed at $\mathbf{R}_4\mathbf{M}_{16}$ reaction was confirmed to be a hydrogel, as it maintained its tube shape when immersed in water (Figure 2.4a). We noted that the size of the hydrogel was easily produced at centimeter scale and can be readily scaled up. As expected, this hydrogel emitted green fluorescence after staining with a DNA-specific dye GelGreen (Figure 2.4b), indicating that the entire hydrogel was composed of DNA. Rheology data further confirmed that the $\mathbf{R}_4\mathbf{M}_{16}$ was a true gel since the shear-storage modulus (G', representing the elasticity) was constantly higher than the shear-loss modulus (G'', representing the viscosity) over the entire frequency range (Figure 2.4c).

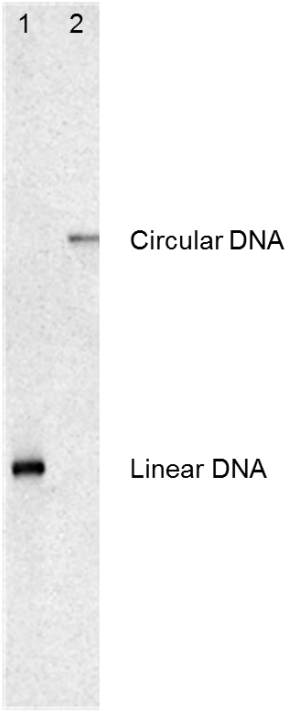

Figure 2.2. Gel electrophoresis image of linear and circular DNA template. Lane 2 indicated circular template DNA which showed slower mobility than linear DNA (Lane 1) after circularization.[154]

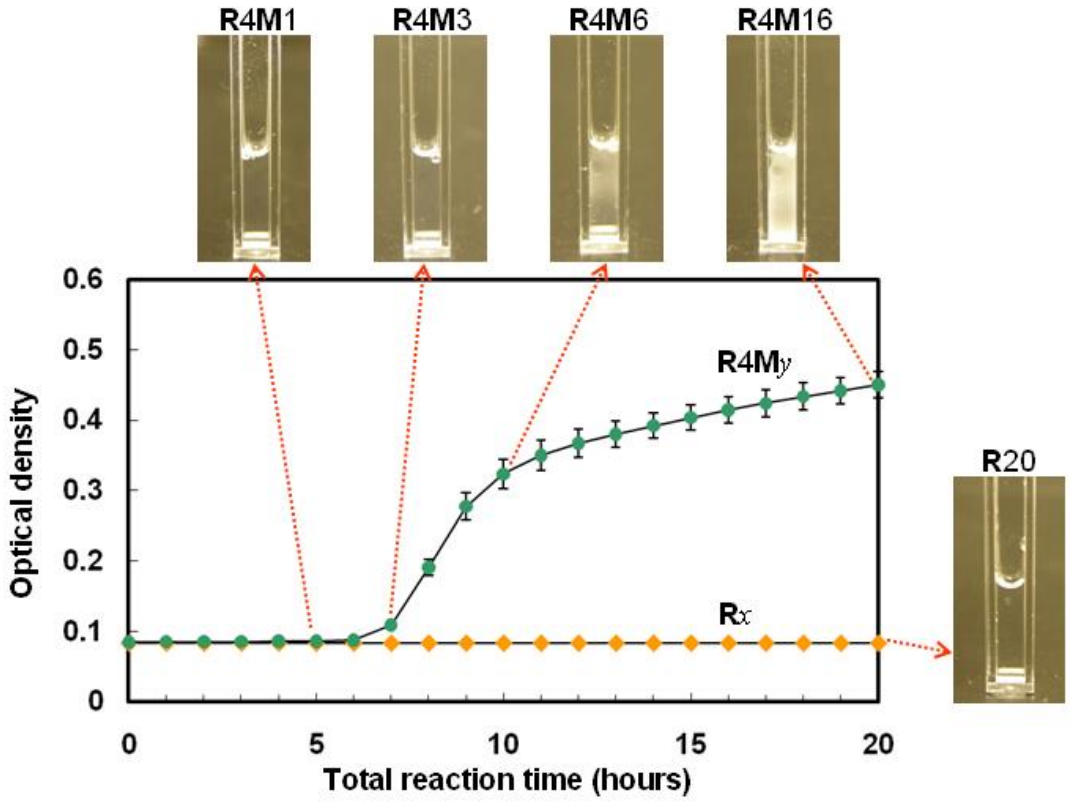

Figure 2.3. Monitoring the gel formation by optical density. OD of only RCA up to 20 h without MCA (●, R_x) and 4 h RCA with MCA up to 16 h (●, R_4M_y) were measured at a wavelength of 600 nm. Photographs of the cuvette containing R_4M_1, R_4M_3, R_4M_6, and R_4M_{16} showed clear visual changes of the gel going from transparent to opaque. However, R_x remained transparent up to 20 h.[154]

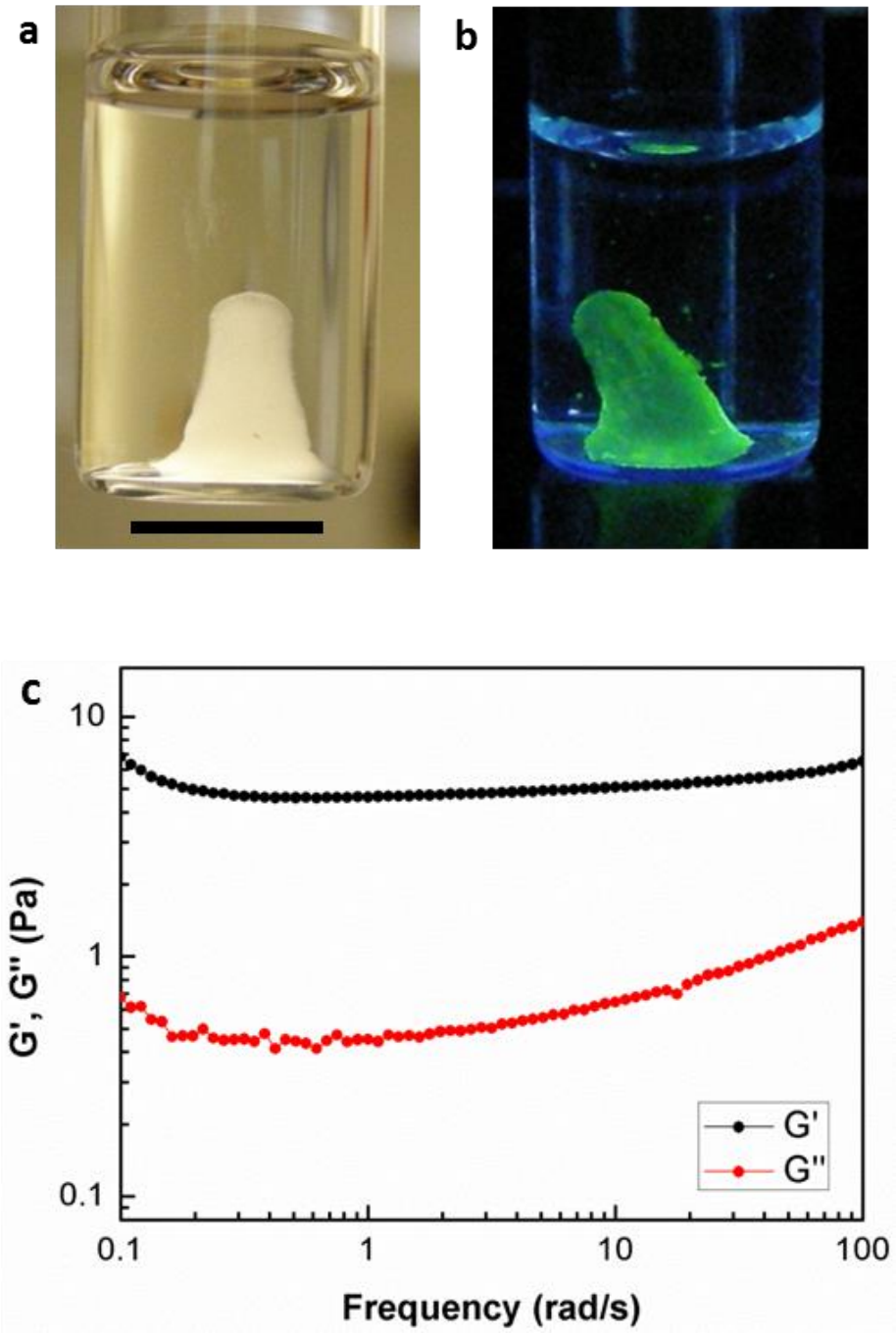

Figure 2.4. Characterization of the R_4M_{16} DNA hydrogel. a. Photograph of R_4M_{16} hydrogel. The scale bar is 10 mm. **b**. Stained hydrogels with GelGreen, a DNA specific dye. **c**. Storage (G') and shear loss (G'') modulus of $\mathbf{R_4M_{16}}$ hydrogel from a Rheometer measurement.[154]

2.3.3 Unique internal structures of the DNA hydrogel

Unlike conventional hydrogels, whose internal structures are amphorous[138, 150, 156], our $\mathbf{R}_4\mathbf{M}_{16}$ hydrogel had strikingly unique hierarchical internal structures, indicated by the field emission scanning electron microscopy (FE-SEM). At the micro-scale, DNA microspheres were densely packed in the hydrogel (Figure 2.5a). These unique microspheres had uniform size (1.6 μm ± 0.2 μm) and wove together by DNA. Within each microsphere, internal porous nanostructures were observed by cutting the DNA microsphere into half via focused ion beam (Figure 2.5 b-c). To the best of our knowledge, this type of hierarchical structure has never been seen before in conventional hydrogel, and may contribute to its unique properties.

We further selectively tuned the hierarchical structures by simply changing the reaction time of **R** and **M** separately. More specifically, by elongating the **R**-process from 0 hrs to 8 hrs, while keeping the **M**-process constant at 16 hrs (i.e., $\mathbf{R}_0\mathbf{M}_{16}$, $\mathbf{R}_1\mathbf{M}_{16}$, $\mathbf{R}_2\mathbf{M}_{16}$, $\mathbf{R}_4\mathbf{M}_{16}$ and $\mathbf{R}_8\mathbf{M}_{16}$), we obtained denser populated DNA microsphere with almost identical size (Figure 2.5 d-h, from 10 ± 2/100 μm^2 in $\mathbf{R}_0\mathbf{M}_{16}$ to 35 ± 5/100 μm^2 in $\mathbf{R}_8\mathbf{M}_{16}$). On the other hand, by increasing the **M**-process reaction time from 1 hr to 16 hrs, while keeping **R**-process constant at 4 hrs (i.e., $\mathbf{R}_4\mathbf{M}_1$, $\mathbf{R}_4\mathbf{M}_3$, $\mathbf{R}_4\mathbf{M}_6$, and $\mathbf{R}_4\mathbf{M}_{16}$), we produced a more developed DNA microspheres (Figure 2.6 a-d). The diameter of the DNA microsphere increased from ~ 0.3 μm in $\mathbf{R}_4\mathbf{M}_1$ to ~ 1.6 μm in $\mathbf{R}_4\mathbf{M}_{16}$. We emphasize that these differently tuned hierarchical internal structures were easily accomplished by designing and controlling the enzymatic reactions of $\mathbf{R}_x\mathbf{M}_y$.

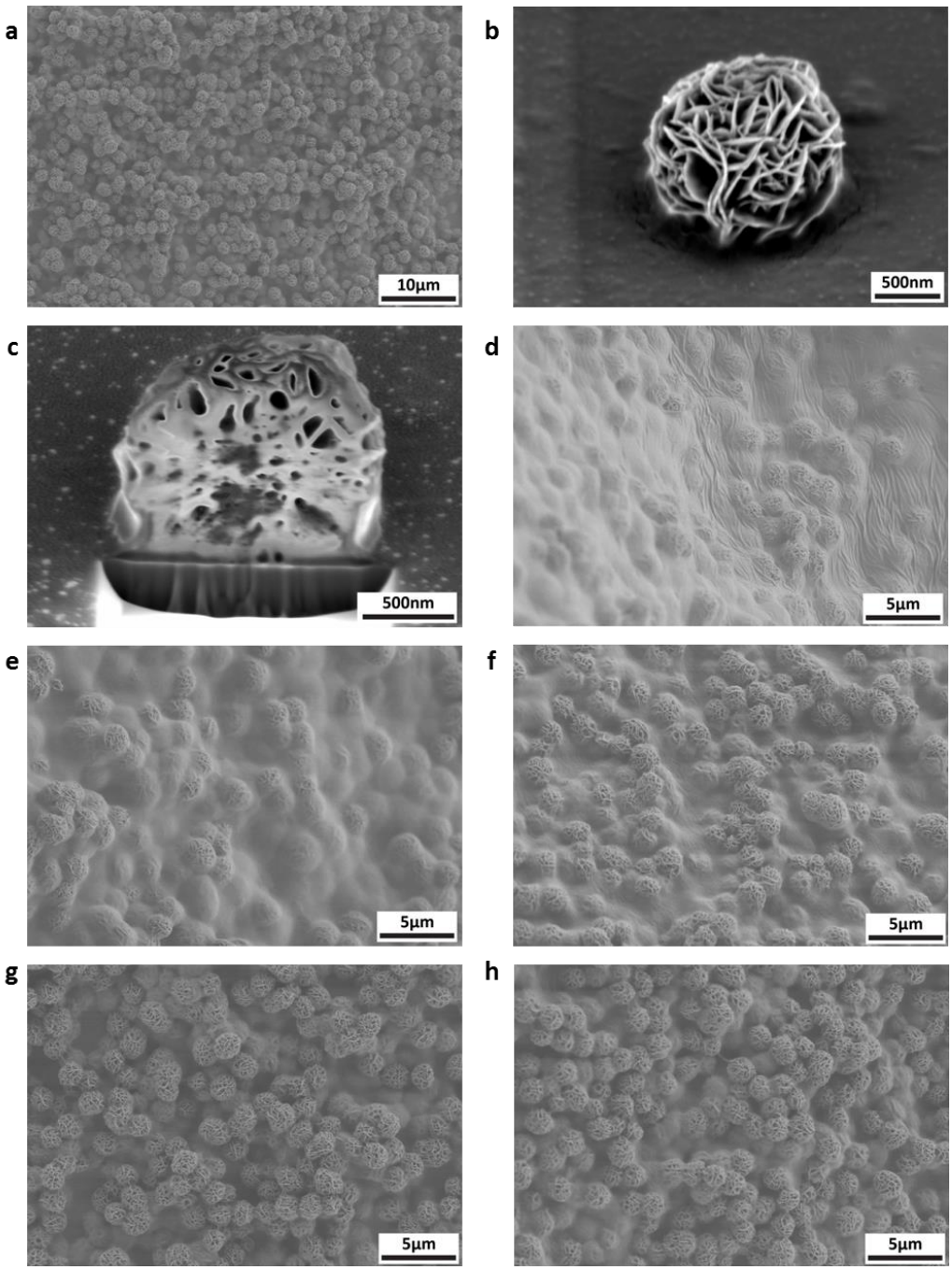

Figure 2.5. Morphology of the DNA hydrogel with different RCA-process time. a, SEM images of R_4M_{16} DNA hydrogel. b,c, SEM images of an individual microsphere that was isolated (**b**), and cut with focused ion beam (**c**). **d-h,** SEM images for different RCA time: $\mathbf{R_0M_{16}}$ (**d**), $\mathbf{R_1M_{16}}$ (**e**), $\mathbf{R_2M_{16}}$ (**f**), $\mathbf{R_4M_{16}}$ (**g**) and $\mathbf{R_8M_{16}}$ (**h**).[154]

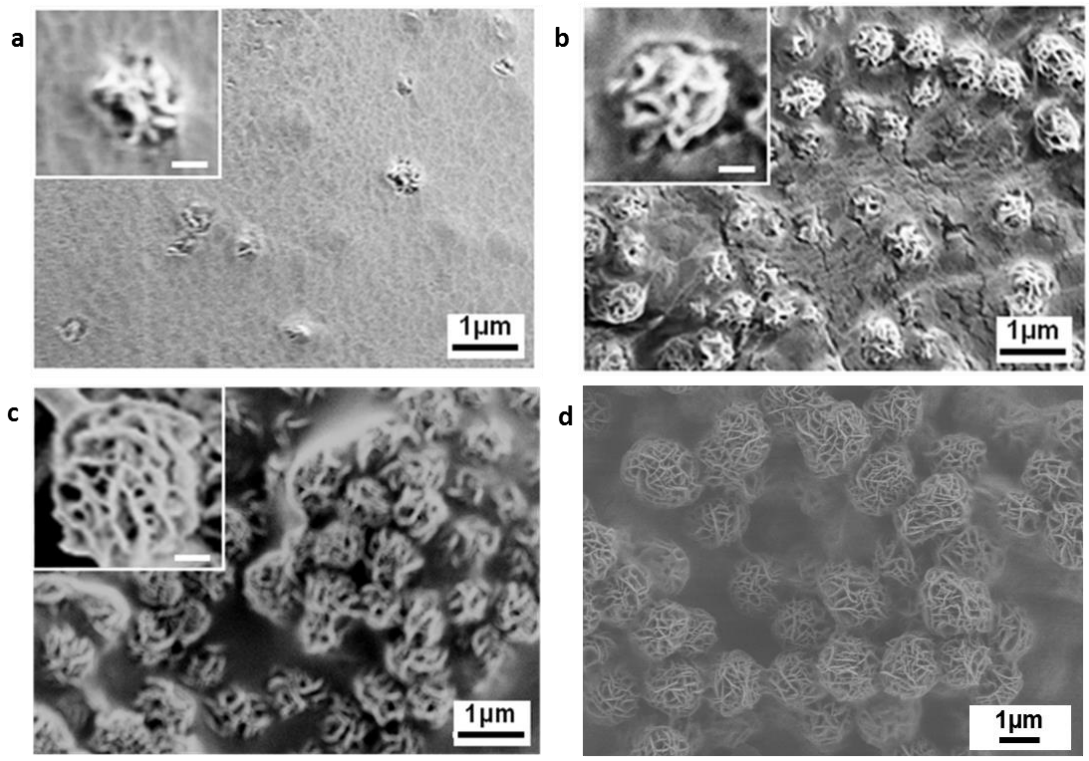

Figure 2.6: Morphology of the DNA hydrogel with different MCA-process time. **a**, $\mathbf{R_4M_1}$, **b**, $\mathbf{R_4M_3}$, **c**, $\mathbf{R_4M_6}$, **d**, $\mathbf{R_4M_{16}}$. Scale bars in insets, 200nm. Not only the number of the DNA microsphere were increasing, but also the diameters of DNA microsphere were growing from 350 ± 80nm for $\mathbf{R_4M_1}$, 550 ± 100nm for $\mathbf{R_4M_3}$, 790 ± 150nm for $\mathbf{R_4M_6}$ and 1600 ± 200nm for $\mathbf{R_4M_{16}}$.[154]

2.3.4 Unusual mechanical properties of the DNA hydrogel

Unexpectedly, we discovered unusual mechanical properties of our DNA hydrogel that were not found in nature: it had both liquid-like and solid-like properties. When the gel was taken out of water, it became a "liquid" and flew freely in the tube (Figure 2.7a), and conformed to the shape of its container, such as star-shape, circle-shape, rectangle-shape, triangle-shape and cross-shape (Figure 2.7b). However, when the gel was put back into water, it metamorphosed into a solid gel. Surprisingly, the gel always returned to its birth shape in water, regardless of how many different shapes it had taken in the liquid-like state. To further investigate this unusual property, we first formed $\mathbf{R}_4\mathbf{M}_{16}$ hydrogel in molds with defined geometries in the shape of the English letters "D", "N" and "A" (Figure 2.7c). After removing water, each hydrogel behaved like a liquid by conforming to the shape of the vial (Figure 2.7d). However, when the water was reintroduced, the hydrogels returned to their birth shapes ("D", "N", and "A", Figure 2.7e). This shape transition of the gel was monitored in real time (Figure 2.7f). When the water is introduced, the gel started to metamorphose within the first 3 s (from t = 0 s to 3 s). The gel continued to transform back to its birth shape gradually and smoothly (from t = 3 s to 9 s). The final shape of "D" was restored within 15 s (t = 15 s). These liquid-to-solid transition and returning-to-original-shape processes can be repeated as many times as one likes. These results clearly demonstrated the unprecedented DNA hydrogel with unusual mechanical properties that have never been created before.

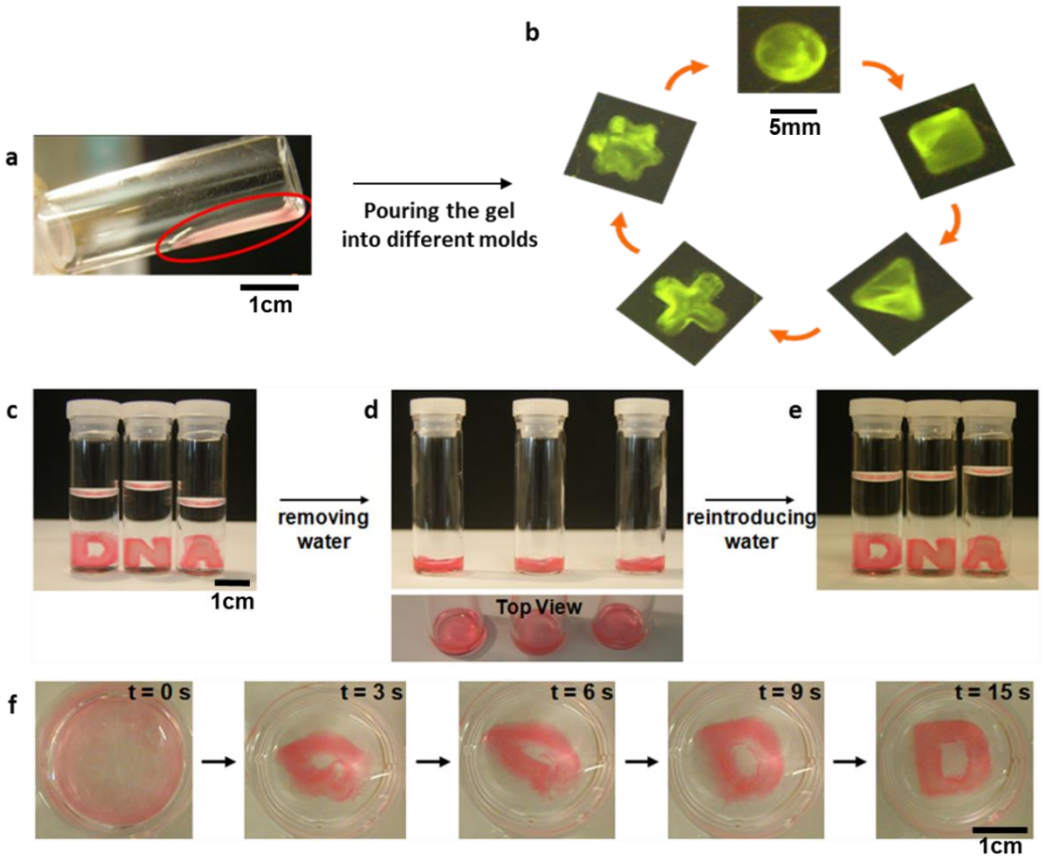

Figure 2.7. Liquid-like and Solid-like property of R_4M_{16} hydrogel. a, When out of water, the hydrogel flowed freely in the tube. **b,** When the hydrogel was poured into different shaped-containers consecutively and repeatedly (from circular to square to triangular to X-shaped to star-shaped and back to circular), it conformed to the shape of its container, just like a liquid. The gel was stained with GelGreen. **c,** "D", "N", and "A"-shaped hydrogel are successfully formed and tested its solid-like property by removing and replacing water. **d,** Series of photographs showing the process of DNA hydrogel going back to the birth shape after reintroducing water at 25 ℃: the gels started to metamorphose within the first 3 s (from t = 0 s to 3 s). The gel continued to transform back to its birth shape gradually and smoothly (from t = 3 s to 9 s). The final shape of "D" was restored within 15 s (t = 15 s).[154]

2.3.5 Mechanism for the unusual mechanical properties

To understand the mechanism for this unusual mechanical behavior, we carefully analyzed the stresses applied to the gel. There are two stresses involved in deforming a hydrogel when the gel is placed in the air. They are surface tension stress γ/L and gravitational stress ρgL. On the other hand, elastic stress εE of the hydrogel resists the deformation. Here, γ is the surface tension, L is the length scale of the gel, ρ is the specific gravity of the gel, g is the gravitational constant, ε is magnitude of the strain and E is the Young's modulus. For a hydrogel with the length scale of 1 cm, the surface tension is 7.2 N/m^2 and the gravitational stress is 98 N/m^2. Here we use γ = 0.072 N/m, $\rho = 1000$ kg/m^3 and g = 9.8 m/s^2.

For most hydrogel, the elastic modulus is in the range of KPa to MPa[138, 145, 157]. The strain induced by the surface tension and gravity is negligible, thus the gel supports itself and keeps its original shape when it is in the air. However, for our DNA hydrogel, the elastic modulus is as low as 5 Pa (Figure 2.4). The surface tension and gravity is able to deform the hydrogel as much as 21 times. If our hydrogel is elastic and is not damaged by those two stresses, it will behave like a liquid. To test the elasticity of the hydrogel, we anchored the gel between two clippers with the initial length of 3 mm. By gradually stretching the two clippers apart from each other, the gel was elongated to as much as 51 mm without breaking (Figure 2.8). Because of the high elasticity and the low elastic modulus of the hydrogel, it possessed the unusual mechanical properties.

Chemically, the DNA hydrogel was composed of DNA chains (both ssDNA

and dsDNA) and physically entangled crosslinking points. This specific molecular structure endowed the hydrogel with very low modulus (~5 Pa). When the hydrogel was in water, it exhibited solid-like property. After water was removed from the chamber, the hydrogel was exposed to air. Because the hydrogel was extremely elastic, it could not keep its shape under the surface tension and gravitational stresses, thus it was deformed at the water/air interface. After all the water was totally removed from the chamber, under the stresses of surface tension and gravity, the gel conformed to the shape of the chamber, resembling the property of water. After the hydrogel was re-immersed in the water, the gravity was canceled by the buoyance stress. Thus the gel restored to its original shape via elastic stress, exhibiting the solid-like property (Figure 2.9).

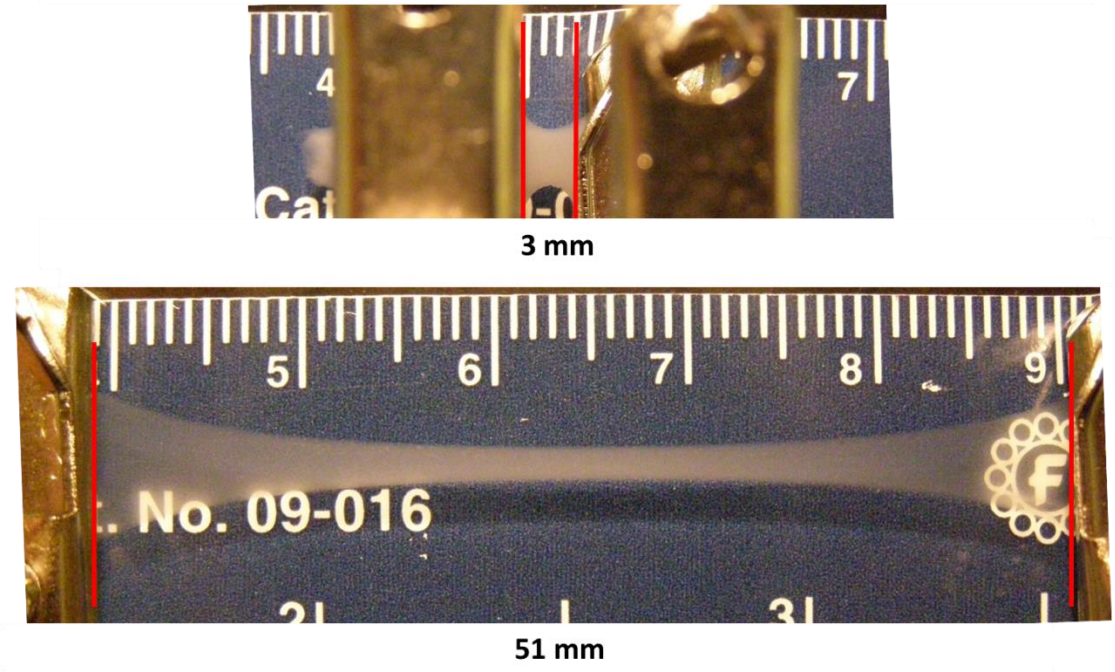

Figure 2.8. Elasticity of the DNA hydrogel. The DNA hydrogel (white color) was anchored between two clippers with the original length of 3 mm. After stretching the two clippers apart from each other, the gel was elongated to as much as 51 mm, representing a 17 fold deformation.

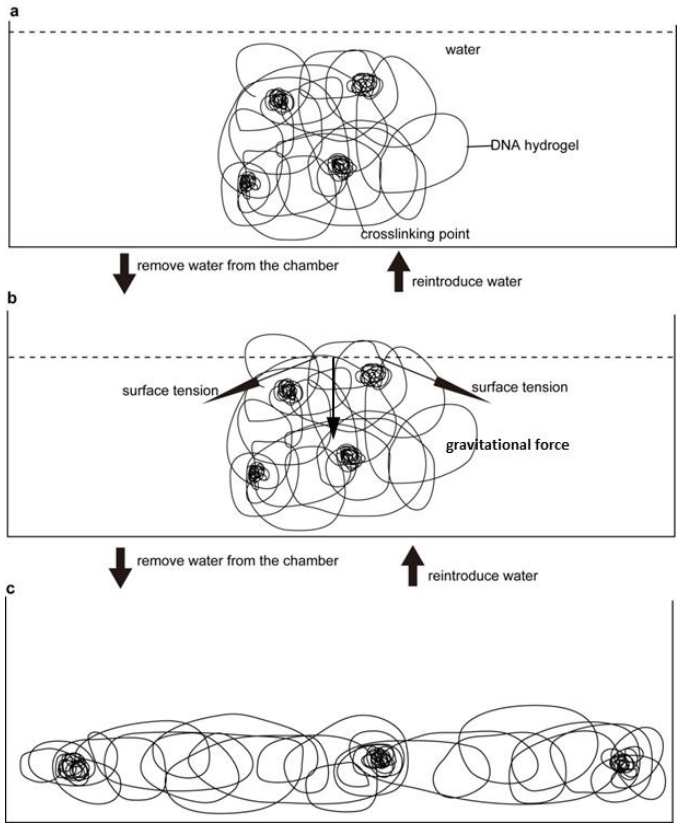

Figure 2.9. Schematic molecular mechanism of the liquid-like and solid-like properties of the DNA hydrogel. a, The DNA meta-hydrogel was composed of DNA chains (both ssDNA and dsDNA) and the entangled crosslinking points. This specific molecular structure endowed the hydrogel with very low modulus (~5 Pa). b, After water was removed from the chamber, the hydrogel was exposed to air. Because the hydrogel was extremely soft, it could not keep its shape under the surface tension and gravitational stress, thus it was deformed at the water/air interface. c, After all the water was totally removed from the chamber, under the action of surface tension and gravity, the gel conformed to the shape of the chamber, resembling the property of water. After reintroducing water into the chamber, the hydrogel returned to its birth shape, exhibiting the solid-like property.[154]

2.3.6 Applications of the unusual mechanical properties

Many applications can be envisioned by using our DNA hydrogel. We first explored our hydrogel's potential as a controlled drug release system. A unique advantage is that both the gel material building blocks (DNA) and the gel itself (physical enclosure) can be used as drug reservoirs. We loaded our DNA hydrogel with drugs, DOX and insulin, by chemical intercalation and physical entrapment, respectively. As expected, the physically entrapped drug had a much faster releasing profile than the chemically intercalated drug (Figure 2.10). This property can be potentially applied to the release of different drugs in a time-controlled fashion.

In addition, applications can also take advantage of using either or both liquid-like and solid-like properties of our hydrogel. As an example we designed a DNA-hydrogel-based electric circuit which used water as a switch (Figure 2.11). When the surrounding water was removed, the DNA hydrogel (doped with 10 nm gold nanoparticle to attain electric conductivity) became "liquid-like" and thus conformed to the shape of the channel linking the two electrodes together. As a result, the circuit was turned on (Figure 2.11 "ON"). By simply adding water back to the meta-hydrogel, DNA hydrogel became "solid-like" and thus remembered its birth shape (which was shorter) actuating the gel to move away rapidly from the electrode and consequently shutting off the current completely (Figure 2.10, "OFF").

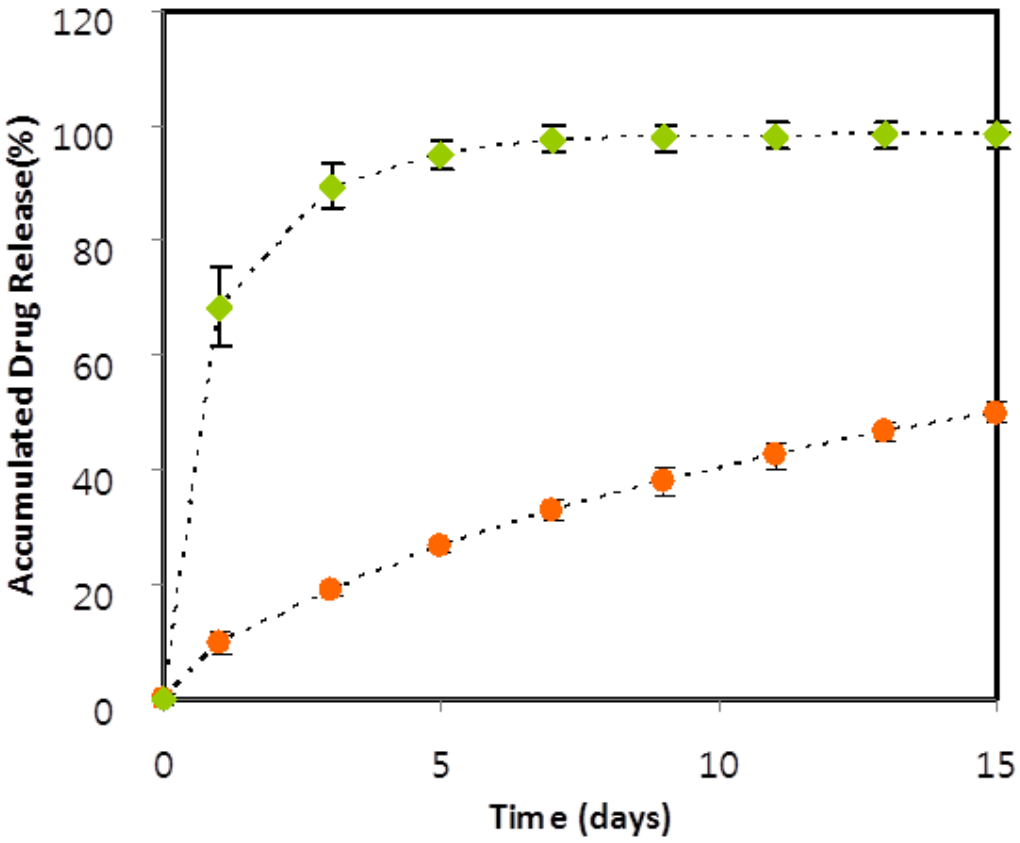

Figure 2.10. Drug release profiles of $\mathbf{R}_4\mathbf{M}_{16}$ DNA hydrogel. Controlled drug release profiles with insulin (♦) and doxorubicin (●). The volume of the DNA hydrogel was 70µl. [154]

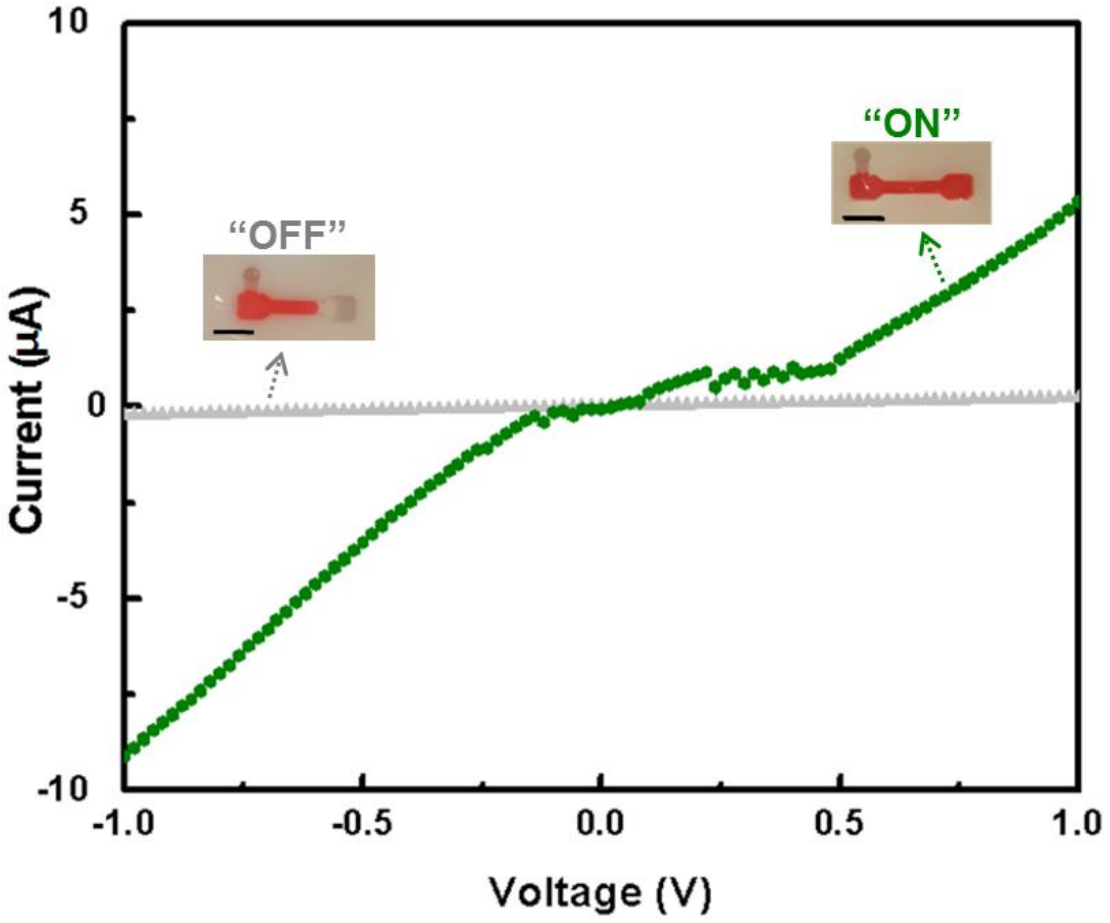

Figure 2.11. Electric circuit switches by using liquid-like and solid-like properties of DNA hydrogel. With liquid-like property of gel, the circuit can be covered by DNA gel encapsulating 10 nm AuNP (●, "On"). By simply adding water the gel metamorphosed to its birth shape which was shorter, resulting in the gel moving away rapidly (within seconds) from the electrode and consequently shutting off the current completely (▲, "off"). The scale bars of inset are 5mm.[154]

Table 2.1. Oligonucleotide sequences of linear ssDNA and primers for the DNA hydrogel.

Strand	**Sequence**
Linear ssDNA	5'-Phosphate-**TCGTTTGATGTTCCTAACGTACCAACGCACACGCAGTATTATGGACTGGTAAAAGCTTTCCGAGGTAGCCTGGAGCATAGAGGCATTGGCTG**-3'
Primer1	5'-**TAGGAACATCAAACGACAGCCA**-3'(complementary to **TGGCTGTCGTTTGATGTTCCTA** in circular template)
Primer2	5'-**ACGCAGTATTATGGACTG**-3'
Primer3	5'-**TGGTACGTTAGGAACATC**-3'(complementary to **GATGTTCCTAACG TACCA** in circular template)

Table 2.2. Influence of RCA and MCA process durations on the solid-like and liquid-like properties of DNA hydrogel.

Gel type (R_xM_y)	**Solid-like property**	**Liquid-like property**
$\mathbf{R_0M_{16}}$*	NO	YES
$\mathbf{R_1M_{16}}$*	NO	YES
$\mathbf{R_2M_{16}}$	YES	YES
$\mathbf{R_4M_{16}}$	YES	YES
$\mathbf{R_8M_{16}}$	YES	YES
$\mathbf{R_{12}M_{16}}$*	NO	YES
$\mathbf{R_{16}M_{16}}$*	NO	YES
$\mathbf{R_4M_1}$	NO	YES
$\mathbf{R_4M_3}$	NO	YES
$\mathbf{R_4M_6}$	NO	YES
$\mathbf{R_4M_{20}}$	YES	YES
$\mathbf{R_4M_{24}}$	YES	YES

*: These reactions resulted in turbid solutions with liquid-like properties (e.g. "flow"). However when they were transferred back into water, they did not maintain their original shapes. Thus we defined them not having solid-like property.[154]

2.4 Conclusion

We have successfully created a bulk-scale physically entangled DNA hydrogel based on pure enzymatic amplification for the first time. By designing two enzymatic processes, rolling circle amplification and multi-primed chain amplification, DNA chains are greatly amplified, both in length and in quantity, to entangle with each other to form a DNA hydrogel. Due to the amplification power of the enzymatic amplification, the hydrogel is synthesized at low cost and can be readily scaled up. Interestingly, our hydrogel possesses an internal hierarchical micro-structure that gives rise to the unusual mechanical properties that have not been found in nature of any kind: it behaves like a liquid and flows freely when taken out of water, and becomes solid and goes back to its original shape when immersed in water. Our work will significantly expand DNA materials repertoire with great potential for real-world applications, including drug release, cell therapy, protein expression, electric switch, flexible circuits, and others.

CHAPTER 3: BIOMEDICAL APPLICATIONS OF THE PHYSICALLY ENTANGLED DNA HYDROGELS *

3.1 Introduction

Modern drug discovery started in the early twentieth century with rational syntheses of small-molecule drugs and advanced 50 years later to large-molecule biologics via recombinant DNA technology and monoclonal antibody technology. Currently, nucleic acid (DNA and RNA) has been demonstrated as one of the most recent biologics for disease prevention and treatment, including nucleic acid diagnostics[97, 158, 159], siRNA therapy[105, 160, 161], gene therapy[162] and DNA vaccines[163, 164]. While most of these applications relied on the protein coding sequences, a special class of DNA that was composed of only non-coding, unmethylated CpG motifs was developed as a promising immunotherapy drug through the innate immune system[106, 107, 165, 166]. The CpG motif specifically interacts with the toll-like receptor 9 (TLR9) presented in the endocytic vesicles after being endocytosed[167]. This specific interaction directly activates immunostimulatory cascades[165] characterized by the elevated productions of proinflammatory cytokines including tumor necrosis factor alpha (TNF-α) and interleukin 6 (IL-6)[99, 168]. As of now, more than a dozen of CpG-based DNA drugs are in clinical trials as vaccine adjuvants, anti-allergens, and cancer immunotherapy drugs[108, 109, 169].

---

*: A paper based on this chapter has been submitted with the authors: Songming Peng, Chuangying Xu, Chunyan Li, Mark R. Hartman, Yan Yu, Wei Han, Qiangbin Wang and Dan Luo.

Even though promising, the lack of potency and fast degradation *in vivo* of DNA remain to be two important hurdles. To address the issue of inadequate potency, four different classes of CpG-containing DNA, each with distinct flanking sequences, were developed in order to elicit stronger immune responses[108]. To mitigate the degradation problem, instead of using natural DNA with phosphodiester bonds (poDNA), DNA backbones replaced by phosphorothioate bonds (psDNA) were employed[108]; psDNA was not a substrate of nucleases thus resisted the degradation. Fundamentally, both hurdles are related to the dose issue. If one can administer a much larger effective dose, in theory the efficacy will increase and degradation will have minimal impact. However, the therapeutic window limits how high the dose one can reach. In fact, this is also a general challenge for almost all drugs: how to formulate a very high effective dose without causing toxicities.

Our physically entangled DNA hydrogel revealed a striking internal micro-structure, a huge amount of uniformly sized DNA microspheres. Those microspheres can be easily isolated from the hydrogel with high yield, and to our surprise, we discovered that the DNA density in the microsphere reached as high as human chromosome density in the metaphase. Such high density might be able to serve as a great platform to condense high dose of DNA drugs, such as CpG motifs. Indeed, by designing CpG motif into the circular DNA template, we created a novel DNA structure termed as super-condensed, ultra-high dose DNA (scudDNA); the scudDNA was composed of over several million doses of CpG motifs (Figure 3.1a-d). Importantly, such an unprecedented high dose was super-condensed into only one single microsphere, serving as a self-releasing system without causing much toxicity.

Excitingly, scudDNA elicited enhanced cell immune responses *in vitro* and successfully suppressed tumor growth *in vivo*, while the same DNA with the same dose without scudDNA structure failed to do so (Figure 3.1e-g). To the best of our knowledge, this was the first time that millions of therapeutic CpG motifs were condensed into one microsphere and that the condensed structure itself served as an effective drug formulation. Our scudDNA structure can incorporate any past or future CpG sequences, or any other therapeutic sequences, providing a novel platform for all nucleic acid-based drugs.

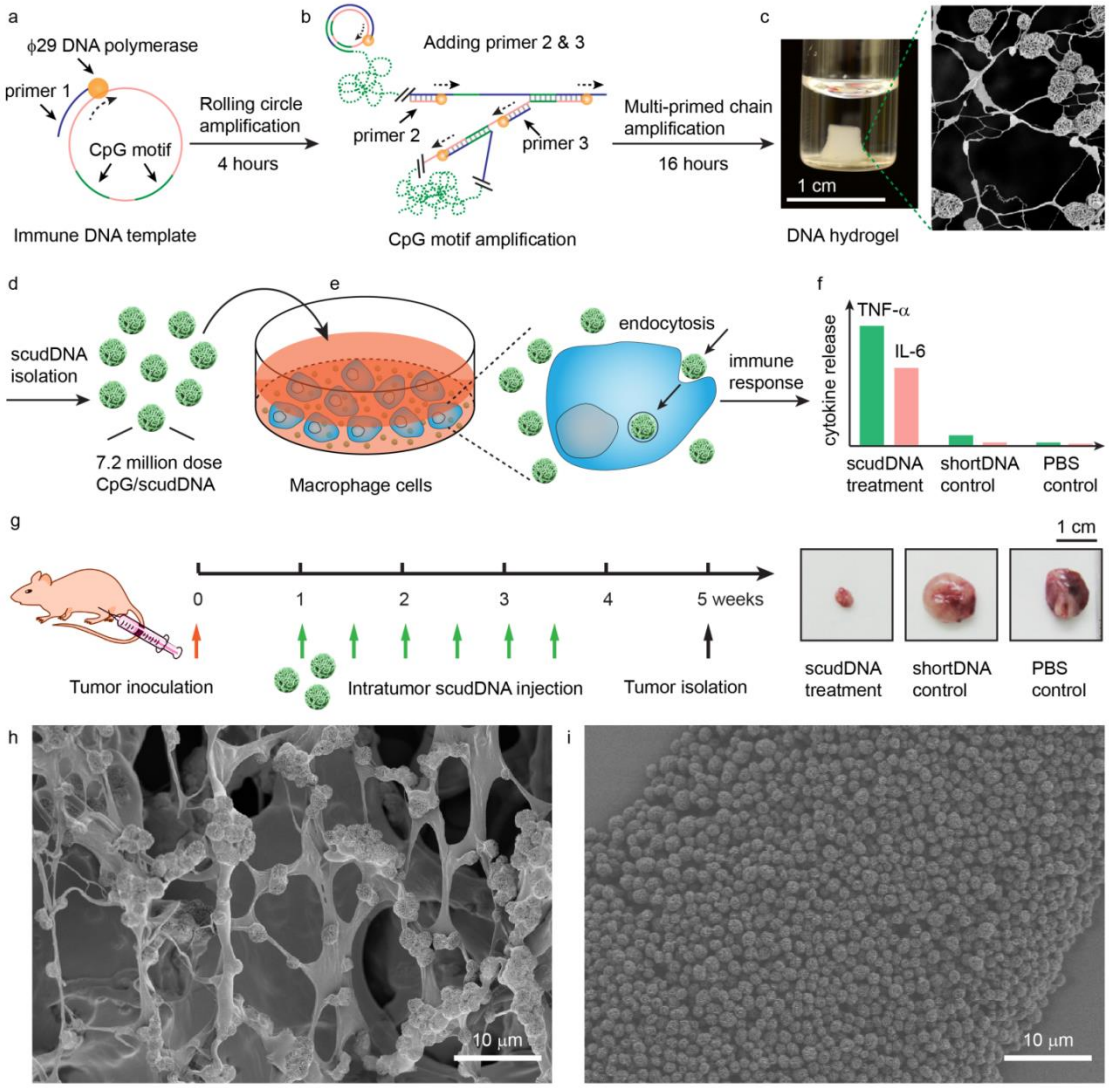

Figure 3.1. Schematic illustration of the production and function of the scudDNA. **a,** The circular immune DNA template was designed to have two CpG motifs. Upon binding with primer 1, the rolling circle amplification was initiated by the Φ29 DNA polymerase to produce long DNA. **b,** After adding primer 2 and primer 3, multi-primed chain reaction was initiated. The amplified long DNA chains, which contained large amounts of CpG motifs, were entangled to form a DNA hydrogel. **c,** The DNA hydrogel was immersed in water, and was composed of DNA microspheres (scudDNA) and DNA bundles. **d,** The scudDNA was isolated from the hydrogel by

mechanically breaking the DNA bundles. **e,** By incubating with macrophage cells, the scudDNA was effectively endocytosed. **f,** The scudDNA elicited enhanced immunostimulatory effects, characterized by the TNF-α and IL-6 release, compared to the control shortDNA and PBS. **g,** Mice were inoculated with tumor cells, and after one week, injections of scudDNA were administered for three weeks at a frequency of twice a week. The tumor was retrieved at week five. The tumor size indicated that the scudDNA effectively suppressed the tumor growth, while the control shortDNA failed to do so. **h-i,** The microstructure of scudDNA in the hydrogel (**h**) and isolated scudDNA (**i**) was revealed by scanning electron microscopy.

3.2 Materials and Methods

3.2.1 Chemicals, cells and animals

Φ29 DNA polymerase was purchased from Epicentre Biotechnologies (Madison, WI). Inorganic pyrophosphatase was purchased from New England Biolabs (Beverly, MA). Oligonucleotides were commercially synthesized and PAGE purified (Integrated DNA Technologies, Coralville, Iowa). Sequences of the oligonucleotides are listed in Table 3.1. Enzyme-linked immunosorbent assay (ELISA) kits for TNF-α and IL-6 detection were purchased from Syd Labs (Natick, MA). Mice macrophage cell line Raw 264.7 was purchased from American Type Culture Collection (ATCC, Manassas, VA). Mice colon tumor cancer cell line (CT26.WT) was obtained from Shanghai Cell Bank (Shanghai, China). 6-week-old female BALB/c mice were purchased from Shanghai SLRC Laboratory Animal Company (Shanghai, China).

3.2.2 Super-condensed ultra-high dose DNA (scudDNA) fabrication

Ligated circular immune DNA template (50 nM), which was hybridized with primer 1 (50 nM), was incubated with Φ 29 DNA polymerase (1 unit/μl) in the reaction buffer (40 mM Tris-HCl, 50 mM KCl, 10 mM $MgCl_2$, 5 mM $(NH_4)_2SO_4$, 4 mM dithiothreitol, 200 μg/ml bovin serum albumin and 10 mM dNTP) at 30 ^oC. After 4 hours, primer 2 and primer 3 (50 μM) were added to the reaction to initiate the multi-primed chain reaction for another 16 hours, which resulted in a DNA hydrogel composed of scudDNA. The scudDNA was isolated from the hydrogel by mechanically breaking the DNA bundles between them. The isolated scudDNA was then purified by repeatedly centrifuging at 8000 rcf (2 min) and washing with milliQ

water 3-4 times, until no absorption at 260 nm was detected in the supernatant. The obtained scudDNA was dispersed in milliQ water and stored at 4 ^{o}C. By simply using Cy5 or Alexa 488-labled primer 2, red or green fluorescent scudDNA was produced. To reveal the microstructure of the scudDNA, it was coated with Au/Pd and imaged by the LEO 1550 FESEM (Carl Zeiss). The composition of scudDNA was examined by incubating it with the inorganic pyrophosphatase (0.01 unit/μl) in the reaction buffer (40mM Tris-HCl, 10mM $MgCl_2$) at room temperature. The optical density at 600 nm was measured by a microplate reader (BioTek Instruments) every hour. Elemental analysis of the scudDNA was carried out using a Tecnai T12 TEM (FEI).

3.2.3 scudDNA mass, density and dose calculation

The mass of each scudDNA was quantified using the following method. First, the number of scudDNA in the solution was counted using a hemocytometer. Then the scudDNA was treated with excess amounts of Exonuclease I and Exonuclease III for 24 hours to totally degrade the DNA into nucleotides. After digestion, the absorbance by the nucleotides at 260 nm was measured and the concentration was determined according to the standard nucleotide absorption curve. The average mass of each scudDNA was determined to be 0.15 pg, through dividing the nucleotide concentration by the number density of the scudDNA in solution.

Since most of the scudDNA had a spherical morphology, the formula for the volume of a sphere was used to estimate volume of the scudDNA. The scudDNA had an average diameter of 1.3 μm (Figure 3.2), and the volume of the scudDNA was calculated to be 1.15 μm^3. Thus, the average density of the scudDNA was 0.13

$pg/\mu m^3$.

The compaction ratio and CpG dose in each scudDNA was calculated as followings:

• Mass of the 82 base immune DNA template

$= 25088$ g/mol $= 25088/(6.02\times10^{23}) = 4.17\times10^{-8}$ pg

• Average repeating immune DNA template in each scudDNA

$= 0.15pg/(4.17\times10^{-8}\ pg) = 3.6\times10^{6}$

• Average compaction ratio

$= 3.6\times10^{6}\times82(base)\times0.34(nm/base)/(1300nm) = 7.7\times10^{4}$

• Average molecular weight of each scudDNA

$= 3.6\times10^{6}\times25088$ (g/mol) $= 9\times10^{10}$ g/mol

Since each immune DNA template contains two copies of CpG motif

• Average CpG motif in each scudDNA

$= 3.6\times10^{6}\times2 = 7.2$ million

3.2.4 In vitro immunostimulatory effects of the scudDNA

Mice macrophage cell line Raw 264.7 was maintained in Dulbecco's Modified Eagle Medium (DMEM), with 10 % fetal bovine serum (FBS) and 1% penicillin/streptomycin. Before the experiment, cells were seeded in a 48-well cell culture plate at a density of 160,000/well. After overnight incubation, the cell culture medium was discarded and the cells were subjected to scudDNA^{+CpG} or shortDNA^{+CpG} for the potency and stability test. To test the potency of the scudDNA^{+CpG} and shortDNA^{+CpG}, Opti-Modified Essential Medium (Opti-MEM, a reduced-serum

medium, 200 μl) with different concentrations of scudDNA^{+CpG} or shortDNA^{+CpG} (1, 2.5, 5 and 10 μg/ml, equal to 80, 200, 400 and 800 nM of CpG motif) were added to the cells. After 8 h (for TNF-α) or 24 h (for IL-6) incubation, the supernatant was collected and stored at -80 ^{o}C for later use. On the other hand, to test the stability of the scudDNA^{+CpG} and shortDNA^{+CpG} against serum degradation, the DNA samples were pretreated in 200 μl DMEM with 10 % FBS for different amounts of time (0, 2, 4, 8, 16 and 24 hours) with a concentration of 5 μg/ml at 37 ^{o}C. The serum treated scudDNA^{+CpG} and shortDNA^{+CpG} were either examined by agarose gel electrophoresis to check their stability or incubated with the Raw 264.7 cells for 8 h (for TNF-α) or 24 h (for IL-6) to test their immunostimulatory functions. Measurements of the secreted TNF-α and IL-6 ($n \geq 3$) were determined by the ELISA according the provided protocols. The DNA degradation was quantified by Image-J.

3.2.5 Cell uptake and release of the scudDNA

Raw 264.7 cells were seeded in a 4-well chamber slide (Thermo Fisher Scientific) at a density of 170,000/well and cultured overnight. Red fluorescence labeled scudDNA^{+CpG} (0.75 μg, equal to 29 scudDNA/cell) in 400 μl DMEM with 10 % FBS was added to the well and incubated at 37 ^{o}C or 4 ^{o}C for 8 h. The cells were then washed with 500 μl PBS for 3 times, and fixed with 4 % paraformaldehyde in PBS for 15 min. After incubating with 0.1 % Triton-X-100 in PBS for 4 min, the cells was stained with Alexa-488 Phalloidin (Life Technologies) to visualize the filamentous actin according to the provided protocol. The slide was then incubated with DAPI (250 ng/ml in PBS) to stain the cell nuclei. Prolong Gold anti-fade solution

was dropped onto the slide to avoid fluorescence bleaching. The slide was sealed with nail polish and imaged with LSM710 confocal microscopy (Carl Zeiss). To test whether the scudDNA^{+CpG} was colocalized with the endo-lysosome, we used a 4-well cell culture dish with glass bottom (CELLview, Greiner Bio-One). Cells were seeded at a density of 80,000/well and cultured overnight, and then incubated with green fluorescence labeled scudDNA^{+CpG} (0.35 μg, equal to 29 scudDNA/cell) in 200 μl DMEM with 10 % FBS at 37 ^{o}C for 8 h. After that, the cells were washed with DMEM for 3 times and incubated with deep red LysoTracker (Life Technologies, 15,000X dilution of the stock) in DMEM for another 2 h at 37 ^{o}C. Hoechst 34580 (Life Technologies, 1 μg/ml) was then added to the cells to stain the nuclei for 30 min. The live cells were imaged under the LSM710 confocal microscopy.

To test the release of the scudDNA^{+CpG}, the scudDNA^{+CpG} was incubated with 100 mM PBS buffer (pH = 7.4, 6.5 and 6.0) or 100 mM sodium acetate buffer (pH = 5.5, 5.0, 4.5 and 4.0) for 2 hours at 37 ^{o}C. The solution was briefly centrifuged to collect the leftover scudDNA^{+CpG}. The DNA released was quantified by measuring the absorbance at 260 nm in the supernatant.

3.2.6 Toxicity of the scudDNA

The toxicity of scudDNA^{+CpG} was examined both *in vitro* and *in vivo*. To test the *in vitro* toxicity, scudDNA^{+CpG} of different concentrations (0.1, 1, 5, 10 and 20 μg/ml) was incubated with the Raw 264.7 cells overnight. The cell viability was assessed by the MTT assay. To test the *in vivo* toxicity, scudDNA^{+CpG} (10 μg, 50 μL) was subcutaneously injected into the right flank of the 6-week-old female BALB/c

mice (n = 6 for each group) at a frequency of two injections per week for three weeks. PBS was used as a control. The mice were sacrificed at day 21. Blood samples were collected from the mice fundus artery and centrifuged at 3000 rpm for 30 min to separate blood cells and blood plasma. Major organs including livers, kidneys and spleens were also harvested, fixed in 4 % formalin/PBS solution, embedded in OCT resin, and then sectioned and stained with hematoxylin/eosin. The blood biochemistry, hematological analysis and histological examinations of different organs were examined to assess the *in vivo* toxicity.

3.2.7 In vivo tumor suppression of the scudDNA

The mice colon tumor cancer cell line (CT26.WT) was maintained in RPMI 1640 media supplemented with 10 % FBS. The tumor cells (1×10^6) were subcutaneously injected into the right flank of the 6-week-old female BALB/c mice. The tumor was allowed to grow for one week (at which time the size reached ~ 2 mm in diameter). The mice were then weighed, randomly coded and divided into four different groups (n = 8 for each group). PBS, control shortDNA^{+CpG}, control scudDNA^{-CpG} or scudDNA^{+CpG} (10 μg, 50 μL) was intratumorly injected into the mice at a frequency of two injections per week for three weeks. The tumor size was measured every three days. Tumor volume was estimated according to the formula $V = 0.52ab^2$, where a is the largest superficial diameter and b is the smallest superficial diameter. To monitor the tumor weight, the mice was sacrificed by cervical dissociation one week after the treatment was finished, and the tumors were removed from the mice and weighed. To monitor the survival rate, another group of mice (n = 8) was cultured for another seven weeks after the treatment was finished and the

number of dead mice was recorded.

3.2.8 In vivo tracking of the scudDNA

To label the scudDNA^{+CpG} with tissue-penetrating infra-red quantum dots (Ag_2S QD), 5' amine modified primer 2 (160 μM) was first conjugated to carboxylic group modified QD (4 μM) catalyzed by the 1-Ethyl-3-(3-dimethylaminopropyl) carbodiimide (EDC, 2 mM) and N-Hydroxysuccinimide (NHS, 2 mM) in pH = 7.4 PBS buffer for 6 hours. The conjugated DNA-QD was purified by removing the free DNA, EDC and NHS using the YM-50 centrifuge column (Mw = 50,000 cutoff membrane, Millipore) for 3-4 times, until no DNA was detected in the flow-through solution. The QD-DNA was added to the MCA reactions to produce the QD-labeled scudDNA^{+CpG}. The QD-labeled shortDNA^{+CpG} was obtained using a similar method. The QD-scudDNA^{+CpG} or QD-shortDNA^{+CpG} (30 μg/ml, 50 μl) was injected into the tumor-bearing mice and the near-infrared fluorescence images were collected in real-time by a 640×512 pixel two-dimensional InGaAs/SWIR camera (Photonic Science, UK) equipped with 880 nm and 1100 nm filters (Daheng Optics and Fine Mechanics Co., Ltd, China). A near-infrared lens pair SWIR-35 (Navitar, US) was used to focus the image onto the detector. The excitation light was provided by an 808-nm diode laser (Starway Laser Inc., China) and the excitation power density at the imaging plane was 35.6 mW/cm^2.

3.2.9 Data analysis

Data are expressed as means ± standard deviation. For toxicity study, tumor growth and tumor weight, statistical difference was calculated using a one-way Anova

method, followed by an unpaired, two-tailed t test. Significance for Kaplan-Meier curves was determined by the log-rank test. *p*-values less than 0.05 were considered statistically significant.

3.3 Results and Discussion

3.3.1 Formation and mechanism of scudDNA structure

The scudDNA structure was inspired by a unique enzymatic chain reaction reported in our previous bulk-scale DNA hydrogel[154]. For this work, we designed the CpG motif into the DNA template (Figure 3.1a & Table 3.1). After two-step enzymatic processes: rolling circle amplification (RCA) and multi-primed chain amplification (MCA), the DNA template with CpG motif was greatly amplified and resulted in a hydrogel with large amounts of uniformly sized DNA microspheres (Figure 3.1b-c & 3.1h). More importantly, each of the microspheres was consist of unprecedentedly high dose of CpG motif up to several million copies. The microsphere was isolated from the hydrogel by mechanically breaking the DNA bundles between them (Figure 3.1d, 3.1i & Figure 3.2).

To our surprise, by measuring the average mass and base number in each microsphere, we discovered that the microsphere (i.e. scudDNA) were hugely compacted (77000 fold) and reached a density as high as 0.13 pg/μm^3, which was similar to the greatly condensed chromosome DNA in the metaphase of cell circle[170].

Unlike chromosomes (or any other traditionally condensed DNA complexes), in which DNA was packed by the positively charged reagents such as histones (or cationic polymers), our scudDNA was entirely self-condensed without introducing any

cationic compacting reagent. This was quite counterintuitive due to the fact that negatively charged DNA repelled each other. To understand the underlying process of this unusual self-compaction, we carefully examined the RCA and MCA enzymatic reactions. During the polymerase catalyzed DNA chain elongation, an S_N2 nucleophilic substitution, the nucleophile was the oxygen of the 3'-hydroxyl group of the propagating DNA, and the leaving group was the β and γ - phosphate (pyrophosphate) of the dNTP. Upon binding with the Mg^{2+}, the metal-bound hydroxyl group became more nucleophilic than the sole hydroxyl group. Similarly, another Mg^{2+} aided the leaving group, resulting in the generation of a new phosphodiester bond along with a pyrophosphate as a byproduct (Figure 3.3). We noted that during each step, due to the proximity and participation of the Mg^{2+}, magnesium pyrophosphate precipitates were generated *in situ* (as opposed to forming the precipitates after the completion of the chain elongation). We also noted that a similar metal salt, calcium phosphate, was among the first transfection reagents used for condensing DNA[171]. Thus, we speculated that the *in situ* generated magnesium pyrophosphate condensed DNA in real-time.

Indeed, by incubating the scudDNA with the inorganic pyrophosphatase, an enzyme hydrolyzed magnesium pyrophosphate to more soluble magnesium phosphate[172], we observed that scudDNA totally disappeared after the treatment (Figure 3.4 a-b). In addition, the optical density 600 (OD 600) gradually decreased with increasing incubation time (Figure 3.5). Furthermore, scanning electron microscopy (SEM) images showed that, after the pyrophosphatase treatment, the size of the scudDNA microsphere diminished and that the microsphere disentangled into

fibers (Figure 3.4 c-d). Moreover, elemental analysis data also indicated the presence of Mg^{2+} within the DNA microspheres (Figure 3.6). Taken together, these data revealed that during the DNA elongation process, extremely long DNA entangled while at the same time were self-condensed by magnesium pyrophosphate generated *in situ*.

We noted that in other polymerase reaction, magnesium pyrophosphate was also produced. However, polymerase reaction typically do not condense the DNA, which is probably due to the fact that only short DNA strands (in the range of several thousand bases, as produced by Taq polymerase) or only small amounts of DNA strands (as produced by conventional RCA which lacks the multi-primed chain reaction) are produced. Our unique two enzymatic processes not only generated long DNA strands (in the range of million bases), but also produced a huge amount of them (~1000 fold compared to RCA only). These long DNA strands were entangled with each other and condensed by the *in situ* generated magnesium pyrophosphate, forming the scudDNA. Furthermore, co-precipitating the immune DNA template with magnesium pyrophosphate failed to produce the scudDNA (data not shown), suggesting that *in situ* condensation was essential for forming such compact structure.

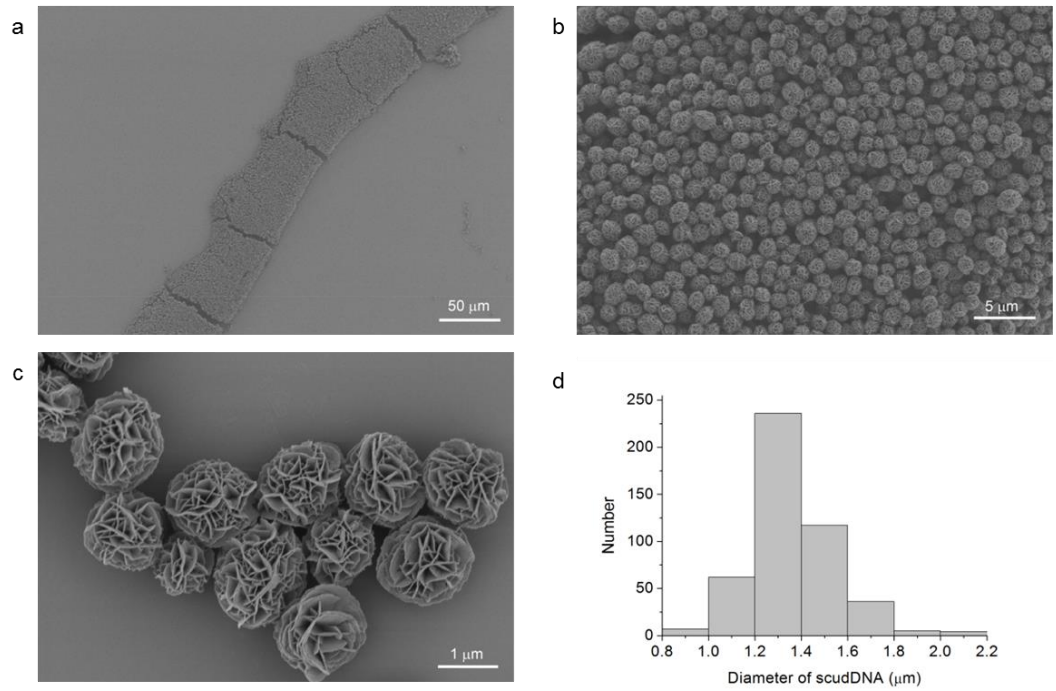

Figure 3.2. SEM images and size distribution of the scudDNA. **a-c**, The scudDNA can be prepared in bulk-scale. **d**, The scudDNA had an average size of 1.3 μm.

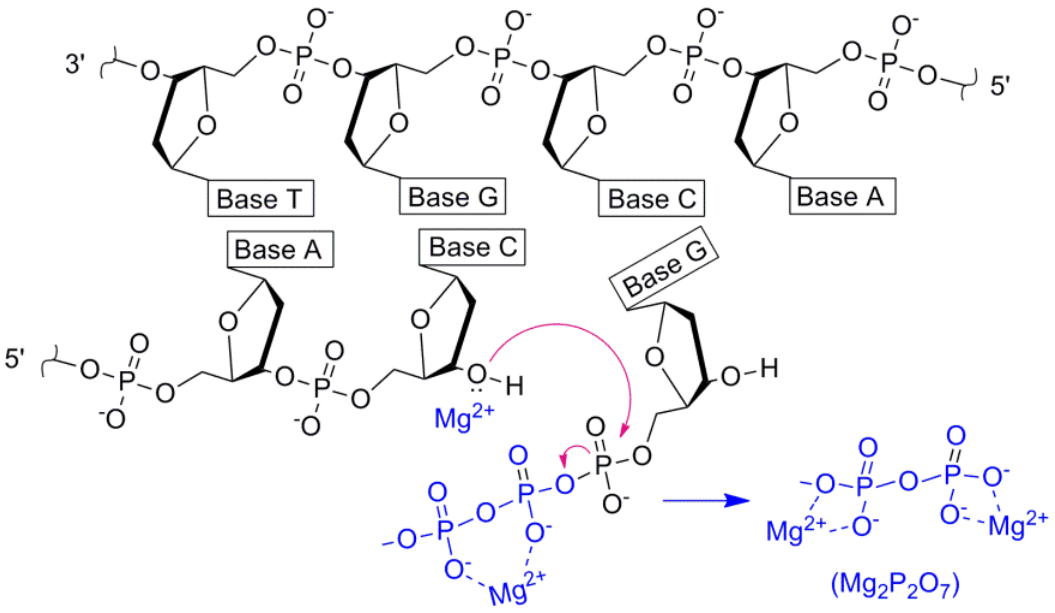

Figure 3.3. Schematic illustration of magnesium pyrophosphate generated *in situ*.

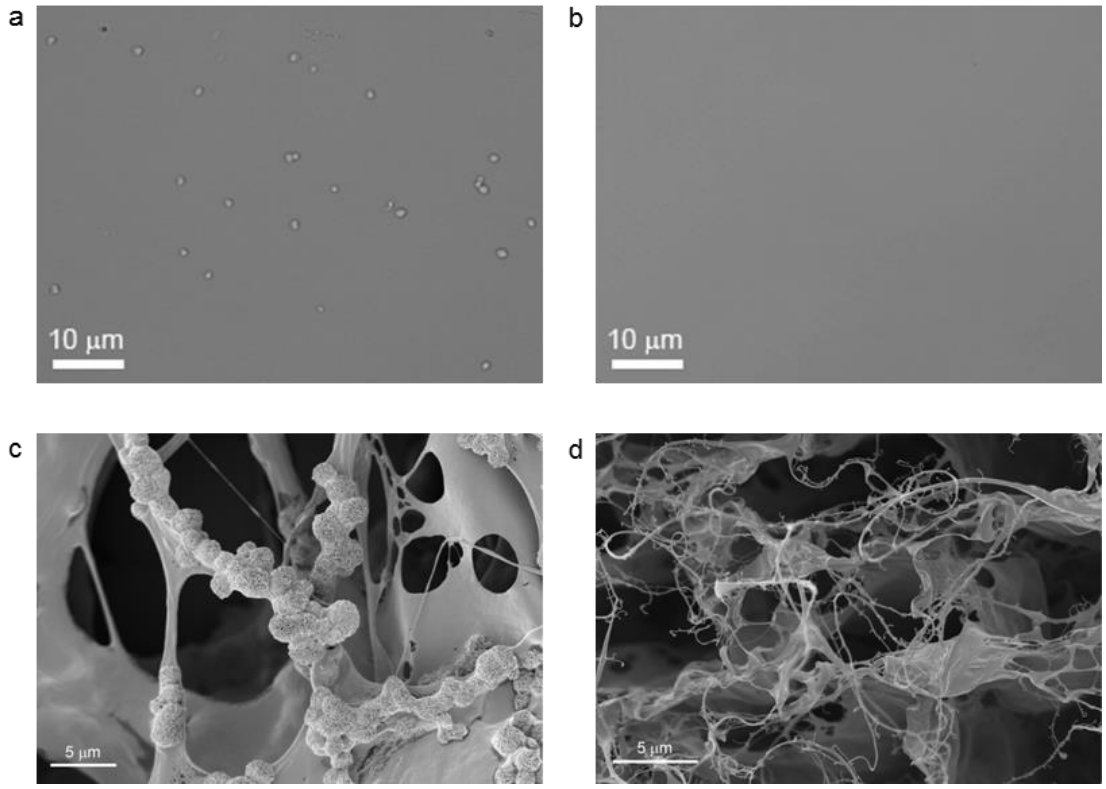

Figure 3.4. Optical and SEM images of the scudDNA treated with pyrosphosphatase. a-b, Light microscopy images of the scudDNA before (a) and after (b) inorganic pyrophosphatase. c-d, SEM images of DNA hydrogel before (**a**) and after (**b**) inorganic pyrophosphatase treatment. The DNA fibers compacted in the scudDNA were released after the enzyme treatment.

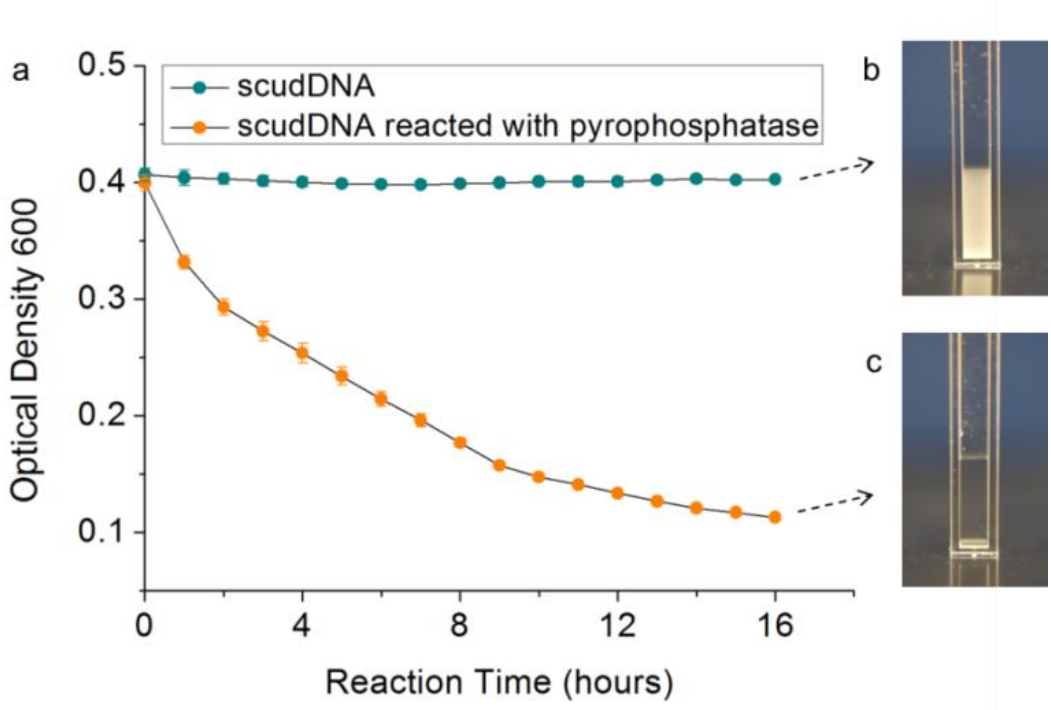

Figure 3.5. Optical density of the scudDNA treated with inorganic pyrophosphatase. **a,** The optical density at 600 nm remained the same for scudDNA without treatment, while it gradually decreased for the scudDNA treated with pyrophosphatase **b,c,** Photographs showed clear visual changes that the scudDNA turned from opaque (**b**) to transparent (**c**) after pyrophosphatase treatment.

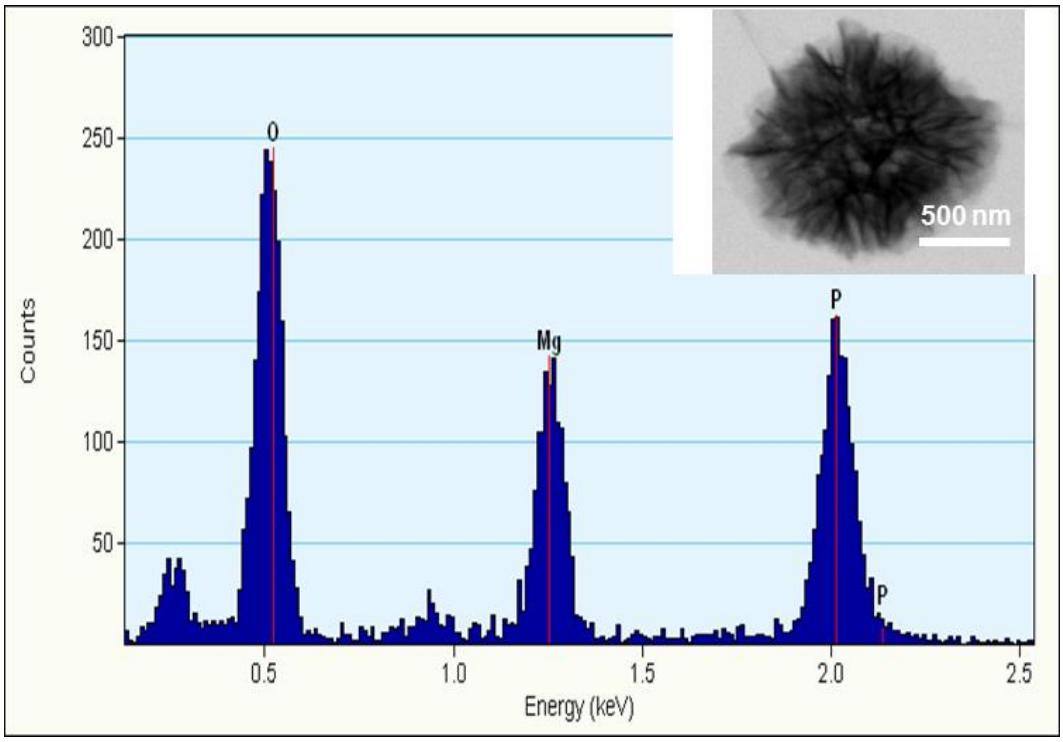

Figure 3.6. Elemental analysis of the scudDNA. The elemental analysis revealed that the scudDNA contained the elements of oxygen, magnesium and phosphorus, furthing indicating the presence of magesium pyrophosphate in the scudDNA structure. Other elements including carbon and nitrogen are beyond the detection capability of the X-ray setting in the TEM. Inset: TEM image of the scudDNA.

3.3.2 Enhanced immunostimulatory effects of scudDNA structure

Since each scudDNA comprised 7.2 million copies of the CpG motifs within one single microsphere (scudDNA or scudDNA^{+CpG}), and since CpG motif was known to elicit immune responses, we investigated the immunostimulatory effects of the scudDNA by incubating them with the mouse macrophage cells. The single-stranded CpG short DNA (shortDNA or shortDNA^{+CpG}) with the exact same CpG dose without scudDNA structure was used as controls throughout experiments. As expected, both scudDNA and shortDNA elicited the immunostimulatory response, characterized by the secretion of the TNF-α and IL-6 (Figure 3.7 a-b). Surprisingly, the scudDNA triggered a much stronger, up to 12 fold TNF-α and 88 fold IL-6 stimulatory responses compared to the shortDNA control (Figure 3.7 a-b), even though the CpG dose used were exactly the same. In addition, little stimulatory effect was observed for the scudDNA control, in which the CpG motif was not present in the scudDNA structure (scudDNA^{-CpG}, Figure 3.7c). These results clearly revealed that it was the scudDNA structure alone that greatly enhanced the potency of the CpG motif. For both scudDNA and shortDNA, the immunostimulatory effects exhibited generally a linear dose response to the concentration tested (from 0 to 800 nM, Figure 3.7 a-b). In addition, the CpG dose in each scudDNA can be readily tuned by designing DNA templates with different numbers of CpG motif, from 0 - 4 CpG/template, which corresponded to 0 - 14.4 million CpG/scudDNA (Figure 3.7c & Table 3.1). As a result, we adjusted scudDNA immunostimulatory effects both up and down effectively (Figure 3.7c). Moreover, the immune responses from scudDNA were further controlled, up and down again with different incubation time (Figure 3.8). Taken

together, our results suggested that scudDNA offered a wide window for tuning the immune responses by changing the dose per scudDNA, concentration, or incubation time.

In addition to the aforementioned built-in flexibility in tuning the immune responses, our scudDNA was stable both structurally and functionally against serum degradation. After 24 hour incubation with serum-containing cell culture media, most of the scudDNA was intact, while less than 1% shortDNA control remained (Figure 3.7d & Figure 3.9). The resistivity to degradation was probably due to the super-condensed structure that protected the DNA from being totally exposed to enzymes. From the functionality perspective, we exposed the scudDNA to the mouse macrophage cells after pretreating them for different amount of time. We found out that the scudDNA maintained most of the immunostimulatory activities (Figure 3.7 e-f), while the shortDNA control lost its entire function within 4 hours.

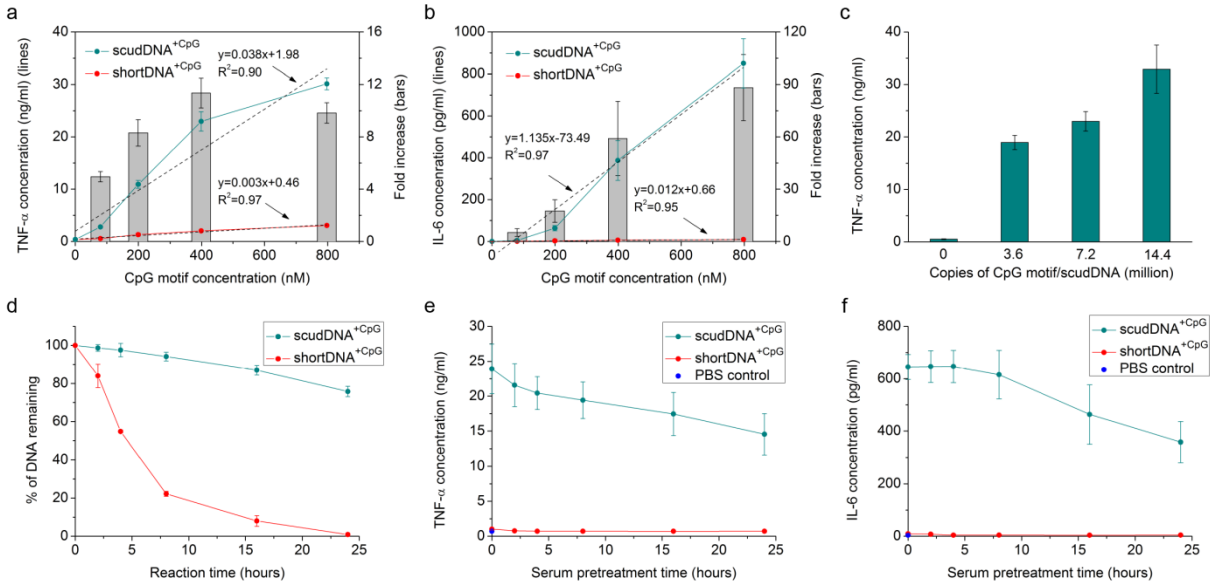

Figure 3.7. *In vitro* immunostimulatory effects of the scudDNA. **a-b,** TNF-α (**a**) and IL-6 (**b**) secreted by macrophage cells incubated with different concentrations of scudDNA^{+CpG} and control shortDNA^{+CpG} (1, 2,5, 5 and 10 μg/ml, equal to 80, 200, 400 and 800 nM of CpG motifs). **c**, The scudDNA was designed to have different doses of CpG motifs (0, 3.6, 7.2 and 14.4 million, respectively). Immunostimulatory effects of these four different scudDNA (scudDNA concentration was fixed at 5 μg/ml) was characterized by TNF-α secretion. **d**, Degradation of scudDNA^{+CpG} and shortDNA^{+CpG} in 10 % serum-containing cell culture media. **e-f,** The scudDNA^{+CpG} and shortDNA^{+CpG} (5 μg/ml) were pretreated with 10 % serum-containing cell culture media for various time (0, 2, 4, 8, 16 and 24 hours, respectively). The treated scudDNA^{+CpG} and shortDNA^{+CpG} were then incubated with the macrophage cells and the secreted TNF-α (**e**) and IL-6 (**f**) were detected. Error bars represent the standard deviation.

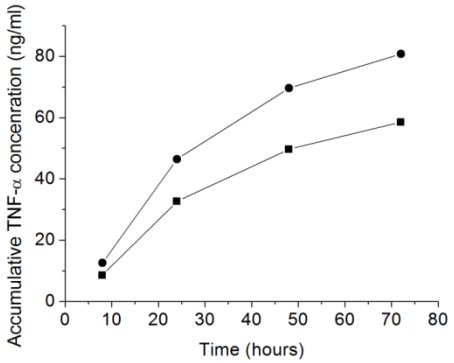

Figure 3.8. Time response curve of the accumulative TNF-α secretion. Macrophage cells were seeded in 48-well cell culture plate at a density of 40,000/well. After overnight incubation, the full cell culture medium was discarded. scudDNA^{+CpG} (10 μg/ml) in 200 μl DMEM with 10 % FBS were incubated with the cells for 8 hour and 10 μl supernatant was taken out and stored at -80 ^{o}C. The cells were incubated with the same media for another 16 hour and the supernatant was carefully replaced by 200 μl fresh DMEM with 10 % FBS. The media was changed every 24 hours and the TNF-α secreted into the media was quantified by ELISA.

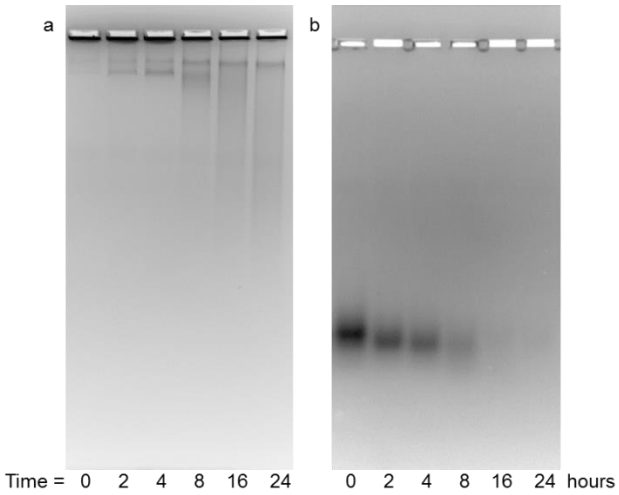

Figure 3.9. Agarose gel images for the degradation of scudDNA. The scudDNA^{+CpG} (a) and shortDNA^{+CpG} (b) were treated with the 10 % fetal bovine serum.

3.3.3 Uptake and release of scudDNA structure

CpG-based immune responses are mainly governed by the TLR9-mediated signal pathways[165], which require the interaction of CpG motif with the TLR9 located in the endosome[167], as well as maturation and acidification of the endosome[173, 174]. To explore whether or not immune cells can uptake our scudDNA without any transfection reagent, we first covalently labeled the scudDNA with a red fluorescence dye (Cy5, Figure 3.10); we then incubated the labeled scudDNA with the macrophage cells. Surprisingly, epifluorescence microscopy revealed that delivery efficiency reached 73% (Figure 3.11 a-b & Figure 3.12). The uptake was mainly due to the endocytosis, because little uptake was observed when the macrophage cells were incubated at 4 ^{o}C, a temperature that inhibited the endocytosis pathways (Figure 3.11 b-c). To further demonstrate the endocytosis-based uptake mechanism, we stained the cells with Lysotracker, a red dye specifically stained the endo-lysosome, and we observed that the green fluorescence-labeled scudDNA (Alex 488, Figure 3.10) was colocalized with the endo-lysosome (Figure 3.11 d-g). These results strongly indicated that our scudDNA efficiently entered the cell through endocytosis without adding any transfection reagent and was located within the endo-lysosome.

A critical question was how scudDNA, which was super-condensed, triggered immune response after endocytosed. We hypothesized that scudDNA self-released inside the endo-lysosome at low pH. Indeed, by incubating the scudDNA with different buffer solutions mimicking the endo-lysosome pH, we discovered that the DNA was gradually released from the scudDNA following the acidification of the solutions (Figure 3.11 g). The released DNA fibers from the scudDNA were

confirmed by the SEM images (Figure 3.11 h-i). In addition, fluorescence images showed that the intact scudDNA swelled at low pH (Figure 3.13). This volumetric swelling led to the de-condensing of the scudDNA, concurring to a low pH-triggered self-release mechanism. Similar to the aforementioned pyrophosphatase that hydrolyzed magnesium pyrophosphate to a more soluble magnesium phosphate, low pH also dissolved the magnesium pyrophosphate within the scudDNA, exposing the CpG motifs. All these data pointed to a pathway where our scudDNA was first endocytosed and then self-released DNA fibers upon low pH. These DNA fibers consist of ultra-high dose CpG motifs that were exposed and responsible for the interaction with the TLR9, leading towards an enhanced immune response in cultured cells.

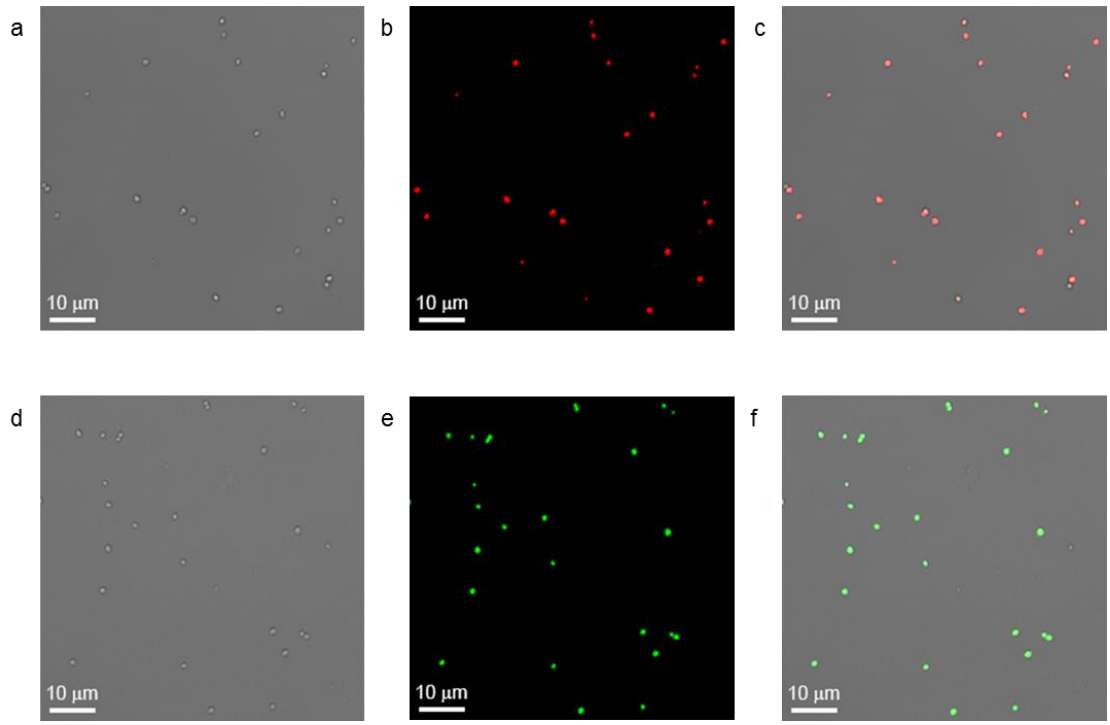

Figure 3.10. Optical microscopy images of the fluorescent scudDNA. Fluorescent labeled (cy-5 and Alexa 488) Primer-2 were used to generate fluorescent scudDNA. **a-c**, cy5-labeled red fluorescent scudDNA. **a,** bright field image. **b**, fluorescence image. **c**, merged image. **d-f,** Alexa 488-labeled green fluorescent scudDNA. **d**, bright field image. **e**, fluorescence image. **f**, merged image.

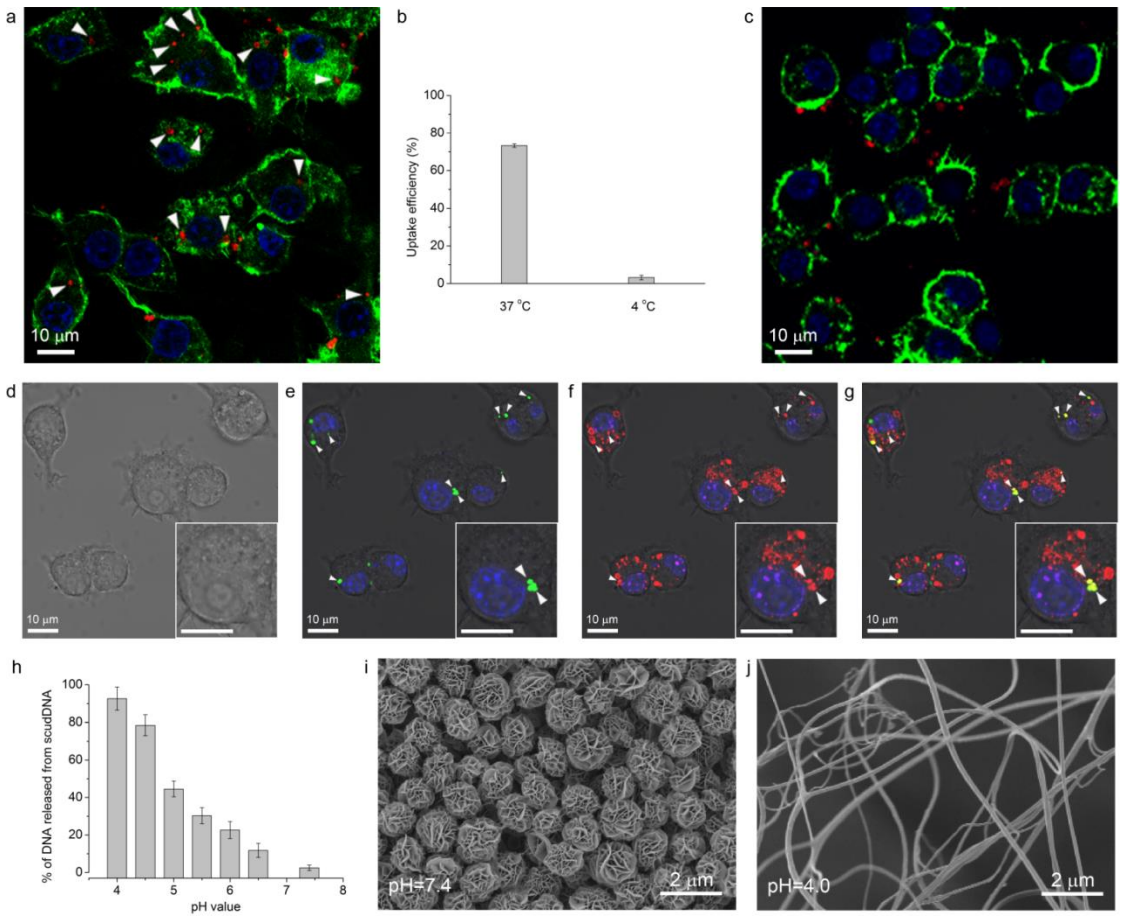

Figure 3.11. Cell uptake and self-releasing of the scudDNA. **a-c,** Macrophage cell uptake of the red fluorescence labeled scudDNA at 37 ^{o}C (**a**) and 4 ^{o}C (**c**). The actin in the cell was stained with green fluorescent color. Uptake efficiency of the scudDNA was quantified at 37 ^{o}C and 4 ^{o}C (**b**). **d-g,** Colocalization of the scudDNA with the endo-lysosome. Bright field microscopy image of the macrophage cells (**d**). The scudDNA was labeled with green fluorescence (**e**), and the endo-lysosome was stained with red fluorescence (**f**). The yellow fluorescence was the merged color (**g**), indicating that the endocytosed scudDNA was located in the endo-lysosome. The inset scale bar was 10 μm. **h,** scudDNA release in different pH buffers. **i-j**, SEM image of scudDNA treated with pH = 7.4 PBS (**i**) and pH = 4.0 sodium acetate buffer (**j).**

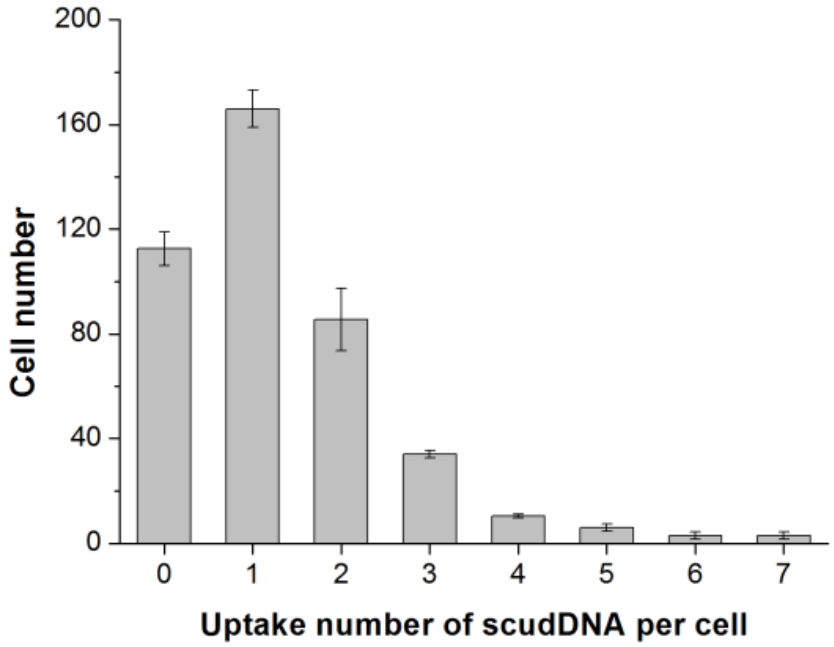

Figure 3.12. Number of scudDNA endocytosed by each cell.

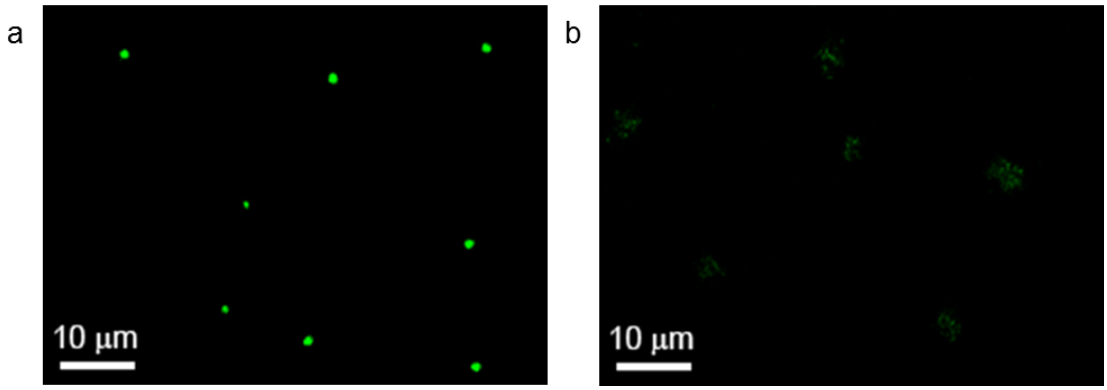

Figure 3.13. Fluorescent microscopy images of scudDNA treated with different pH buffer. a**,** pH = 7.4 PBS buffer. **b**, pH = 4.0 sodium acetate buffer.

3.3.4 Toxicity of scudDNA structure

Encouraged by the promising *in vitro* results, we tested our condensed DNA *in vivo* as a novel cancer immunotherapy drug. First, cytotoxicity was examined before injecting the scudDNA^{+CpG} into the mouse. No cytotoxicity was observed when the scudDNA^{+CpG} concentration reached as high as 20 μg/ml (equal to 1600 nM CpG concentration and 166 scudDNA/cell, Figure 3.14); this was expected mainly due to the fact that the scudDNA^{+CpG} was entirely composed of natural poDNA. The absence of any transfection reagents also contributed to the low cytotoxicity[171]. Second, injecting scudDNA^{+CpG} into the normal mice did not induce any measurable toxicity indicated by the blood chemistry, hematological analysis and histological analysis (Figure 3.15 & Figure 3.16).

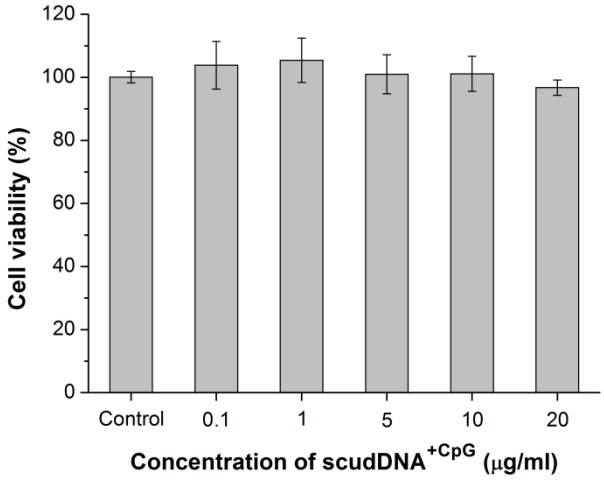

Figure 3.14. Cell viability after treating with scudDNA. Different concentrations of scudDNA^{+CpG} were incubated with mouse macrophage cells for overnight. The cell viability was evaluated by the MTT assay.

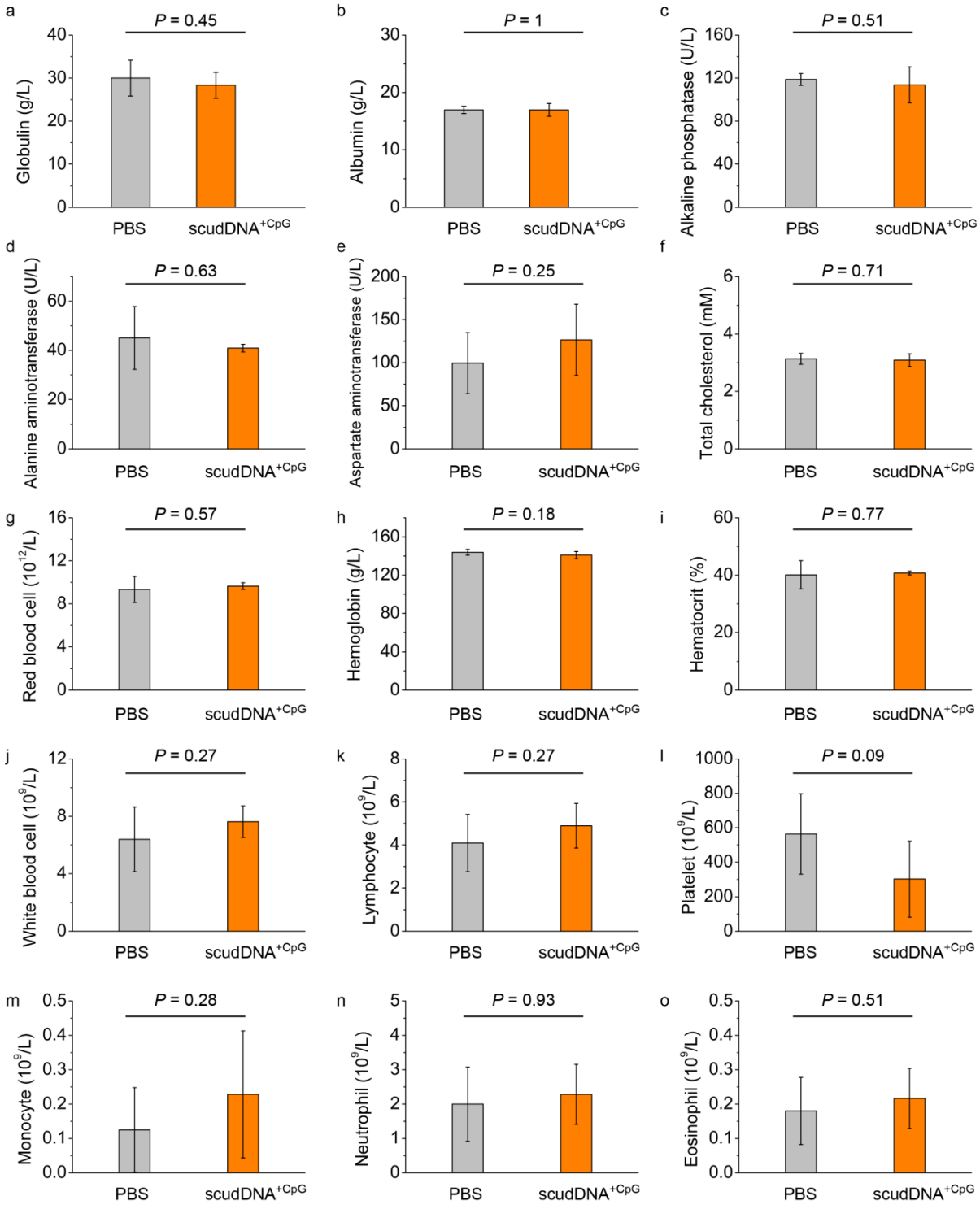

Figure 3.15. Blood toxicity of mice treated with scudDNA and PBS. Blood biochemistry (**a-f**) and hematology analysis (**g-o**) revealed that no significant

difference (determined by two-sample *t* test assuming unequal variances) was observed between scudDNA^{+CpG} treated mice (n = 6) and PBS controls, suggesting that scudDNA^{+CpG} did not induce *in vivo* toxicity. *p*-value larger than 0.05 was considered as not significant.

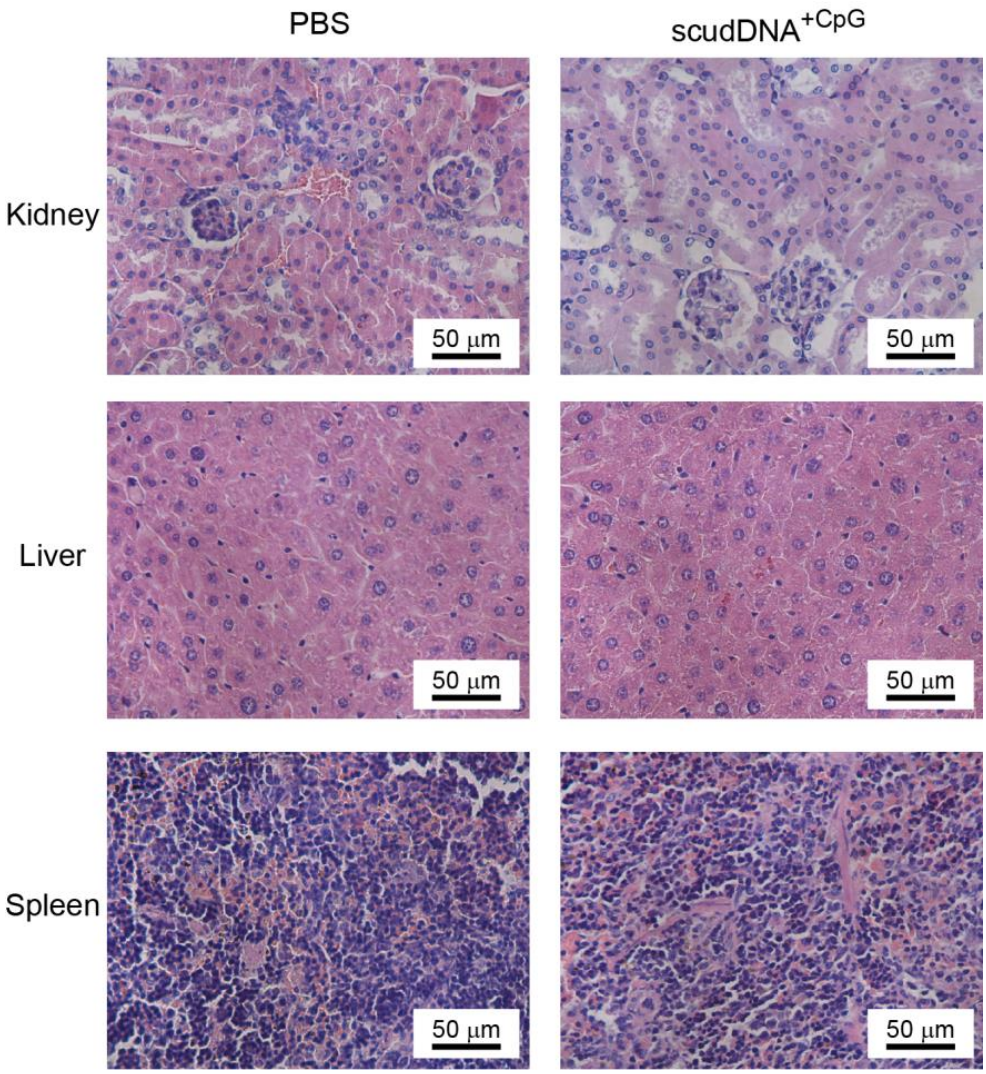

Figure 3.16. Organ toxicity of mice treated with scudDNA and PBS. The normal mice were treated with PBS, or scudDNA^{+CpG}. The mice kidney, live and spleen were harvested, fixed and sectioned for histological examination. No observable tissue damage, necrosis, or inflammation was observed.

3.3.5 Suppression of tumor growth in a mouse model by scudDNA structure

We then used an established murine colon carcinoma model and subjected tumor-bearing mice with our murine-specific CpG scudDNA (Figure 1g). Controls were scudDNA^{-CpG} and shortDNA^{+CpG}. Two days after injection, histology staining revealed that in the tumor tissue treated with scudDNA, abundant neutrophils were recruited with a great number of necrotic debris presented, indicating an inflammatory response was present (Figure 3.17a). On the other hand, few neutrophils were observed with obvious large amount of tumor cells for the controls (Figure 3.17 b-d). The tumor growth curve indicated an expected increase of tumor volume for the PBS control (Figure 3.18a, black squares). Injection of scudDNA^{-CpG} and shortDNA^{+CpG} controls did not affect tumor growth (Figure 3.18a, blue circles and red triangles, respectively). However, injection of our CpG scudDNA almost completely prevented the tumor from growing for all the mice (Figure 3.18a, inverted cyan triangles & Figure 3.19). Indeed, this dramatic inhibition of tumor growth was visualized by the retrieved tumors at day 34 from eight different mice (Figure 3.18b). Similarly, the average tumor weight from PBS, scudDNA^{-CpG} and shortDNA^{+CpG} controls reached 0.4 g after 34 days, respectively. In contrast, the average tumor weight was only 0.07 g for CpG scudDNA (Figure 3.18c). The survival rate of the mouse treated with scudDNA reached 87.5 % after 80 days, much higher compared to the control mice: the survival rate for PBS and scudDNA^{-CpG} was 0 % and 25 %, respectively (Figure 3.18d). Interestingly, the survival rate of shortDNA^{+CpG} control, which included the exact same amount of CpG motifs as our scudDNA, was 0 %, suggesting that both the scudDNA structure and the CpG motif were needed as a cancer immunotherapy drug.

It was of paramount importance to understand why the scudDNA structure enhanced CpG-based immunotherapy *in vivo*. From this research, at least four unique attributes of our scudDNA contributed to the therapeutic effects. First, our scudDNA compacted an unprecedentedly high dose of CpG motifs within one unit. Second, the condensed structure protected these high dose CpG motifs against serum degradation. Third, after uptake, the scudDNA self-released at endo-lysosome low pH and intracellular pyrophosphatase. And fourth, the scudDNA displayed superior local targeting *in vivo* (Figure 3.20i). In more detail, scudDNA, labeled with a tissue-penetrating infra-red fluorescent quantum dot (Ag_2S[175], Figure 3.20a), was administered intratumorly; their fate was followed in live animals in real-time (Figure 3.20b). Even though the same amount of the labeled shortDNA^{+CpG} and scudDNA were injected, the labeled shortDNA^{+CpG} rapidly disappeared from the tumor site within five minutes and diminished to 16 % after 24 hours (Figure 3.20b & Figure 3. 20c). In contrast, much more scudDNA were presented at the tumor site within five minutes compared to shortDNA^{+CpG} and 76 % still remained even after 24 hours (Figure 3.20b & Figure 3. 20c).

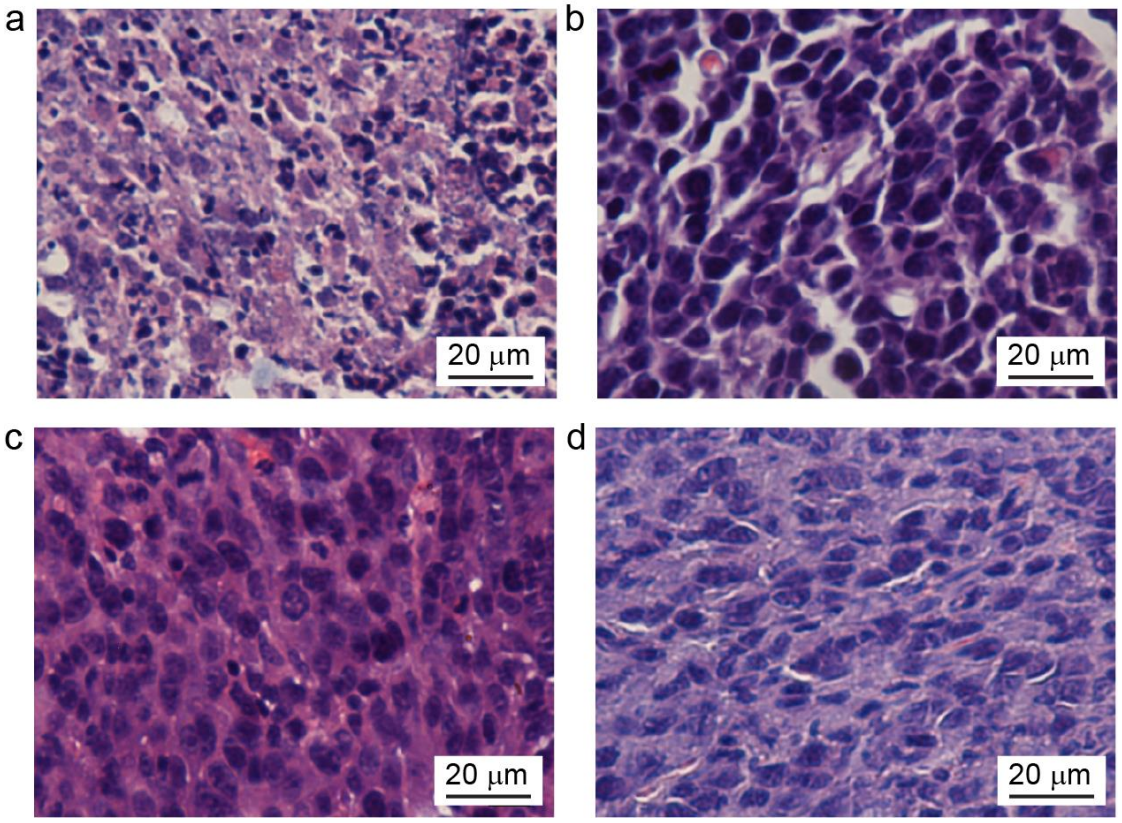

Figure 3.17. Histology stain of the tumor tissue after scudDNA treatment. **a-d,** Histological stain of the tumor tissue treated with scudDNA^{+CpG} (**a**), PBS (**b**), control scudDNA^{-CpG} (**c**), and control shortDNA^{+CpG} (**d**).

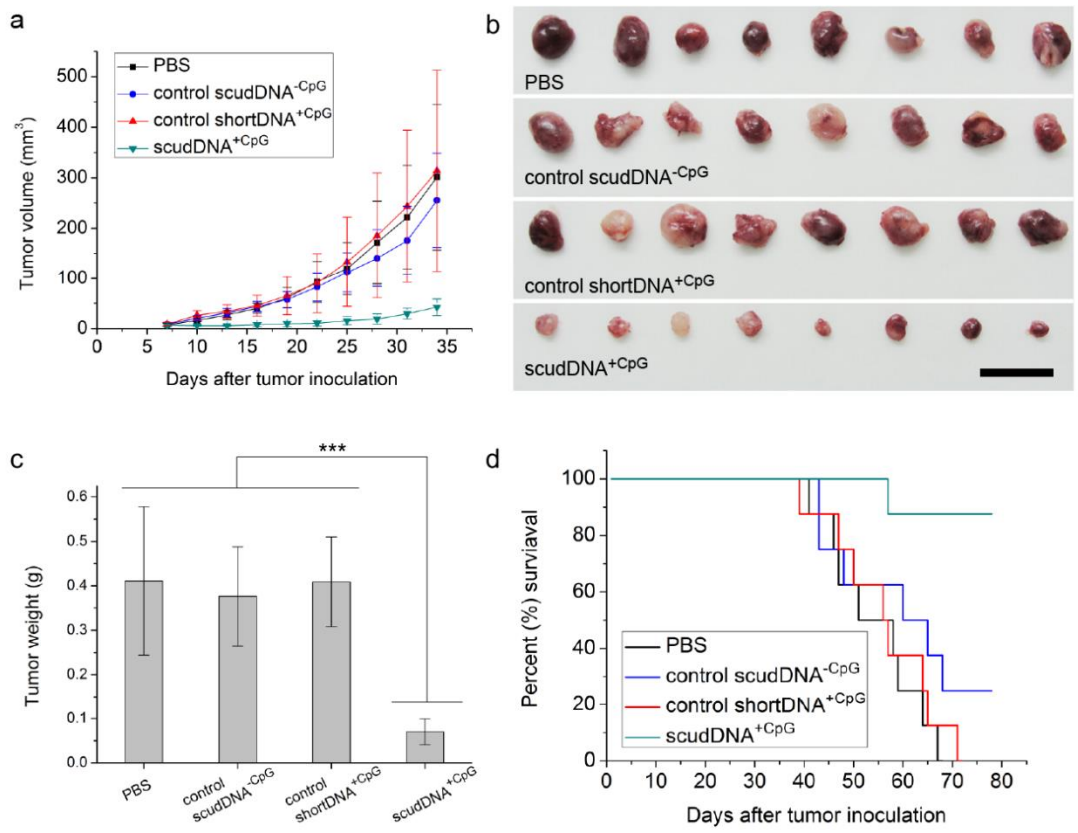

Figure 3.18. *In vivo* suppression of tumor growth by the scudDNA. **a**, Average tumor volume versus time of mice treated with scudDNA^{+CpG} and controls (PBS, scudDNA^{-CpG} and shortDNA^{+CpG}) (n = 8) ($P < 0.01$). **b-c**, Images (**b**) and weight (**c**) of the retrieved tumors at day 34. Scale bar: 2 cm. *** $P < 0.001$. **d**, Kaplan-Meier survival curves of mice treated with scudDNA^{+CpG} and controls (PBS, scudDNA^{-CpG} and shortDNA^{+CpG}) (n = 8). scudDNA^{+CpG} increased survival significantly over controls; for *p*-values for all comparisons, determined by log-rank test, see Table 3.2.

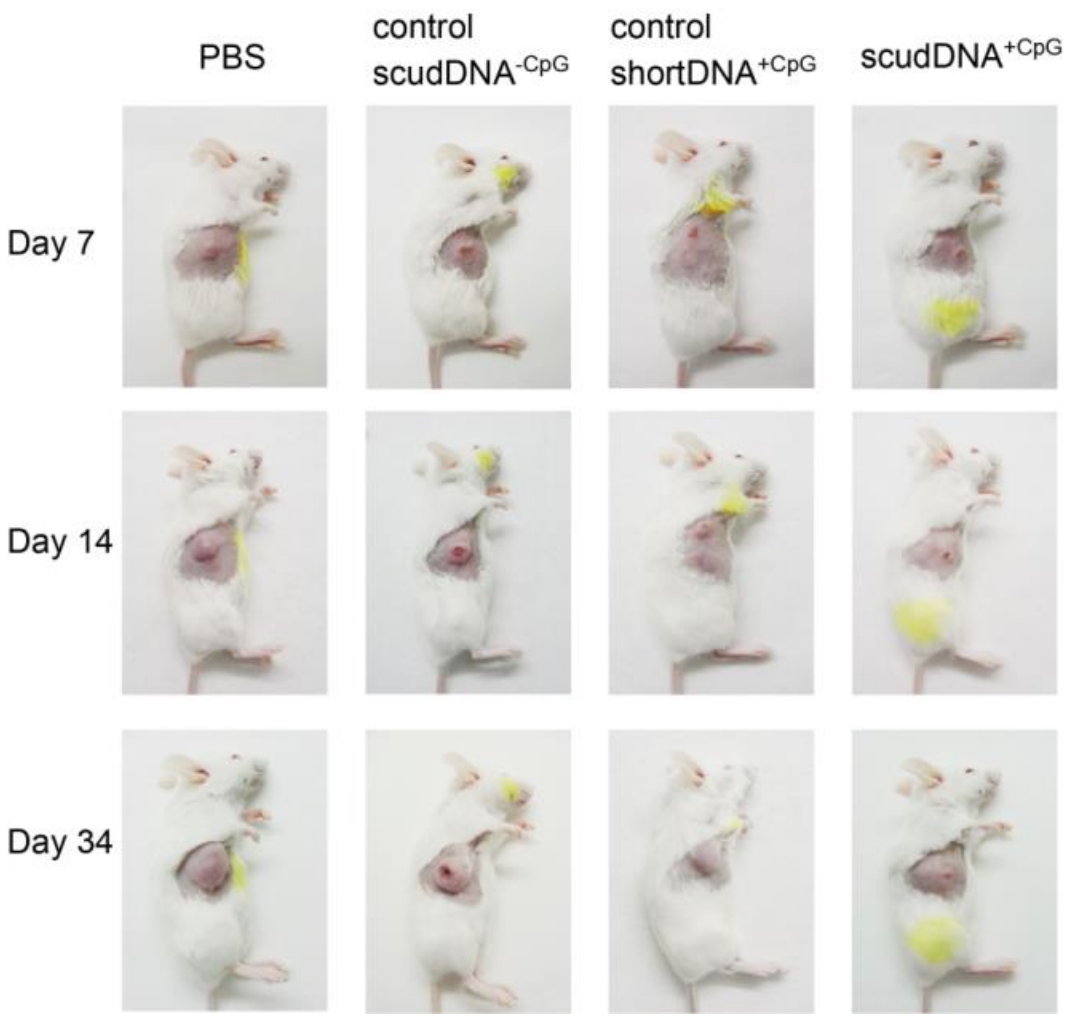

Figure 3.19. Representative images of tumor-bearing mice after treatment. The mice were treated with PBS, control scudDNA^{-CpG}, control shortDNA^{+CpG}, and scudDNA^{+CpG}. Representative images were taken.

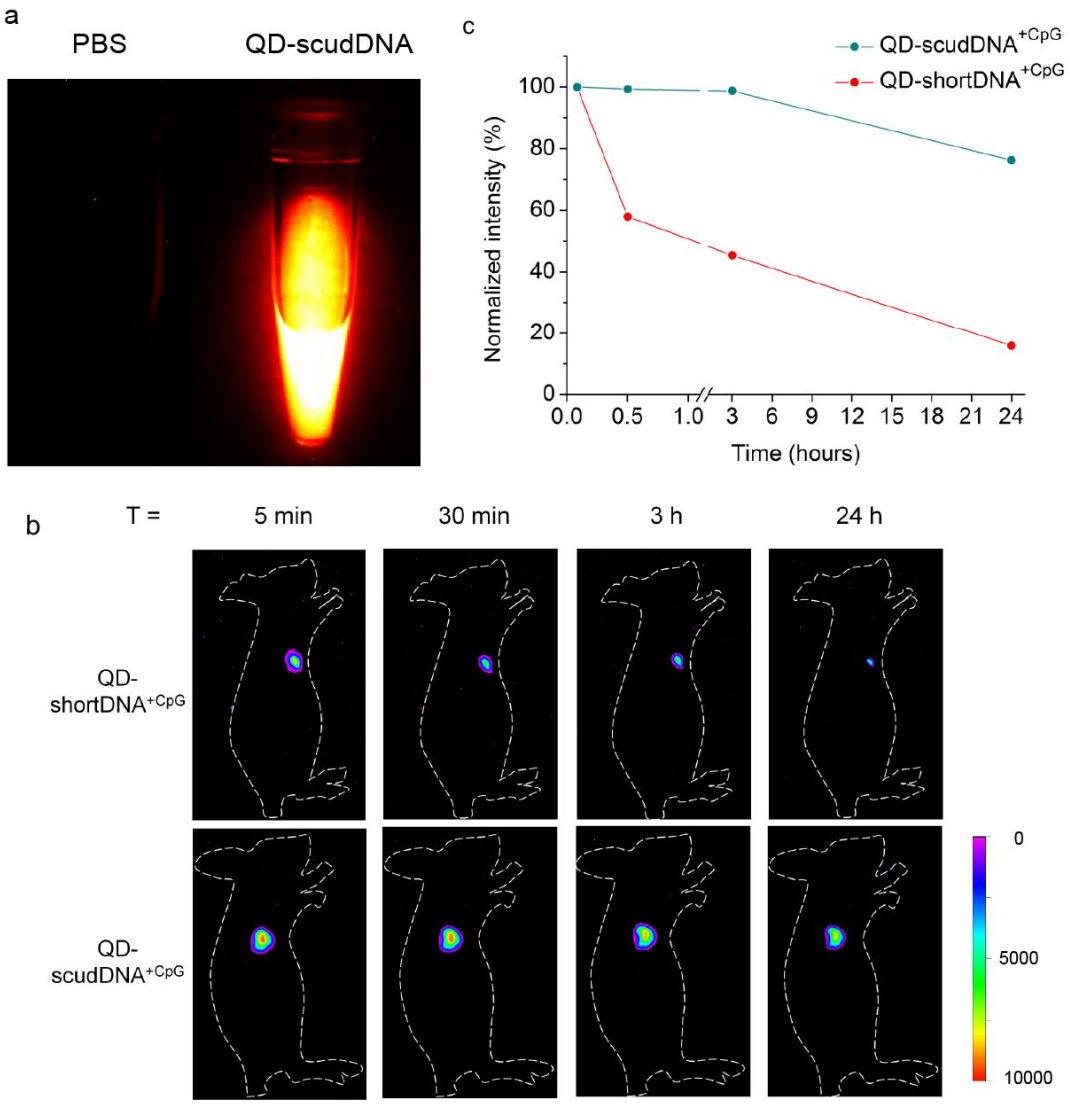

Figure 3.20. *In vivo* tracking of the scudDNA. **a**, Infra-red fluorescent image of the PBS and QD-labeled scudDNA^{+CpG}. **b**, Infra-red fluorescent images of the mice treated with QD-labeled shortDNA^{+CpG} and QD-labeled scudDNA^{+CpG}. **c**, Normalized *in vivo* infra-red fluorescence intensity of QD-labeled scudDNA^{+CpG} and QD-labeled shortDNA^{+CpG} versus time. The infra-red intensities at 30 min, 3 h and 24 h were normalized to the infra-red intensity at 5 min.

3.4 Conclusion

We have demonstrated for the first time that a scudDNA structure, which compacted more than seven million doses of CpG in a single microsphere, elicited much higher immune responses *in vitro*. In particular, this scudDNA almost completely suppressed tumor growth *in vivo* without causing any measurable toxicity, providing an exciting novel DNA-based drug for cancer immunotherapy. Our research indicated that a super-condensed DNA physical structure can be effectively used for addressing the grand challenge of formulating a very high effective dose without causing toxicities.

Excitingly, our scudDNA is not limited to CpG motifs. Other immunostimulatory or immunosuppressive DNA sequences can be easily designed into the scudDNA structure. In addition, gene sequence has also been successfully employed to produce scudDNA for protein production (data not shown), which can be utilized for gene therapy and DNA vaccines. Moreover, by using RNA-dependent RNA polymerase, scudRNA can be achieved for RNAi-based therapies. Thus, our scudDNA provides a versatile platform to effectively compact and deliver the nucleic-acid based therapeutics.

Table 3.1: DNA sequences for producing the scudDNA.

Strand	Sequence
Immune DNA template (shortDNA^{+CpG})	5'-phosphate-TAGTTTTCCATGACGTTCCTGACGTTAAGCAGTATTATGAACTCTCCATGAGCTTCCTGAGCTTGATGTTCCTAACCTACCA
Primer 1	5'-GTCATGGAAAACTATGGTAGGTTAGGAAC
Primer 2	5'-AAGCAGTATTATGAACTC
Primer 3	5'-TGGTAGGTTAGGAACATC
0 CpG template	5'- phosphate-TAGTTTTCCATGAGCTTCCTGAGCTTAAGCAGTATTATGAACTCTCCATGAGCTTCCTGAGCTTGATGTTCCTAACCTACCA
1 CpG template	5'- phosphate-TAGTTTTCCATGACGTTCCTGAGCTTAAGCAGTATTATGAACTCTCCATGAGCTTCCTGAGCTTGATGTTCCTAACCTACCA
4 CpG template	5'- phosphate-TAGTTTTCCATGACGTTCCTGACGTTAAGCAGTATTATGAACTCTCCATGACGTTCCTGACGTTGATGTTCCTAACCTACCA

Table 3.2: *P*-values determined by log-rank test for survival curve comparisons.

	PBS	control scudDNA^{-CpG}	control shortDNA^{+CpG}
control scudDNA^{-CpG}	N.S.	---	N.S.
control shortDNA^{+CpG}	N.S.	N.S.	---
scudDNA^{+CpG}	0.0004	0.0151	0.0003

p-value larger than 0.05 was considered as not significant (N.S.).

CHAPTER 4: CONCLUSION AND FUTURE PERSPECTIVE

4.1 Conclusion

A physically entangled bulk-scale DNA hydrogel has been created for the first time. The hydrogel is produced from two specially designed enzymatic processes: multi-primed chain amplification and rolling circle amplification. These enzymatic amplification processes generate a great amount of ultra-long DNA chains and weave them together to form a hydrogel. Due to the amplification power of polymerase reaction, the DNA hydrogel is synthesized with high efficiency and low cost, and can be readily scaled up. Our method provides a novel approach to produce bulk-scale DNA materials for real-world application.

Interestingly, our hydrogel has unusual mechanical properties that are not found in nature of any kind: it has both solid-like and liquid-like properties. When the gel is immersed in water, it memorizes its original shape and behaves like a solid. However, the hydrogel becomes free-flowing “liquid” after taken out of water, and metamorphoses back to its original shape upon addition of water. This liquid-to-solid transition can be repeated as many times as wanted. The unusually mechanical property of the DNA hydrogel is explained by its unique internal hierarchical structures and the stresses applied to the hydrogel. The hydrogel is composed of ultra-long DNA chains, which are not chemically linked but physically entangled with each other. This special composition enables the gel to possess an ultra-low elastic modulus, while have an extremely high elasticity. Thus, when the gel is taken out of water, the gravity and surface tension are able to deform the gel as much as 20 fold,

giving the gel to a liquid-like behavior. On the other hand, when the gel is immersed in water, the gravitational stress is canceled by the buoyance stress, and the surface tension is practically zero, thus the gel returns to its original shape and behaves like a solid.

More interestingly, the hydrogel is composed of a huge amount of uniformly sized DNA microspheres. These microspheres can be easily isolated from the DNA hydrogel with high efficiency and yield. To our surprise, the DNA density in the microspheres reaches as high as the human chromosome density in the metaphase. Such high DNA density might be able to condense ultra-high dose of DNA drugs. Indeed, by using immunostimulatory CpG drug as an example, we create for the first time a super-condensed ultra-high dose DNA (scudDNA) structure, which compacted more than seven million doses of CpG in a single microsphere.

Our scudDNA triggers a significantly enhanced immunostimulatory responses *in vitro* compared to the linear CpG DNA without the scudDNA structure. The superior potency is due to the fact that sucdDNA effectively protects the condensed DNA, efficiently enters the cell and releases the DNA. More importantly, this scudDNA almost completely suppresses tumor growth *in vivo* without causing any measurable toxicity, providing an exciting novel DNA-based drug for cancer immunotherapy. On the other hand, linear CpG DNA with the exact same amount dose of the scudDNA but without the scudDNA structure does not show any therapeutic effect. Our results indicate that this super-condensed physical structure can serve as an effectively drug formulation used for addressing the grand challenge of formulating a very high effective dose without causing toxicities.

4.2 Future perspective

4.21 Synthesis of the physically entangled DNA hydrogel

One of the grand challenges of creating DNA materials for real-world applications is how to prepare DNA materials with high yield, large scale and low cost. While our physically entangled DNA hydrogel might be able to address this challenge, further improvements can be made. The main cost for the physically entangled DNA hydrogel is the Φ29 and dNTP. Methods to further reduce the cost are desirable.

We have demonstrated the gel has a unique internal structure, which results the unusual mechanical properties. However, the internal structure is only revealed at the nanometer to micrometer scale. Studying the structure from the molecular level, such as using labeled primers to track the gel formation process in real time, would greatly deepen our understanding in the unique structures and the unusual properties. In addition, in the current circular DNA template design, we intentionally avoid any secondary structure in the template. While this design greatly helps increase the yield of DNA polymerization, it always results in a similar DNA structure. Building secondary structures into the template, such as hairpin structures, might be able to produce a DNA hydrogel with different internal structure, which may lead to entirely different bulk-scale mechanical properties.

Furthermore, due to the generality of enzymatic reactions, our two-step enzymatic amplification processes can be extended to synthesize other nucleic acid based hydrogels. For instance, RNA has shown tremendous biomedical application. However, preparing RNA materials in bulk scale is even more challenging than DNA

materials, because of the fast degradation of RNA as well as the abundance of ribonuclease in the environment. Thus, no RNA hydrogel has ever been synthesized so far. Our method can be easily applied to the RNA hydrogel synthesis by replacing the DNA dependent polymerase to RNA dependent polymerase.

In addition to the preparing pure nucleic acid material, our DNA hydrogel can also be explored in producing hybrid materials. Our DNA hydrogel has a superb elastic behavior with up to 2000 % strain. However, the strength of the gel is very low. One interesting research direction is whether introducing other materials, such as forming interpenetrating network, would be able to increase the strength of the DNA hydrogel while maintain its elasticity to achieve ultra-tough and ultra-elastic materials.

4.22 Applications of the physically entangled DNA hydrogel

From the macroscopic, no other hydrogels can flow like a liquid as our DNA hydrogel. By taking advantage of this unique property, we have demonstrated a circuit using water as an electrical switch. Other applications can also be imaged. For instance, hydrogels have been utilized for wound healing, due to the facts including high water content, porous structure allowing the oxygen penetration, and capability to load drugs. However, it is very difficult for the conventional solid hydrogel to totally cover the wound, which usually cause the infection of the uncovered wound. Our liquid-like DNA hydrogel can easily address this challenge. In addition, different drugs can be loaded to the gel either during the gelation process or after the gelation. Moreover, our gel is prepared in a physiologically relevant buffer condition, making it conveniently to be adapted to the biomedical application.

From the microscopic, we have isolated the DNA microsphere from the DNA

hydrogel, creating a super-condensed ultra-high dose DNA (scudDNA) as a novel immunotherapy drug. Besides cancer therapy, our scudDNA can also be used as vaccine adjuvant, due to its great potency to trigger the immune system. More excitingly, our scudDNA is not limited to immunostimulotary CpG motifs. Other immunostimulatory or immunosuppressive DNA sequences can be easily designed into the scudDNA structure. In addition, gene sequence has also been successfully employed to produce scudDNA for protein production, which can be utilized for gene therapy and DNA vaccines. Moreover, by using RNA-dependent RNA polymerase, scudRNA can be achieved for RNAi-based therapies. Thus, our scudDNA provides a versatile platform to effectively compact and deliver the nucleic-acid based therapeutics.

BIBLIOGRAPHY

1. Peng, S.M., Derrien, T.L., Cui, J.H., Xu, C.Y. & Luo, D. From cells to DNA materials. *Mater Today* **15**, 190-194 (2012).
2. Roh, Y.H., Ruiz, R.C.H., Peng, S.M., Lee, J.B. & Luo, D. Engineering DNA-based functional materials. *Chem Soc Rev* **40**, 5730-5744 (2011).
3. Luo, D. The road from biology to materials. *Mater Today* **6**, 38-43 (2003).
4. Roberts, R.J., Vincze, T., Posfai, J. & Macelis, D. REBASE - enzymes and genes for DNA restriction and modification. *Nucleic Acids Res* **35**, D269-D270 (2007).
5. Roberts, R.J., Vincze, T., Posfai, J. & Macelis, D. REBASE-a database for DNA restriction and modification: enzymes, genes and genomes. *Nucleic Acids Res* **38**, D234-D236 (2010).
6. Caruthers, M. Gene synthesis machines: DNA chemistry and its uses. *Science* **230**, 281-285 (1985).
7. Kosuri, S. & Church, G.M. Large-scale de novo DNA synthesis: technologies and applications. *Nature methods* **11**, 499-507 (2014).
8. Dormitzer, P.R. et al. Synthetic Generation of Influenza Vaccine Viruses for Rapid Response to Pandemics. *Sci Transl Med* **5** (2013).
9. Sano, T., Smith, C.L. & Cantor, C.R. Immuno-Pcr - Very Sensitive Antigen-Detection by Means of Specific Antibody-DNA Conjugates. *Science* **258**, 120-122 (1992).
10. Niemeyer, C.M., Wacker, R. & Adler, M. Combination of DNA-directed

immobilization and immuno-PCR: very sensitive antigen detection by means of self-assembled DNA-protein conjugates. *Nucleic Acids Res* **31** (2003).

11. Wilner, O.I. et al. Enzyme cascades activated on topologically programmed DNA scaffolds. *Nat Nanotechnol* **4**, 249-254 (2009).
12. Bailey, R.C., Kwong, G.A., Radu, C.G., Witte, O.N. & Heath, J.R. DNA-encoded antibody libraries: A unified platform for multiplexed cell sorting and detection of genes and proteins. *J Am Chem Soc* **129**, 1959-1967 (2007).
13. Niemeyer, C.M. The developments of semisynthetic DNA-protein conjugates. *Trends Biotechnol* **20**, 395-401 (2002).
14. Niemeyer, C.M. Functional devices from DNA and proteins. *Nano Today* **2**, 42-52 (2007).
15. Niemeyer, C.M. Semisynthetic DNA-Protein Conjugates for Biosensing and Nanofabrication. *Angew Chem Int Edit* **49**, 1200-1216 (2010).
16. Kwong, G.A. et al. Modular Nucleic Acid Assembled p/MHC Microarrays for Multiplexed Sorting of Antigen-Specific T Cells. *J Am Chem Soc* **131**, 9695-9703 (2009).
17. Alemdaroglu, F.E., Wang, J., Borsch, M., Berger, R. & Herrmann, A. Enzymatic control of the size of DNA block copolymer nanoparticles. *Angew Chem Int Edit* **47**, 974-976 (2008).
18. Gibbs, J.M. et al. Polymer-DNA hybrids as electrochemical probes for the detection of DNA. *J Am Chem Soc* **127**, 1170-1178 (2005).
19. Immoos, C.E., Lee, S.J. & Grinstaff, M.W. DNA-PEG-DNA triblock macromolecules for reagentless DNA detection. *J Am Chem Soc* **126**, 10814-

10815 (2004).

20. Kwak, M. & Herrmann, A. Nucleic Acid/Organic Polymer Hybrid Materials: Synthesis, Superstructures, and Applications. *Angew Chem Int Edit* **49**, 8574-8587 (2010).

21. Safak, M., Alemdaroglu, F.E., Li, Y., Ergen, E. & Herrmann, A. Polymerase chain reaction as an efficient tool for the preparation of block copolymers. *Adv Mater* **19**, 1499-+ (2007).

22. Watson, K.J., Park, S.J., Im, J.H., Nguyen, S.T. & Mirkin, C.A. DNA-block copolymer conjugates. *J Am Chem Soc* **123**, 5592-5593 (2001).

23. Cheng, W.L., Park, N.Y., Walter, M.T., Hartman, M.R. & Luo, D. Nanopatterning self-assembled nanoparticle superlattices by moulding microdroplets. *Nat Nanotechnol* **3**, 682-690 (2008).

24. Cheng, W.L. et al. Free-standing nanoparticle superlattice sheets controlled by DNA. *Nat Mater* **8**, 519-525 (2009).

25. Tan, S.J., Campolongo, M.J., Luo, D. & Cheng, W.L. Building plasmonic nanostructures with DNA. *Nat Nanotechnol* **6**, 268-276 (2011).

26. Mirkin, C.A., Letsinger, R.L., Mucic, R.C. & Storhoff, J.J. A DNA-based method for rationally assembling nanoparticles into macroscopic materials. *Nature* **382**, 607-609 (1996).

27. Alivisatos, A.P. et al. Organization of 'nanocrystal molecules' using DNA. *Nature* **382**, 609-611 (1996).

28. Park, S.Y. et al. DNA-programmable nanoparticle crystallization. *Nature* **451**, 553-556 (2008).

29. Elghanian, R., Storhoff, J.J., Mucic, R.C., Letsinger, R.L. & Mirkin, C.A. Selective colorimetric detection of polynucleotides based on the distance-dependent optical properties of gold nanoparticles. *Science* **277**, 1078-1081 (1997).

30. Nykypanchuk, D., Maye, M.M., van der Lelie, D. & Gang, O. DNA-guided crystallization of colloidal nanoparticles. *Nature* **451**, 549-552 (2008).

31. Smith, S.B., Cui, Y.J. & Bustamante, C. Overstretching B-DNA: The elastic response of individual double-stranded and single-stranded DNA molecules. *Science* **271**, 795-799 (1996).

32. Cluzel, P. et al. DNA: An extensible molecule. *Science* **271**, 792-794 (1996).

33. Hagerman, P.J. Flexibility of DNA. *Annu Rev Biophys Bio* **17**, 265-286 (1988).

34. Tinland, B., Pluen, A., Sturm, J. & Weill, G. Persistence length of single-stranded DNA. *Macromolecules* **30**, 5763-5765 (1997).

35. Seeman, N.C. Nucleic-Acid Junctions and Lattices. *J Theor Biol* **99**, 237-247 (1982).

36. Aldaye, F.A., Palmer, A.L. & Sleiman, H.F. Assembling materials with DNA as the guide. *Science* **321**, 1795-1799 (2008).

37. Torring, T., Voigt, N.V., Nangreave, J., Yan, H. & Gothelf, K.V. DNA origami: a quantum leap for self-assembly of complex structures. *Chem Soc Rev* **40**, 5636-5646 (2011).

38. Chen, J.H. & Seeman, N.C. Synthesis from DNA of a Molecule with the Connectivity of a Cube. *Nature* **350**, 631-633 (1991).

39. Winfree, E., Liu, F.R., Wenzler, L.A. & Seeman, N.C. Design and self-

assembly of two-dimensional DNA crystals. *Nature* **394**, 539-544 (1998).

40. Zheng, J.P. et al. From molecular to macroscopic via the rational design of a self-assembled 3D DNA crystal. *Nature* **461**, 74-77 (2009).

41. Rothemund, P.W.K. Folding DNA to create nanoscale shapes and patterns. *Nature* **440**, 297-302 (2006).

42. Douglas, S.M. et al. Self-assembly of DNA into nanoscale three-dimensional shapes. *Nature* **459**, 414-418 (2009).

43. Han, D.R. et al. DNA Origami with Complex Curvatures in Three-Dimensional Space. *Science* **332**, 342-346 (2011).

44. He, Y. et al. Hierarchical self-assembly of DNA into symmetric supramolecular polyhedra. *Nature* **452**, 198-U141 (2008).

45. Douglas, S.M., Bachelet, I. & Church, G.M. A Logic-Gated Nanorobot for Targeted Transport of Molecular Payloads. *Science* **335**, 831-834 (2012).

46. Wei, B., Dai, M.J. & Yin, P. Complex shapes self-assembled from single-stranded DNA tiles. *Nature* **485**, 623-+ (2012).

47. Ke, Y.G., Ong, L.L., Shih, W.M. & Yin, P. Three-Dimensional Structures Self-Assembled from DNA Bricks. *Science* **338**, 1177-1183 (2012).

48. Liedl, T., Sobey, T.L. & Simmel, F.C. DNA-based nanodevices. *Nano Today* **2**, 36-41 (2007).

49. Li, H.Y., Carter, J.D. & LaBean, T.H. Nanofabrication by DNA self-assembly. *Mater Today* **12**, 24-32 (2009).

50. Feldkamp, U. & Niemeyer, C.M. Rational design of DNA nanoarchitectures. *Angew Chem Int Edit* **45**, 1856-1876 (2006).

51. Pinheiro, A.V., Han, D.R., Shih, W.M. & Yan, H. Challenges and opportunities for structural DNA nanotechnology. *Nat Nanotechnol* **6**, 763-772 (2011).

52. Seeman, N.C. DNA in a material world. *Nature* **421**, 427-431 (2003).

53. Woo, S. & Rothemund, P.W.K. Programmable molecular recognition based on the geometry of DNA nanostructures. *Nat Chem* **3**, 620-627 (2011).

54. Seeman, N.C. Nanomaterials Based on DNA. *Annu Rev Biochem* **79**, 65-87 (2010).

55. Sharma, J. et al. Control of Self-Assembly of DNA Tubules Through Integration of Gold Nanoparticles. *Science* **323**, 112-116 (2009).

56. Deng, Z.X., Tian, Y., Lee, S.H., Ribbe, A.E. & Mao, C.D. DNA-encoded self-assembly of gold nanoparticles into one-dimensional arrays. *Angew Chem Int Edit* **44**, 3582-3585 (2005).

57. Wang, G.L. & Murray, R.W. Controlled assembly of monolayer-protected gold clusters by dissolved DNA. *Nano Lett* **4**, 95-101 (2004).

58. Le, J.D. et al. DNA-templated self-assembly of metallic nanocomponent arrays on a surface. *Nano Lett* **4**, 2343-2347 (2004).

59. Zheng, J.W. et al. Two-dimensional nanoparticle arrays show the organizational power of robust DNA motifs. *Nano Lett* **6**, 1502-1504 (2006).

60. Cheng, W.L. et al. Probing in Real Time the Soft Crystallization of DNA-Capped Nanoparticles. *Angew Chem Int Edit* **49**, 380-384 (2010).

61. Maye, M.M., Kumara, M.T., Nykypanchuk, D., Sherman, W.B. & Gang, O. Switching binary states of nanoparticle superlattices and dimer clusters by

DNA strands. *Nat Nanotechnol* **5**, 116-120 (2010).

62. Rosi, N.L. & Mirkin, C.A. Nanostructures in biodiagnostics. *Chem Rev* **105**, 1547-1562 (2005).

63. Storhoff, J.J., Elghanian, R., Mucic, R.C., Mirkin, C.A. & Letsinger, R.L. One-pot colorimetric differentiation of polynucleotides with single base imperfections using gold nanoparticle probes. *J Am Chem Soc* **120**, 1959-1964 (1998).

64. Pathak, S., Choi, S.K., Arnheim, N. & Thompson, M.E. Hydroxylated quantum dots as luminescent probes for in situ hybridization. *J Am Chem Soc* **123**, 4103-4104 (2001).

65. Gerion, D. et al. Room-temperature single-nucleotide polymorphism and multiallele DNA detection using fluorescent nanocrystals and microarrays. *Anal Chem* **75**, 4766-4772 (2003).

66. Han, M.Y., Gao, X.H., Su, J.Z. & Nie, S. Quantum-dot-tagged microbeads for multiplexed optical coding of biomolecules. *Nat Biotechnol* **19**, 631-635 (2001).

67. Parak, W.J. et al. Conjugation of DNA to silanized colloidal semiconductor nanocrystalline quantum dots. *Chem Mater* **14**, 2113-2119 (2002).

68. Keren, K., Berman, R.S., Buchstab, E., Sivan, U. & Braun, E. DNA-Templated Carbon Nanotube Field-Effect Transistor. *Science* **302**, 1380-1382 (2003).

69. Zheng, M. et al. Structure-Based Carbon Nanotube Sorting by Sequence-Dependent DNA Assembly. *Science* **302**, 1545-1548 (2003).

70. Baughman, R.H., Zakhidov, A.A. & de Heer, W.A. Carbon Nanotubes--the

Route Toward Applications. *Science* **297**, 787-792 (2002).

71. Tu, X.M., Manohar, S., Jagota, A. & Zheng, M. DNA sequence motifs for structure-specific recognition and separation of carbon nanotubes. *Nature* **460**, 250-253 (2009).

72. Niemeyer, C.M., Sano, T., Smith, C.L. & Cantor, C.R. Oligonucleotide-Directed Self-Assembly of Proteins - Semisynthetic DNA Streptavidin Hybrid Molecules as Connectors for the Generation of Macroscopic Arrays and the Construction of Supramolecular Bioconjugates. *Nucleic Acids Res* **22**, 5530-5539 (1994).

73. Niemeyer, C.M., Koehler, J. & Wuerdemann, C. DNA-directed assembly of bienzymic complexes from in vivo biotinylated NAD(P)H : FMN oxidoreductase and luciferase. *Chembiochem* **3**, 242-245 (2002).

74. Piperberg, G., Wilner, O.I., Yehezkeli, O., Tel-Vered, R. & Willner, I. Control of Bioelectrocatalytic Transformations on DNA Scaffolds. *J Am Chem Soc* **131**, 8724-+ (2009).

75. Wang, F., Lu, C.H. & Willner, I. From Cascaded Catalytic Nucleic Acids to Enzyme-DNA Nanostructures: Controlling Reactivity, Sensing, Logic Operations, and Assembly of Complex Structures. *Chem Rev* **114**, 2881-2941 (2014).

76. Niemeyer, C.M., Adler, M. & Wacker, R. Detecting antigens by quantitative immuno-PCR. *Nat Protoc* **2**, 1918-1930 (2007).

77. Niemeyer, C.M., Adler, M. & Wacker, R. Lmmuno-PCR: high sensitivity detection of proteins by nucleic acid amplification. *Trends Biotechnol* **23**, 208-

216 (2005).

78. Malou, N. & Raoult, D. Immuno-PCR: a promising ultrasensitive diagnostic method to detect antigens and antibodies. *Trends Microbiol* **19**, 295-302 (2011).

79. Alemdaroglu, F.E., Safak, M., Wang, J., Berger, R. & Herrmann, A. DNA multiblock copolymers. *Chem Commun*, 1358-1359 (2007).

80. Li, Z., Zhang, Y., Fullhart, P. & Mirkin, C.A. Reversible and chemically programmable micelle assembly with DNA block-copolymer amphiphiles. *Nano Lett* **4**, 1055-1058 (2004).

81. Alemdaroglu, F.E., Ding, K., Berger, R. & Herrmann, A. DNA-templated synthesis in three dimensions: Introducing a micellar scaffold for organic reactions. *Angew Chem Int Edit* **45**, 4206-4210 (2006).

82. Alemdaroglu, F.E., Alemdaroglu, N.C., Langguth, P. & Herrmann, A. DNA block copolymer micelles - A combinatorial tool for cancer Nanotechnology. *Adv Mater* **20**, 899-+ (2008).

83. Lin, D.C., Yurke, B. & Langrana, N.A. Mechanical Properties of a Reversible, DNA-Crosslinked Polyacrylamide Hydrogel. *Journal of Biomechanical Engineering* **126**, 104-110 (2004).

84. Yang, H., Liu, H., Kang, H. & Tan, W. Engineering Target-Responsive Hydrogels Based on Aptamer−Target Interactions. *J Am Chem Soc* **130**, 6320-6321 (2008).

85. Zhu, Z. et al. An Aptamer Cross-Linked Hydrogel as a Colorimetric Platform for Visual Detection. *Angew Chem Int Edit* **49**, 1052-1056 (2010).

86. Wei, B., Cheng, I., Luo, K.Q. & Mi, Y. Capture and Release of Protein by a Reversible DNA-Induced Sol–Gel Transition System. *Angewandte Chemie* **120**, 337-339 (2008).

87. Xiong, X.L. et al. Responsive DNA-Based Hydrogels and Their Applications. *Macromol Rapid Comm* **34**, 1271-1283 (2013).

88. Dave, N., Chan, M.Y., Huang, P.J.J., Smith, B.D. & Liu, J.W. Regenerable DNA-Functionalized Hydrogels for Ultrasensitive, Instrument-Free Mercury(II) Detection and Removal in Water. *J Am Chem Soc* **132**, 12668-12673 (2010).

89. Liu, J.W. Oligonucleotide-functionalized hydrogels as stimuli responsive materials and biosensors. *Soft Matter* **7**, 6757-6767 (2011).

90. Khimji, I., Kelly, E.Y., Helwa, Y., Hoang, M. & Liu, J.W. Visual optical biosensors based on DNA-functionalized polyacrylamide hydrogels. *Methods* **64**, 292-298 (2013).

91. Qi, H. et al. DNA-directed self-assembly of shape-controlled hydrogels. *Nat Commun* **4** (2013).

92. Li, Y.G. et al. Controlled assembly of dendrimer-like DNA. *Nat Mater* **3**, 38-42 (2004).

93. Sil, D., Lee, J.B., Luo, D., Holowka, D. & Baird, B. Trivalent ligands with rigid DNA spacers reveal structural requirements for IgE receptor signaling in RBL mast cells. *Acs Chem Biol* **2**, 674-684 (2007).

94. Fréchet, J.M.J., Tomalia, D.A., Wiley, J. & Sons, I. Dendrimers and other dendritic polymers. (Wiley New York, 2001).

95. Freedman, K.O. et al. Diffusion of single star-branched dendrimer-like DNA. *J Phys Chem B* **109**, 9839-9842 (2005).

96. Li, Y.G., Cu, Y.T.H. & Luo, D. Multiplexed detection of pathogen DNA with DNA-based fluorescence nanobarcodes. *Nat Biotechnol* **23**, 885-889 (2005).

97. Lee, J.B. et al. Multifunctional nanoarchitectures from DNA-based ABC monomers. *Nat Nanotechnol* **4**, 430-436 (2009).

98. Feng, X. et al. Fluorescence Logic-Signal-Based Multiplex Detection of Nucleases with the Assembly of a Cationic Conjugated Polymer and Branched DNA. *Angewandte Chemie International Edition* **48**, 5316-5321 (2009).

99. Rattanakiat, S., Nishikawa, M., Funabashi, H., Luo, D. & Takakura, Y. The assembly of a short linear natural cytosine-phosphate-guanine DNA into dendritic structures and its effect on immunostimulatory activity. *Biomaterials* **30**, 5701-5706 (2009).

100. Nishikawa, M. et al. Biodegradable CpG DNA hydrogels for sustained delivery of doxorubicin and immunostimulatory signals in tumor-bearing mice. *Biomaterials* **32**, 488-494 (2011).

101. Luo, D., Li, Y., Um, S. & Cu, Y. in DNA Vaccines, Vol. 127. (eds. W.M. Saltzman, H. Shen & J. Brandsma) 115-125 (Humana Press, 2006).

102. Um, S.H., Lee, J.B., Kwon, S.Y., Li, Y. & Luo, D. Dendrimer-like DNA-based fluorescence nanobarcodes. *Nat Protoc* **1**, 995-1000 (2006).

103. Tran, T.N.N. et al. A Universal DNA-Based Protein Detection System. *J Am Chem Soc* **135**, 14008-14011 (2013).

104. Lee, C.C., MacKay, J.A., Frechet, J.M.J. & Szoka, F.C. Designing dendrimers

for biological applications. *Nat Biotechnol* **23**, 1517-1526 (2005).

105. Roh, Y.H. et al. DNAsomes: Multifunctional DNA-Based Nanocarriers. *Small* **7**, 74-78 (2011).

106. Krieg, A.M. et al. Cpg Motifs in Bacterial-DNA Trigger Direct B-Cell Activation. *Nature* **374**, 546-549 (1995).

107. Vollmer, J. & Krieg, A.M. Immunotherapeutic applications of CpG oligodeoxynucleotide TLR9 agonists. *Adv Drug Deliver Rev* **61**, 195-204 (2009).

108. Bode, C., Zhao, G., Steinhagen, F., Kinjo, T. & Klinman, D.M. CpG DNA as a vaccine adjuvant. *Expert Rev Vaccines* **10**, 499-511 (2011).

109. Krieg, A.M. CpG Still Rocks! Update on an Accidental Drug. *Nucleic Acid Ther* **22**, 77-89 (2012).

110. Klinman, D.M. et al. Therapeutic potential of oligonucleotides expressing immunosuppressive TTAGGG motifs. *Ann Ny Acad Sci* **1058**, 87-95 (2005).

111. Trieu, A., Roberts, T.L., Dunn, J.A., Sweet, M.J. & Stacey, K.J. DNA motifs suppressing TLR9 responses. *Crit Rev Immunol* **26**, 527-544 (2006).

112. Peter, M. et al. Characterization of suppressive oligodeoxynucleotides that inhibit Toll-like receptor-9-mediated activation of innate immunity. *Immunology* **123**, 118-128 (2008).

113. Liu, Y. et al. Biomimetic enzyme nanocomplexes and their use as antidotes and preventive measures for alcohol intoxication. *Nat Nanotechnol* **8**, 187-192 (2013).

114. Censi, R., Di Martino, P., Vermonden, T. & Hennink, W.E. Hydrogels for

protein delivery in tissue engineering. *J Control Release* **161**, 680-692 (2012).

115. Lee, S.C., Kwon, I.K. & Park, K. Hydrogels for delivery of bioactive agents: A historical perspective. *Adv Drug Deliver Rev* **65**, 17-20 (2013).

116. Gupta, P., Vermani, K. & Garg, S. Hydrogels: from controlled release to pH-responsive drug delivery. *Drug Discov Today* **7**, 569-579 (2002).

117. Lin, C.C. & Metters, A.T. Hydrogels in controlled release formulations: Network design and mathematical modeling. *Adv Drug Deliver Rev* **58**, 1379-1408 (2006).

118. Peppas, N.A., Hilt, J.Z., Khademhosseini, A. & Langer, R. Hydrogels in biology and medicine: From molecular principles to bionanotechnology. *Adv Mater* **18**, 1345-1360 (2006).

119. Hoare, T.R. & Kohane, D.S. Hydrogels in drug delivery: Progress and challenges. *Polymer* **49**, 1993-2007 (2008).

120. Garcia, A.J. PEG-Maleimide Hydrogels for Protein and Cell Delivery in Regenerative Medicine. *Ann Biomed Eng* **42**, 312-322 (2014).

121. Silva, R., Fabry, B. & Boccaccini, A.R. Fibrous protein-based hydrogels for cell encapsulation. *Biomaterials* (2014).

122. Kloxin, A.M., Kloxin, C.J., Bowman, C.N. & Anseth, K.S. Mechanical Properties of Cellularly Responsive Hydrogels and Their Experimental Determination. *Adv Mater* **22**, 3484-3494 (2010).

123. Lutolf, M.P., Gilbert, P.M. & Blau, H.M. Designing materials to direct stem-cell fate. *Nature* **462**, 433-441 (2009).

124. Seliktar, D. Designing Cell-Compatible Hydrogels for Biomedical

Applications. *Science* **336**, 1124-1128 (2012).

125. Huh, D., Hamilton, G.A. & Ingber, D.E. From 3D cell culture to organs-on-chips. *Trends Cell Biol* **21**, 745-754 (2011).

126. Khetan, S. & Burdick, J.A. Patterning hydrogels in three dimensions towards controlling cellular interactions. *Soft Matter* **7**, 830-838 (2011).

127. Slaughter, B.V., Khurshid, S.S., Fisher, O.Z., Khademhosseini, A. & Peppas, N.A. Hydrogels in Regenerative Medicine. *Adv Mater* **21**, 3307-3329 (2009).

128. Balakrishnan, B. & Banerjee, R. Biopolymer-Based Hydrogels for Cartilage Tissue Engineering. *Chem Rev* **111**, 4453-4474 (2011).

129. Patterson, J., Martino, M.M. & Hubbell, J.A. Biomimetic materials in tissue engineering. *Mater Today* **13**, 14-22 (2010).

130. Lutolf, M.P. & Hubbell, J.A. Synthetic biomaterials as instructive extracellular microenvironments for morphogenesis in tissue engineering. *Nat Biotechnol* **23**, 47-55 (2005).

131. Drury, J.L. & Mooney, D.J. Hydrogels for tissue engineering: scaffold design variables and applications. *Biomaterials* **24**, 4337-4351 (2003).

132. Lee, K.Y. & Mooney, D.J. Hydrogels for tissue engineering. *Chem Rev* **101**, 1869-1879 (2001).

133. Hoffman, A.S. Hydrogels for biomedical applications. *Adv Drug Deliver Rev* **64**, 18-23 (2012).

134. Tomatsu, I., Peng, K. & Kros, A. Photoresponsive hydrogels for biomedical applications. *Adv Drug Deliver Rev* **63**, 1257-1266 (2011).

135. Burdick, J.A. & Prestwich, G.D. Hyaluronic Acid Hydrogels for Biomedical

Applications. *Adv Mater* **23**, H41-H56 (2011).

136. Yan, C.Q. & Pochan, D.J. Rheological properties of peptide-based hydrogels for biomedical and other applications. *Chem Soc Rev* **39**, 3528-3540 (2010).

137. Hoffman, A.S. Hydrogels for biomedical applications. *Adv Drug Deliver Rev* **54**, 3-12 (2002).

138. Um, S.H. et al. Enzyme-catalysed assembly of DNA hydrogel. *Nat Mater* **5**, 797-801 (2006).

139. Hur, J. et al. DNA hydrogel-based supercapacitors operating in physiological fluids. *Sci Rep-Uk* **3** (2013).

140. Zinchenko, A., Miwa, Y., Lopatina, L.I., Sergeyev, V.G. & Murata, S. DNA Hydrogel as a Template for Synthesis of Ultrasmall Gold Nanoparticles for Catalytic Applications. *Acs Appl Mater Inter* **6**, 3226-3232 (2014).

141. Mandal, C. & Nandi, U.S. Kinetic Studies on the Interaction of Gold(Iii) with Nucleic-Acids .1. Native DNA-Au(Iii) System - Spectrophotometric Studies. *P Indian as-Chem Sci* **88**, 263-278 (1979).

142. Pillai, C.K.S. & Nandi, U.S. Binding of Gold(Iii) with DNA. *Biopolymers* **12**, 1431-1435 (1973).

143. Cheng, E.J. et al. A pH-Triggered, Fast-Responding DNA Hydrogel. *Angew Chem Int Edit* **48**, 7660-7663 (2009).

144. Gehring, K., Leroy, J.L. & Gueron, M. A Tetrameric DNA-Structure with Protonated Cytosine.Cytosine Base-Pairs. *Nature* **363**, 561-565 (1993).

145. Xing, Y.Z. et al. Self-Assembled DNA Hydrogels with Designable Thermal and Enzymatic Responsiveness. *Adv Mater* **23**, 1117-1121 (2011).

146. Jin, J. et al. A Triggered DNA Hydrogel Cover to Envelop and Release Single Cells. *Adv Mater* **25**, 4714-4717 (2013).

147. Schiffenbauer, Y.S. et al. A cell chip for sequential imaging of individual non-adherent live cells reveals transients and oscillations. *Lab on a chip* **9**, 2965-2972 (2009).

148. Kim, S.H., Yamamoto, T., Fourmy, D. & Fujii, T. Electroactive Microwell Arrays for Highly Efficient Single-Cell Trapping and Analysis. *Small* **7**, 3239-3247 (2011).

149. Nishikawa, M. et al. Injectable, self-gelling, biodegradable, and immunomodulatory DNA hydrogel for antigen delivery. *J Control Release* **180**, 25-32 (2014).

150. Park, N., Um, S.H., Funabashi, H., Xu, J.F. & Luo, D. A cell-free protein-producing gel. *Nat Mater* **8**, 432-437 (2009).

151. Hartman, M.R. et al. Thermostable Branched DNA Nanostructures as Modular Primers for Polymerase Chain Reaction. *Angew Chem Int Edit* **52**, 8699-8702 (2013).

152. Cimino, G.D., Gamper, H.B., Isaacs, S.T. & Hearst, J.E. Psoralens as Photoactive Probes of Nucleic Acid Structure and Function: Organic Chemistry, Photochemistry, and Biochemistry. *Annual Review of Biochemistry* **54**, 1151-1193 (1985).

153. Blanco, L. et al. Highly Efficient DNA-Synthesis by the Phage Phi-29 DNA-Polymerase - Symmetrical Mode of DNA-Replication. *J Biol Chem* **264**, 8935-8940 (1989).

154. Lee, J. et al. A mechanical metamaterial made from a DNA hydrogel. *Nat Nanotechnol* **7**, 816-820 (2012).

155. Slater, G.W. DNA gel electrophoresis: The reptation model(s). *ELECTROPHORESIS* **30**, S181-S187 (2009).

156. Roh, Y.H. et al. Photocrosslinked DNA Nanospheres for Drug Delivery. *Macromolecular Rapid Communications* **31**, 1207-1211 (2010).

157. CauichRodriguez, J.V., Deb, S. & Smith, R. Effect of cross-linking agents on the dynamic mechanical properties of hydrogel blends of poly(acrylic acid)-poly(vinyl alcohol vinyl acetate). *Biomaterials* **17**, 2259-2264 (1996).

158. Zhu, G.Z. et al. Noncanonical Self-Assembly of Multifunctional DNA Nanoflowers for Biomedical Applications. *J Am Chem Soc* **135**, 16438-16445 (2013).

159. Hartman, M.R. et al. Point-of-care nucleic acid detection using nanotechnology. *Nanoscale* **5**, 10141-10154 (2013).

160. Lee, J.B., Hong, J., Bonner, D.K., Poon, Z. & Hammond, P.T. Self-assembled RNA interference microsponges for efficient siRNA delivery. *Nat Mater* **11**, 316-322 (2012).

161. Whitehead, K.A., Langer, R. & Anderson, D.G. Knocking down barriers: advances in siRNA delivery. *Nat Rev Drug Discov* **8**, 129-138 (2009).

162. Kay, M.A. State-of-the-art gene-based therapies: the road ahead. *Nat Rev Genet* **12**, 316-328 (2011).

163. Kutzler, M.A. & Weiner, D.B. DNA vaccines: ready for prime time? *Nat Rev Genet* **9**, 776-788 (2008).

164. Rice, J., Ottensmeier, C.H. & Stevenson, F.K. DNA vaccines: precision tools for activating effective immunity against cancer. *Nat Rev Cancer* **8**, 108-120 (2008).

165. Klinman, D.M. Immunotherapeutic uses of CpG oligodeoxynucleotides. *Nat Rev Immunol* **4**, 248-257 (2004).

166. Weiner, G.J. CpG oligodeoxynucleotide-based therapy of lymphoid malignancies. *Adv Drug Deliver Rev* **61**, 263-267 (2009).

167. Hemmi, H. et al. A Toll-like receptor recognizes bacterial DNA. *Nature* **408**, 740-745 (2000).

168. Ouyang, X.Y. et al. Rolling Circle Amplification-Based DNA Origami Nanostructrures for Intracellular Delivery of Immunostimulatory Drugs. *Small* **9**, 3082-3087 (2013).

169. Krieg, A.M. Development of TLR9 agonists for cancer therapy. *J Clin Invest* **117**, 1184-1194 (2007).

170. Bennett, M.D., Heslopharrison, J.S., Smith, J.B. & Ward, J.P. DNA Density in Mitotic and Meiotic Metaphase Chromosomes of Plants and Animals. *J Cell Sci* **63**, 173-179 (1983).

171. Luo, D. & Saltzman, W.M. Synthetic DNA delivery systems. *Nat Biotechnol* **18**, 33-37 (2000).

172. Cooperman, B.S. The mechanism of action of yeast inorganic pyrophosphatase. *Methods in enzymology* **87**, 526-548 (1982).

173. Hacker, H. et al. CpG-DNA-specific activation of antigen-presenting cells requires stress kinase activity and is preceded by non-specific endocytosis and

endosomal maturation. *Embo J* **17**, 6230-6240 (1998).

174. Yi, A.K. et al. CpG motifs in bacterial DNA activate leukocytes through the pH-dependent generation of reactive oxygen species. *J Immunol* **160**, 4755-4761 (1998).

175. Hong, G.S. et al. In Vivo Fluorescence Imaging with Ag2S Quantum Dots in the Second Near-Infrared Region. *Angew Chem Int Edit* **51**, 9818-9821 (2012).